

**ROUTING AND ACTION  
MEMORANDUM**

---

ROUTING

---

TO: (1) Chemical Sciences Division (Burgess, James)

Report is available for review

(2) Proposal Files    Proposal No.: 71206-CH-ISON

---

DESCRIPTION OF MATERIAL

---

CONTRACT OR GRANT NUMBER: W911NF-18-2-0048

INSTITUTION: Massachusetts Institute of Technology (MIT)

PRINCIPAL INVESTIGATOR: John Joannopoulos

TYPE REPORT: Interim Progress Report

DATE RECEIVED: 8/17/18 10:57AM

PERIOD COVERED: 04-Jan-2018 through 31-July-2018

TITLE:

---

ACTION TAKEN BY DIVISION

---

(x) Report has been reviewed for technical sufficiency and IS ☒ IS NOT ☐ satisfactory.

(x) Material has been given an OPSEC review and it has been determined to be non sensitive and, except for manuscripts and progress reports, suitable for public release.

Approved by SSL\JAMES.BURGESS on 3/9/20 7:28AM

ARO FORM 36-E

<b>REPORT DOCUMENTATION PAGE</b>			Form Approved OMB NO. 0704-0188		
<p>The public reporting burden for this collection of information is estimated to average 1 hour per response, including the time for reviewing instructions, searching existing data sources, gathering and maintaining the data needed, and completing and reviewing the collection of information. Send comments regarding this burden estimate or any other aspect of this collection of information, including suggestions for reducing this burden, to Washington Headquarters Services, Directorate for Information Operations and Reports, 1215 Jefferson Davis Highway, Suite 1204, Arlington VA, 22202-4302. Respondents should be aware that notwithstanding any other provision of law, no person shall be subject to any penalty for failing to comply with a collection of information if it does not display a currently valid OMB control number.</p> <p>PLEASE DO NOT RETURN YOUR FORM TO THE ABOVE ADDRESS.</p>					
1. REPORT DATE (DD-MM-YYYY) 17-08-2018		2. REPORT TYPE Interim Progress Report		3. DATES COVERED (From - To) 4-Jan-2018 - 31-Jul-2018	
4. TITLE AND SUBTITLE ISN 4 - Collaborative Agreement			5a. CONTRACT NUMBER W911NF-18-2-0048		
			5b. GRANT NUMBER		
			5c. PROGRAM ELEMENT NUMBER 611104		
6. AUTHORS			5d. PROJECT NUMBER		
			5e. TASK NUMBER		
			5f. WORK UNIT NUMBER		
7. PERFORMING ORGANIZATION NAMES AND ADDRESSES Massachusetts Institute of Technology (MIT) 77 Massachusetts Avenue NE18-901 Cambridge, MA 02139 -4307			8. PERFORMING ORGANIZATION REPORT NUMBER		
9. SPONSORING/MONITORING AGENCY NAME(S) AND ADDRESS (ES) U.S. Army Research Office P.O. Box 12211 Research Triangle Park, NC 27709-2211			10. SPONSOR/MONITOR'S ACRONYM(S) ARO		
			11. SPONSOR/MONITOR'S REPORT NUMBER(S) 71206-CH-ISN		
12. DISTRIBUTION AVAILABILITY STATEMENT Approved for public release; distribution is unlimited.					
13. SUPPLEMENTARY NOTES The views, opinions and/or findings contained in this report are those of the author(s) and should not be construed as an official Department of the Army position, policy or decision, unless so designated by other documentation.					
14. ABSTRACT					
15. SUBJECT TERMS					
16. SECURITY CLASSIFICATION OF:			17. LIMITATION OF ABSTRACT UU	15. NUMBER OF PAGES	19a. NAME OF RESPONSIBLE PERSON John Joannopoulos
a. REPORT UU	b. ABSTRACT UU	c. THIS PAGE UU			19b. TELEPHONE NUMBER 617-253-4806



**RPPR Interim Progress Report**  
as of 10-Mar-2020

Agency Code:

Proposal Number: 71206CHISN

**Agreement Number: W911NF-18-2-0048**

**INVESTIGATOR(S):**

**Name:** John Joannopoulos joannop@mi

**Email:** joannop@mit.edu

**Phone Number:** 6172534806

**Principal:** Y

Organization: **Massachusetts Institute of Technology (MIT)**

Address: 77 Massachusetts Avenue, Cambridge, MA 021394307

Country: USA

DUNS Number: 001425594

EIN: 042103594

**Report Date:** 31-Aug-2018

Date Received: 17-Aug-2018

**Interim Progress Report** for Period Beginning 04-Jan-2018 and Ending 31-Jul-2018

**Title:** ISN 4 - Collaborative Agreement

**Begin Performance Period:** 04-Jan-2018

**End Performance Period:** 31-Dec-2020

**Report Term:** 1-Annual

Submitted By: John Joannopoulos

Email: joannop@mit.edu

Phone: (617) 253-4806

**Distribution Statement:** 1-Approved for public release; distribution is unlimited.

**STEM Degrees:** 4

**STEM Participants:** 38

**Major Goals:** Founded in 2002, the Institute for Soldier Nanotechnologies (ISN) is a U.S. Army University-Affiliated Research Center (UARC). The ISN was designed as three-member team to leverage the unique capabilities of the U.S. Army, industry, and the Massachusetts Institute of Technology (MIT). The ISN mission is to help the Army and other U.S. military services enable innovative capabilities for Soldiers and warfighters through basic research on nanotechnology by transitioning promising outcomes of that research in partnership with the Army, other U.S. military services, and industry. This mission includes not only decreasing the weight that Soldiers and other warfighters carry but also improving blast and ballistic protection, creating new methods of detecting and detoxifying chemical and biological threats, and providing physiological monitoring and medical treatment.

Information on the Major Goals of each ISN 6.1 project described in this report is included in the compiled Report, attached.

**Accomplishments:** Information on the Accomplishments of each ISN 6.1 project described in this report is included in the compiled Report, attached.

**Training Opportunities:** ISN trains many MIT students and post-doctoral researchers each year. More specific information can be found in the Participants and Students sections of the reporting website.

**Results Dissemination:** ISN shares information about its research in a variety of ways. Each year, ISN hosts hundreds of visitors from the military, academic, and industrial communities. Additionally, ISN researchers are extremely productive in publishing articles in scholarly journals and speaking at scientific conferences. ISN also hold a biennial technical meeting to which more than 100 industry and DoD colleagues are invited, as well as technical seminars on an occasional basis each year.

**Plans Next Period:** Information on the future Plans of each ISN 6.1 project described in this report is included in the compiled Report, attached.

## RPPR Interim Progress Report as of 10-Mar-2020

**Honors and Awards:** Bilge Yildiz - Ross Coffin Purdy Award, June 2018.

Dirk Englund - Awarded tenure, May 2018.

Peter Lu (Graduate Student, Soljacic Research Group) - National Defense Science and Engineering Graduate Fellow - May 2018.

Timothy Swager - Vannevar Bush Faculty Fellowship, April 2018

Paula Hammond - American Chemical Society Award in Applied Polymer Science, Jan 2018.

### Protocol Activity Status:

**Technology Transfer:** Information on the Technology Transfer of each ISN 6.1 project described in this report is included in the compiled Report, attached.

### PARTICIPANTS:

**Participant Type:** PD/PI

**Participant:** Ivan Celanovic

**Person Months Worked:** 1.00

**Funding Support:**

Project Contribution:

International Collaboration:

International Travel:

National Academy Member: N

Other Collaborators:

**Participant Type:** Faculty

**Participant:** John Joannopoulos

**Person Months Worked:** 1.00

**Funding Support:**

Project Contribution:

International Collaboration:

International Travel:

National Academy Member: Y

Other Collaborators:

**Participant Type:** Faculty

**Participant:** Ken Kamrin

**Person Months Worked:** 1.00

**Funding Support:**

Project Contribution:

International Collaboration:

International Travel:

National Academy Member: N

Other Collaborators:

**Participant Type:** Faculty

**Participant:** Marin Solajic

**Person Months Worked:** 1.00

**Funding Support:**

Project Contribution:

International Collaboration:

International Travel:

National Academy Member: N

Other Collaborators:

**Participant Type:** Faculty

**RPPR Interim Progress Report**  
as of 10-Mar-2020

**Participant:** Raul Radovitzky  
**Person Months Worked:** 1.00  
Project Contribution:  
International Collaboration:  
International Travel:  
National Academy Member: N  
Other Collaborators:

**Funding Support:**

**Participant Type:** Faculty  
**Participant:** Steven Johnson  
**Person Months Worked:** 1.00  
Project Contribution:  
International Collaboration:  
International Travel:  
National Academy Member: N  
Other Collaborators:

**Funding Support:**

**Participant Type:** Faculty  
**Participant:** Yoel Fink  
**Person Months Worked:** 1.00  
Project Contribution:  
International Collaboration:  
International Travel:  
National Academy Member: N  
Other Collaborators:

**Funding Support:**

**Participant Type:** Postdoctoral (scholar, fellow or other postdoctoral position)  
**Participant:** Eric Dane  
**Person Months Worked:** 3.00  
Project Contribution:  
International Collaboration:  
International Travel:  
National Academy Member: N  
Other Collaborators:

**Funding Support:**

**Participant Type:** Staff Scientist (doctoral level)  
**Participant:** Aristeidis Karalis  
**Person Months Worked:** 7.00  
Project Contribution:  
International Collaboration:  
International Travel:  
National Academy Member: N  
Other Collaborators:

**Funding Support:**

**Participant Type:** Staff Scientist (doctoral level)  
**Participant:** Alexei Maznev  
**Person Months Worked:** 3.00  
Project Contribution:  
International Collaboration:  
International Travel:  
National Academy Member: N  
Other Collaborators:

**Funding Support:**

**RPPR Interim Progress Report**  
as of 10-Mar-2020

**Participant Type:** Staff Scientist (doctoral level)

**Participant:** David Veysset

**Person Months Worked:** 1.00

**Funding Support:**

Project Contribution:

International Collaboration:

International Travel:

National Academy Member: N

Other Collaborators:

**Participant Type:** Graduate Student (research assistant)

**Participant:** Aaron Baumgarten

**Person Months Worked:** 2.00

**Funding Support:**

Project Contribution:

International Collaboration:

International Travel:

National Academy Member: N

Other Collaborators:

**Participant Type:** Graduate Student (research assistant)

**Participant:** Adam Sliwiak

**Person Months Worked:** 5.00

**Funding Support:**

Project Contribution:

International Collaboration:

International Travel:

National Academy Member: N

Other Collaborators:

**Participant Type:** Graduate Student (research assistant)

**Participant:** Adam Berger

**Person Months Worked:** 2.00

**Funding Support:**

Project Contribution:

International Collaboration:

International Travel:

National Academy Member: N

Other Collaborators:

**Participant Type:** Graduate Student (research assistant)

**Participant:** Ang-yu Lu

**Person Months Worked:** 3.00

**Funding Support:**

Project Contribution:

International Collaboration:

International Travel:

National Academy Member: N

Other Collaborators:

**Participant Type:** Graduate Student (research assistant)

**Participant:** Anton Cottrill

**Person Months Worked:** 1.00

**Funding Support:**

Project Contribution:

International Collaboration:

International Travel:

National Academy Member: N

Other Collaborators:

**RPPR Interim Progress Report**  
as of 10-Mar-2020

**Participant Type:** Graduate Student (research assistant)

**Participant:** Aviram Massuda

**Person Months Worked:** 4.00

**Funding Support:**

Project Contribution:

International Collaboration:

International Travel:

National Academy Member: N

Other Collaborators:

**Participant Type:** Graduate Student (research assistant)

**Participant:** Bradley Walcher

**Person Months Worked:** 6.00

**Funding Support:**

Project Contribution:

International Collaboration:

International Travel:

National Academy Member: N

Other Collaborators:

**Participant Type:** Graduate Student (research assistant)

**Participant:** Cache Hamilton

**Person Months Worked:** 2.00

**Funding Support:**

Project Contribution:

International Collaboration:

International Travel:

National Academy Member: N

Other Collaborators:

**Participant Type:** Graduate Student (research assistant)

**Participant:** Celestine Hong

**Person Months Worked:** 7.00

**Funding Support:**

Project Contribution:

International Collaboration:

International Travel:

National Academy Member: N

Other Collaborators:

**Participant Type:** Graduate Student (research assistant)

**Participant:** Charles Roques-Carnes

**Person Months Worked:** 1.00

**Funding Support:**

Project Contribution:

International Collaboration:

International Travel:

National Academy Member: N

Other Collaborators:

**Participant Type:** Graduate Student (research assistant)

**Participant:** CheeKong Lee

**Person Months Worked:** 5.00

**Funding Support:**

Project Contribution:

International Collaboration:

International Travel:

National Academy Member: N

Other Collaborators:

**RPPR Interim Progress Report**  
as of 10-Mar-2020

**Participant Type:** Graduate Student (research assistant)

**Participant:** Colin Bittner

**Person Months Worked:** 2.00

**Funding Support:**

Project Contribution:

International Collaboration:

International Travel:

National Academy Member: N

Other Collaborators:

**Participant Type:** Graduate Student (research assistant)

**Participant:** Dmitro Martynowych

**Person Months Worked:** 1.00

**Funding Support:**

Project Contribution:

International Collaboration:

International Travel:

National Academy Member: N

Other Collaborators:

**Participant Type:** Graduate Student (research assistant)

**Participant:** Elaine McVay

**Person Months Worked:** 3.00

**Funding Support:**

Project Contribution:

International Collaboration:

International Travel:

National Academy Member: N

Other Collaborators:

**Participant Type:** Graduate Student (research assistant)

**Participant:** Eric Alt

**Person Months Worked:** 5.00

**Funding Support:**

Project Contribution:

International Collaboration:

International Travel:

National Academy Member: N

Other Collaborators:

**Participant Type:** Graduate Student (research assistant)

**Participant:** Eric Sung

**Person Months Worked:** 2.00

**Funding Support:**

Project Contribution:

International Collaboration:

International Travel:

National Academy Member: N

Other Collaborators:

**Participant Type:** Graduate Student (research assistant)

**Participant:** German Hernandez

**Person Months Worked:** 5.00

**Funding Support:**

Project Contribution:

International Collaboration:

International Travel:

National Academy Member: N

**RPPR Interim Progress Report**  
as of 10-Mar-2020

Other Collaborators:

**Participant Type:** Graduate Student (research assistant)

**Participant:** Jamison Sloan

**Person Months Worked:** 1.00

**Funding Support:**

Project Contribution:

International Collaboration:

International Travel:

National Academy Member: N

Other Collaborators:

**Participant Type:** Graduate Student (research assistant)

**Participant:** Jiaojian Shi

**Person Months Worked:** 7.00

**Funding Support:**

Project Contribution:

International Collaboration:

International Travel:

National Academy Member: N

Other Collaborators:

**Participant Type:** Graduate Student (research assistant)

**Participant:** Jonathan Chou

**Person Months Worked:** 2.00

**Funding Support:**

Project Contribution:

International Collaboration:

International Travel:

National Academy Member: N

Other Collaborators:

**Participant Type:** Graduate Student (research assistant)

**Participant:** Jordan Goldstein

**Person Months Worked:** 1.00

**Funding Support:**

Project Contribution:

International Collaboration:

International Travel:

National Academy Member: N

Other Collaborators:

**Participant Type:** Graduate Student (research assistant)

**Participant:** Josue Lopez

**Person Months Worked:** 1.00

**Funding Support:**

Project Contribution:

International Collaboration:

International Travel:

National Academy Member: N

Other Collaborators:

**Participant Type:** Graduate Student (research assistant)

**Participant:** Jude Deschamps

**Person Months Worked:** 2.00

**Funding Support:**

Project Contribution:

International Collaboration:

International Travel:

**RPPR Interim Progress Report**  
as of 10-Mar-2020

National Academy Member: N  
Other Collaborators:

**Participant Type:** Graduate Student (research assistant)

**Participant:** Juliette Alain

**Person Months Worked:** 7.00

**Funding Support:**

Project Contribution:

International Collaboration:

International Travel:

National Academy Member: N

Other Collaborators:

**Participant Type:** Graduate Student (research assistant)

**Participant:** Justin Beroz

**Person Months Worked:** 1.00

**Funding Support:**

Project Contribution:

International Collaboration:

International Travel:

National Academy Member: N

Other Collaborators:

**Participant Type:** Graduate Student (research assistant)

**Participant:** Laura Cooper

**Person Months Worked:** 3.00

**Funding Support:**

Project Contribution:

International Collaboration:

International Travel:

National Academy Member: N

Other Collaborators:

**Participant Type:** Graduate Student (research assistant)

**Participant:** Mohammed Benzaouia

**Person Months Worked:** 6.00

**Funding Support:**

Project Contribution:

International Collaboration:

International Travel:

National Academy Member: N

Other Collaborators:

**Participant Type:** Graduate Student (research assistant)

**Participant:** Peter Lu

**Person Months Worked:** 2.00

**Funding Support:**

Project Contribution:

International Collaboration:

International Travel:

National Academy Member: N

Other Collaborators:

**Participant Type:** Graduate Student (research assistant)

**Participant:** Reginald Avery

**Person Months Worked:** 4.00

**Funding Support:**

Project Contribution:

International Collaboration:



**RPPR Interim Progress Report**  
as of 10-Mar-2020

International Travel:  
National Academy Member: N  
Other Collaborators:

**Participant Type:** Graduate Student (research assistant)

**Participant:** Reyu sakakibara

**Person Months Worked:** 3.00

**Funding Support:**

Project Contribution:

International Collaboration:

International Travel:

National Academy Member: N

Other Collaborators:

**Participant Type:** Graduate Student (research assistant)

**Participant:** Samuel Kim

**Person Months Worked:** 1.00

**Funding Support:**

Project Contribution:

International Collaboration:

International Travel:

National Academy Member: N

Other Collaborators:

**Participant Type:** Graduate Student (research assistant)

**Participant:** Thomas Avila

**Person Months Worked:** 4.00

**Funding Support:**

Project Contribution:

International Collaboration:

International Travel:

National Academy Member: N

Other Collaborators:

**Participant Type:** Graduate Student (research assistant)

**Participant:** Tyler Olsen

**Person Months Worked:** 4.00

**Funding Support:**

Project Contribution:

International Collaboration:

International Travel:

National Academy Member: N

Other Collaborators:

**Participant Type:** Graduate Student (research assistant)

**Participant:** Victor Champagne

**Person Months Worked:** 3.00

**Funding Support:**

Project Contribution:

International Collaboration:

International Travel:

National Academy Member: N

Other Collaborators:

**Participant Type:** Graduate Student (research assistant)

**Participant:** You-Chi Wu

**Person Months Worked:** 4.00

**Funding Support:**

Project Contribution:

**RPPR Interim Progress Report**  
as of 10-Mar-2020

International Collaboration:  
International Travel:  
National Academy Member: N  
Other Collaborators:

**Participant Type:** Graduate Student (research assistant)

**Participant:** Younggyu Kim

**Person Months Worked:** 6.00

**Funding Support:**

Project Contribution:  
International Collaboration:  
International Travel:  
National Academy Member: N  
Other Collaborators:

**Participant Type:** Graduate Student (research assistant)

**Participant:** Yuxuan Lin

**Person Months Worked:** 4.00

**Funding Support:**

Project Contribution:  
International Collaboration:  
International Travel:  
National Academy Member: N  
Other Collaborators:

**Participant Type:** Graduate Student (research assistant)

**Participant:** Gabriel Loke

**Person Months Worked:** 3.00

**Funding Support:**

Project Contribution:  
International Collaboration:  
International Travel:  
National Academy Member: N  
Other Collaborators:

**Participant Type:** Postdoctoral (scholar, fellow or other postdoctoral position)

**Participant:** Alan Lai

**Person Months Worked:** 3.00

**Funding Support:**

Project Contribution:  
International Collaboration:  
International Travel:  
National Academy Member: N  
Other Collaborators:

**Participant Type:** Postdoctoral (scholar, fellow or other postdoctoral position)

**Participant:** Bianca Giovanardi

**Person Months Worked:** 2.00

**Funding Support:**

Project Contribution:  
International Collaboration:  
International Travel:  
National Academy Member: N  
Other Collaborators:

**Participant Type:** Postdoctoral (scholar, fellow or other postdoctoral position)

**Participant:** Boris Spokoyny

**Person Months Worked:** 1.00

**Funding Support:**

**RPPR Interim Progress Report**  
as of 10-Mar-2020

Project Contribution:  
International Collaboration:  
International Travel:  
National Academy Member: N  
Other Collaborators:

**Participant Type:** Postdoctoral (scholar, fellow or other postdoctoral position)

**Participant:** Chong Hou

**Person Months Worked:** 4.00

**Funding Support:**

Project Contribution:  
International Collaboration:  
International Travel:  
National Academy Member: N  
Other Collaborators:

**Participant Type:** Postdoctoral (scholar, fellow or other postdoctoral position)

**Participant:** Daichi Kozawa

**Person Months Worked:** 2.00

**Funding Support:**

Project Contribution:  
International Collaboration:  
International Travel:  
National Academy Member: N  
Other Collaborators:

**Participant Type:** Postdoctoral (scholar, fellow or other postdoctoral position)

**Participant:** David Veysset

**Person Months Worked:** 1.00

**Funding Support:**

Project Contribution:  
International Collaboration:  
International Travel:  
National Academy Member: N  
Other Collaborators:

**Participant Type:** Postdoctoral (scholar, fellow or other postdoctoral position)

**Participant:** Hiroki Isobe

**Person Months Worked:** 7.00

**Funding Support:**

Project Contribution:  
International Collaboration:  
International Travel:  
National Academy Member: N  
Other Collaborators:

**Participant Type:** Postdoctoral (scholar, fellow or other postdoctoral position)

**Participant:** Ji Hoon Park

**Person Months Worked:** 3.00

**Funding Support:**

Project Contribution:  
International Collaboration:  
International Travel:  
National Academy Member: N  
Other Collaborators:

**Participant Type:** Postdoctoral (scholar, fellow or other postdoctoral position)

**Participant:** John Martin

**RPPR Interim Progress Report**  
as of 10-Mar-2020

**Person Months Worked:** 1.00

**Funding Support:**

Project Contribution:

International Collaboration:

International Travel:

National Academy Member: N

Other Collaborators:

**Participant Type:** Postdoctoral (scholar, fellow or other postdoctoral position)

**Participant:** Keun Ah Ryu

**Person Months Worked:** 1.00

**Funding Support:**

Project Contribution:

International Collaboration:

International Travel:

National Academy Member: N

Other Collaborators:

**Participant Type:** Postdoctoral (scholar, fellow or other postdoctoral position)

**Participant:** Lin Zhou

**Person Months Worked:** 2.00

**Funding Support:**

Project Contribution:

International Collaboration:

International Travel:

National Academy Member: N

Other Collaborators:

**Participant Type:** Postdoctoral (scholar, fellow or other postdoctoral position)

**Participant:** Nikesh Koirala

**Person Months Worked:** 3.00

**Funding Support:**

Project Contribution:

International Collaboration:

International Travel:

National Academy Member: N

Other Collaborators:

**Participant Type:** Postdoctoral (scholar, fellow or other postdoctoral position)

**Participant:** Qingqing Ji

**Person Months Worked:** 2.00

**Funding Support:**

Project Contribution:

International Collaboration:

International Travel:

National Academy Member: N

Other Collaborators:

**Participant Type:** Postdoctoral (scholar, fellow or other postdoctoral position)

**Participant:** Shai Maayani

**Person Months Worked:** 2.00

**Funding Support:**

Project Contribution:

International Collaboration:

International Travel:

National Academy Member: N

Other Collaborators:

**Participant Type:** Postdoctoral (scholar, fellow or other postdoctoral position)

**RPPR Interim Progress Report**  
as of 10-Mar-2020

**Participant:** Suyang Xu

**Person Months Worked:** 4.00

**Funding Support:**

Project Contribution:

International Collaboration:

International Travel:

National Academy Member: N

Other Collaborators:

**Participant Type:** Postdoctoral (scholar, fellow or other postdoctoral position)

**Participant:** Veronkia Stelmahk

**Person Months Worked:** 2.00

**Funding Support:**

Project Contribution:

International Collaboration:

International Travel:

National Academy Member: N

Other Collaborators:

**Participant Type:** Postdoctoral (scholar, fellow or other postdoctoral position)

**Participant:** Walker Chan

**Person Months Worked:** 3.00

**Funding Support:**

Project Contribution:

International Collaboration:

International Travel:

National Academy Member: N

Other Collaborators:

**Participant Type:** Postdoctoral (scholar, fellow or other postdoctoral position)

**Participant:** William Bowman

**Person Months Worked:** 1.00

**Funding Support:**

Project Contribution:

International Collaboration:

International Travel:

National Academy Member: N

Other Collaborators:

**Participant Type:** Postdoctoral (scholar, fellow or other postdoctoral position)

**Participant:** Wonseok Shin

**Person Months Worked:** 3.00

**Funding Support:**

Project Contribution:

International Collaboration:

International Travel:

National Academy Member: N

Other Collaborators:

**Participant Type:** Postdoctoral (scholar, fellow or other postdoctoral position)

**Participant:** Wontae Joo

**Person Months Worked:** 1.00

**Funding Support:**

Project Contribution:

International Collaboration:

International Travel:

National Academy Member: N

Other Collaborators:

# RPPR Interim Progress Report

## as of 10-Mar-2020

**Participant Type:** Postdoctoral (scholar, fellow or other postdoctoral position)

**Participant:** Zin Lin

**Person Months Worked:** 4.00

**Funding Support:**

Project Contribution:

International Collaboration:

International Travel:

National Academy Member: N

Other Collaborators:

### ARTICLES:

**Publication Type:** Journal Article

Peer Reviewed: Y

**Publication Status:** 1-Published

**Journal:** Nature

Publication Identifier Type: DOI

Publication Identifier: 10.1038/s41586-018-0185-0

Volume: 558 Issue: 7709

First Page #: 274

Date Submitted: 8/16/18 12:00AM

Date Published: 6/1/18 4:00AM

Publication Location:

**Article Title:** Printing ferromagnetic domains for untethered fast-transforming soft materials

**Authors:** Yoonho Kim, Hyunwoo Yuk, Ruike Zhao, Shawn A. Chester, Xuanhe Zhao

**Keywords:** 3-d printing, ferromagnetic, soft materials, shape change

**Abstract:** Soft materials capable of transforming between three-dimensional (3D) shapes in response to stimuli such as light, heat, solvent, electric and magnetic fields have applications in diverse areas such as flexible electronics<sup>1,2</sup>, soft robotics<sup>3,4</sup> and biomedicine<sup>5–7</sup>. In particular, magnetic fields offer a safe and effective manipulation method for biomedical applications, which typically require remote actuation in enclosed and confined spaces<sup>8–10</sup>. With advances in magnetic field control<sup>11</sup>, magnetically responsive soft materials have also evolved from embedding discrete magnets<sup>12</sup> or incorporating magnetic particles<sup>13</sup> into soft compounds to generating nonuniform magnetization profiles in polymeric sheets<sup>14,15</sup>. Here we report 3D printing of programmed ferromagnetic domains in soft materials that enable fast transformations between complex 3D shapes via magnetic actuation. Our approach is based on direct ink writing<sup>16</sup> of an elastomer composite containing ferromagnetic microparticles. By apply

**Distribution Statement:** 3-Distribution authorized to U.S. Government Agencies and their contractors

Acknowledged Federal Support: Y

**Publication Type:** Journal Article

Peer Reviewed: Y

**Publication Status:** 1-Published

**Journal:** Journal of the Mechanical Behavior of Biomedical Materials

Publication Identifier Type: DOI

Publication Identifier: 10.1016/j.jmbbm.2018.06.016

Volume: 86 Issue:

First Page #: 71

Date Submitted: 8/16/18 12:00AM

Date Published: 10/1/18 8:00AM

Publication Location:

**Article Title:** High-velocity micro-particle impact on gelatin and synthetic hydrogel

**Authors:** David Veyssset, Steven E. Kooi, A.A. ?aznev, Shengchang Tang, Aleksandar S. Mijailovic, Yun Jung Yar

**Keywords:** Gelatin High-speed imaging High-velocity impact Hydrogel Penetration

**Abstract:** The high-velocity impact response of gelatin and synthetic hydrogel samples is investigated using a laser-based microballistic platform for launching and imaging supersonic micro-particles. The micro-particles are monitored during impact and penetration into the gels using a high-speed multi-frame camera that can record up to 16 images with nanosecond time resolution. The trajectories are compared with a Poncelet model for particle penetration, demonstrating good agreement between experiments and the model for impact in gelatin. The model is further validated on a synthetic hydrogel and the applicability of the results is discussed. We find the strength resistance parameter in the Poncelet model to be two orders of magnitude higher than in macroscopic experiments at comparable impact velocities. The results open prospects for testing high-rate behavior of soft materials on the microscale and for guiding the design of drug delivery methods using accelerated microparticles.

**Distribution Statement:** 3-Distribution authorized to U.S. Government Agencies and their contractors

Acknowledged Federal Support: Y

## RPPR Interim Progress Report as of 10-Mar-2020

**Publication Type:** Journal Article      Peer Reviewed: Y      **Publication Status:** 1-Published

**Journal:** Nano Letters

Publication Identifier Type: DOI

Publication Identifier: 10.1021/acs.nanolett.8b01866

Volume: 18

Issue: 8

First Page #: 5057

Date Submitted: 8/16/18 12:00AM

Date Published: 7/1/18 8:00AM

Publication Location:

**Article Title:** Stable, Temperature-Dependent Gas Mixture Permeation and Separation through Suspended Nanoporous Single-Layer Graphene Membranes

**Authors:** Zhe Yuan, Jesse D. Benck, Yannick Eatmon, Daniel Blankschtein, Michael S. Strano

**Keywords:** Graphene membrane gas permeation mixture separation nanopore

**Abstract:** Graphene membranes with nanometer-scale pores could exhibit an extremely high permeance and selectivity for the separation of gas mixtures. However, to date, no experimental measurements of gas mixture separation through nanoporous single-layer graphene (SLG) membranes have been reported. Herein, we report the first measurements of the temperature-dependent permeance of gas mixtures in an equimolar mixture feed containing H<sub>2</sub>, He, CH<sub>4</sub>, CO<sub>2</sub>, and SF<sub>6</sub> from 22 to 208 degrees C through SLG membranes containing nanopores formed spontaneously during graphene synthesis. Five membranes were fabricated by transfer of CVD graphene from catalytic Cu film onto channels framed in impermeable Ni. Two membranes exhibited gas permeances on the order of 10<sup>(-6)</sup> to 10<sup>(-5)</sup> mol m<sup>(-2)</sup> s<sup>(-1)</sup> Pa<sup>(-1)</sup> as well as gas mixture selectivities higher than the Knudsen effusion selectivities predicted by the gas effusion mechanism. We show that a new steric selectivity mechanism explains the permeance data and selectivity

**Distribution Statement:** 3-Distribution authorized to U.S. Government Agencies and their contractors

Acknowledged Federal Support: Y

**Publication Type:** Journal Article

Peer Reviewed: Y

**Publication Status:** 1-Published

**Journal:** Nano Today

Publication Identifier Type: DOI

Publication Identifier: 10.1016/j.nantod.2018.04.012

Volume: 21

Issue:

First Page #: 18

Date Submitted: 8/16/18 12:00AM

Date Published: 8/1/18 8:00AM

Publication Location:

**Article Title:** Emerging trends in 2D nanotechnology that are redefining our understanding of "Nanocomposites"

**Authors:** Pingwei Liu, Anton L. Cottrill, Daichi Kozawa, Volodymyr B. Koman, Dorsa Parviz, Albert Tianxiang Liu,

**Keywords:** Nanotechnology 2D materials Graphene Polymers Nanocomposites Hybrids Nanofillers Fibers

Mechanical reinforcement Multifunctional composites Barrier properties Electrical conduction Thermal conduction Optical properties Liquid-exfoliation Chemical vapor deposition Folding Multilayer

**Abstract:** The goal of this review is to summarize the recent development of nanocomposites of 2D materials, especially polymer nanocomposites with large-area, high-quality 2D sheets, and more importantly, the future direction of this field. Scientists and engineers have a tendency to review and envision the future based on the past, but innovation does not work like this. Herein, we do not provide a comprehensive review of nanocomposites with 2D materials; rather, we highlight unusual or unconventional directions emerging for nanocomposite materials research. This forward-looking perspective of current trends focuses on new research directions. In this review, we summarize the fundamentals of nanocomposites in regards to the mechanical and functional reinforcement at the theoretical limit, and we briefly introduce the synthesis of large-area 2D materials with high quality and their controlled dispersion into matrix materials to achieve the maximum reinforcement predicted by theory. We continue w

**Distribution Statement:** 3-Distribution authorized to U.S. Government Agencies and their contractors

Acknowledged Federal Support: N

## RPPR Interim Progress Report as of 10-Mar-2020

**Publication Type:** Journal Article

Peer Reviewed: Y

**Publication Status:** 1-Published

**Journal:** Science

Publication Identifier Type: DOI

Publication Identifier: 10.1126/science.aap9859

Volume: 359 Issue: 6379

First Page #: 1009

Date Submitted: 8/16/18 12:00AM

Date Published: 3/1/18 5:00AM

Publication Location:

**Article Title:** Observation of bulk Fermi arc and polarization half charge from paired exceptional points

**Authors:** Hengyun Zhou, Chao Peng, Yoseob Yoon, Chia Wei Hsu, Keith A. Nelson, Liang Fu, John D. Joannopoulos

**Keywords:** photonics symmetry lasers

**Abstract:** The ideas of topology have found tremendous success in closed physical systems, but even richer properties exist in the more general open or dissipative framework. We theoretically propose and experimentally demonstrate a bulk Fermi arc that develops from non-Hermitian radiative losses in an open system of photonic crystal slabs. Moreover, we discover half-integer topological charges in the polarization of far-field radiation around the bulk Fermi arc. Both phenomena are shown to be direct consequences of the non-Hermitian topological properties of exceptional points, where resonances coincide in their frequencies and linewidths. Our work connects the fields of topological photonics, non-Hermitian physics, and singular optics, providing a framework to explore more complex non-Hermitian topological systems.

**Distribution Statement:** 3-Distribution authorized to U.S. Government Agencies and their contractors

Acknowledged Federal Support: Y

**Publication Type:** Journal Article

Peer Reviewed: Y

**Publication Status:** 1-Published

**Journal:** Physical Review Letters

Publication Identifier Type: DOI

Publication Identifier: 10.1103/PhysRevLett.120.267201

Volume: 120 Issue: 26

First Page #:

Date Submitted: 8/16/18 12:00AM

Date Published: 6/1/18 8:00AM

Publication Location:

**Article Title:** Quantum Hall Effect with Composites of Magnetic Flux Tubes and Charged Particles

**Authors:** Marija Todoric, Dario Jukic, Danko Radic, Marin Soljacic, Hrvoje Buljan

**Keywords:** charged particles, magnetic flux tubes, anyon, quantum Hall effect

**Abstract:** Composites formed from charged particles and magnetic flux tubes, proposed by Wilczek, are one model for anyons-particles obeying fractional statistics. Here we propose a scheme for realizing charged flux tubes, in which a charged object with an intrinsic magnetic dipole moment is placed between two semi-infinite blocks of a high-permeability ( $\mu_{\{r\}}$ ) material, and the images of the magnetic moment create an effective flux tube. We show that the scheme can lead to a realization of Wilczek's anyons, when a two-dimensional electron system, which exhibits the integer quantum Hall effect, is sandwiched between two blocks of the high- $\mu_{\{r\}}$  material with a temporally fast response (in the cyclotron and Larmor frequency range). The signature of Wilczek's anyons is a slight shift of the resistivity at the plateau of the IQHE. Thus, the quest for high- $\mu_{\{r\}}$  materials at high frequencies, which is underway in the field of metamaterials, and the quest for anyons, are here found to be on the same

**Distribution Statement:** 3-Distribution authorized to U.S. Government Agencies and their contractors

Acknowledged Federal Support: Y



## RPPR Interim Progress Report as of 10-Mar-2020

**Publication Type:** Journal Article      Peer Reviewed: Y      **Publication Status:** 1-Published

**Journal:** Proceedings of the National Academy of Sciences

Publication Identifier Type: DOI

Publication Identifier: 10.1073/pnas.1803261115

Volume: 115

Issue: 26

First Page #: 6614

Date Submitted: 8/16/18 12:00AM

Date Published: 6/1/18 8:00AM

Publication Location:

**Article Title:** A high-efficiency regime for gas-phase terahertz lasers

**Authors:** Fan Wang, Jeongwon Lee, Dane J. Phillips, Samuel G. Holliday, Song-Liang Chua, Jorge Bravo-Abad, .

**Keywords:** continuous wave gas laser laser modeling optically pumped far-infrared laser rotational population inversion terahertz source

**Abstract:** We present both an innovative theoretical model and an experimental validation of a molecular gas optically pumped far-infrared (OPFIR) laser at 0.25 THz that exhibits 10x greater efficiency (39% of the Manley-Rowe limit) and 1,000x smaller volume than comparable commercial lasers. Unlike previous OPFIR-laser models involving only a few energy levels that failed even qualitatively to match experiments at high pressures, our ab initio theory matches experiments quantitatively, within experimental uncertainties with no free parameters, by accurately capturing the interplay of millions of degrees of freedom in the laser. We show that previous OPFIR lasers were inefficient simply by being too large and that high powers favor high pressures and small cavities. We believe that these results will revive interest in OPFIR laser as a powerful and compact source of terahertz radiation.

**Distribution Statement:** 3-Distribution authorized to U.S. Government Agencies and their contractors

Acknowledged Federal Support: Y

**Publication Type:** Journal Article

Peer Reviewed: Y

**Publication Status:** 1-Published

**Journal:** Science Advances

Publication Identifier Type: DOI

Publication Identifier: 10.1126/sciadv.aar4206

Volume: 4

Issue: 6

First Page #:

Date Submitted: 8/16/18 12:00AM

Date Published: 6/1/18 8:00AM

Publication Location:

**Article Title:** Nanophotonic particle simulation and inverse design using artificial neural networks

**Authors:** John Peurifoy, Yichen Shen, Li Jing, Yi Yang, Fidel Cano-Renteria, Brendan G. DeLacy, John D. Joann

**Keywords:** artificial neural networks, light scattering approximation

**Abstract:** We propose a method to use artificial neural networks to approximate light scattering by multilayer nanoparticles. We find that the network needs to be trained on only a small sampling of the data to approximate the simulation to high precision. Once the neural network is trained, it can simulate such optical processes orders of magnitude faster than conventional simulations. Furthermore, the trained neural network can be used to solve nanophotonic inverse design problems by using back propagation, where the gradient is analytical, not numerical.

**Distribution Statement:** 3-Distribution authorized to U.S. Government Agencies and their contractors

Acknowledged Federal Support: Y

## RPPR Interim Progress Report as of 10-Mar-2020

**Publication Type:** Journal Article

Peer Reviewed: Y

**Publication Status:** 1-Published

**Journal:** ACS Nano

Publication Identifier Type: DOI

Publication Identifier: 10.1021/acsnano.7b08231

Volume: 12

Issue: 3

First Page #: 2474

Date Submitted: 8/16/18 12:00AM

Date Published: 3/1/18 5:00AM

Publication Location:

**Article Title:** Active Radiative Thermal Switching with Graphene Plasmon Resonators

**Authors:** Ognjen Ilic, Nathan H. Thomas, Thomas Christensen, Michelle C. Sherrott, Marin Soljačić, Austin J. Min

**Keywords:** graphene near-field radiative heat transfer surface plasmon thermal radiation

**Abstract:** We theoretically demonstrate a near-field radiative thermal switch based on thermally excited surface plasmons in graphene resonators. The high tunability of graphene enables substantial modulation of near-field radiative heat transfer, which, when combined with the use of resonant structures, overcomes the intrinsically broadband nature of thermal radiation. In canonical geometries, we use nonlinear optimization to show that stacked graphene sheets offer improved heat conductance contrast between "ON" and "OFF" switching states and that a >10x higher modulation is achieved between isolated graphene resonators than for parallel graphene sheets. In all cases, we find that carrier mobility is a crucial parameter for the performance of a radiative thermal switch. Furthermore, we derive shape-agnostic analytical approximations for the resonant heat transfer that provide general scaling laws and allow for direct comparison between different resonator geometries dominated by a single mode. T

**Distribution Statement:** 3-Distribution authorized to U.S. Government Agencies and their contractors

Acknowledged Federal Support: Y

**Publication Type:** Journal Article

Peer Reviewed: Y

**Publication Status:** 1-Published

**Journal:** Nature Physics

Publication Identifier Type: DOI

Publication Identifier: 10.1038/s41567-018-0180-2

Volume:

Issue:

First Page #:

Date Submitted: 8/16/18 12:00AM

Date Published: 7/1/18 4:00AM

Publication Location:

**Article Title:** Maximal spontaneous photon emission and energy loss from free electrons

**Authors:** Yi Yang, Aviram Massuda, Charles Roques-Carmes, Steven E. Kooi, Thomas Christensen, Steven G. J

**Keywords:** photon emission, free electrons, Cerenkov, Smith–Purcell, transition radiation

**Abstract:** Free-electron radiation such as Cerenkov<sup>1</sup>, Smith–Purcell<sup>2</sup> and transition radiation<sup>3,4</sup> can be greatly affected by structured optical environments, as has been demonstrated in a variety of polaritonic<sup>5,6</sup>, photonic-crystal<sup>7</sup> and metamaterial<sup>8–10</sup> systems. However, the amount of radiation that can ultimately be extracted from free electrons near an arbitrary material structure has remained elusive. Here we derive a fundamental upper limit to the spontaneous photon emission and energy loss of free electrons, regardless of geometry, which illuminates the effects of material properties and electron velocities. We obtain experimental evidence for our theory with quantitative measurements of Smith–Purcell radiation. Our framework allows us to make two predictions. One is a new regime of radiation operation—at subwavelength separations, slower (non-relativistic) electrons can achieve stronger radiation than fast (relativistic) electrons. The other is a divergence of the emission probability in the

**Distribution Statement:** 3-Distribution authorized to U.S. Government Agencies and their contractors

Acknowledged Federal Support: Y

## RPPR Interim Progress Report as of 10-Mar-2020

**Publication Type:** Journal Article

Peer Reviewed: Y

**Publication Status:** 1-Published

**Journal:** Nature Physics

Publication Identifier Type: DOI

Publication Identifier: 10.1038/s41567-018-0209-6

Volume: Issue:

First Page #:

Date Submitted: 8/16/18 12:00AM

Date Published: 7/1/18 4:00AM

Publication Location:

**Article Title:** Superlight inverse Doppler effect

**Authors:** Xihang Shi, Xiao Lin, Ido Kaminer, Fei Gao, Zhaoju Yang, John D. Joannopoulos, Marin Soljačić, Baile

**Keywords:** inverse Doppler effect, Vavilov–Cherenkov cone, superlight

**Abstract:** It has long been thought<sup>1</sup> that the inverse Doppler frequency shift of light<sup>2–13</sup> is impossible in homogeneous systems with a positive refractive index. Here we break this long-held tenet by predicting a previously unconsidered Doppler effect of light inside a radiation cone, the so-called Vavilov–Cherenkov cone, under specific circumstances. It has been known from the classic work of Ginzburg and Frank that a superlight (that is, superluminal) normal Doppler effect<sup>14–18</sup> appears inside the Vavilov–Cherenkov cone if the velocity of the source  $v$  is larger than the phase velocity of light  $v_p$ . By further developing their theory, we discover that an inverse Doppler frequency shift will arise if  $v > 2v_p$ . We denote this as the superlight inverse Doppler effect. Moreover, we show that the superlight inverse Doppler effect can be spatially separated from the other Doppler effects by using highly squeezed polaritons (such as graphene plasmons), which may facilitate the experimental observation.

**Distribution Statement:** 3-Distribution authorized to U.S. Government Agencies and their contractors

Acknowledged Federal Support: Y

**Publication Type:** Journal Article

Peer Reviewed: Y

**Publication Status:** 1-Published

**Journal:** Nature Photonics

Publication Identifier Type: DOI

Publication Identifier: 10.1038/s41566-018-0176-6

Volume: 12 Issue: 7

First Page #: 423

Date Submitted: 8/16/18 12:00AM

Date Published: 6/1/18 4:00AM

Publication Location:

**Article Title:** Control of semiconductor emitter frequency by increasing polariton momenta

**Authors:** Yaniv Kurman, Nicholas Rivera, Thomas Christensen, Shai Tseskes, Meir Orenstein, Marin Soljačić, Jo

**Keywords:** emitter frequency, polariton momenta, light emission, light absorption

**Abstract:** Light emission and absorption is fundamentally a joint property of both an emitter and its optical environment. Nevertheless, because of the much smaller momenta of photons compared with electrons at similar energies, the optical environment typically modifies only the emission/absorption rates, leaving the emitter transition frequencies practically an intrinsic property. We show here that surface polaritons, exemplified by graphene plasmons, but also valid for other types of polariton, enable substantial and tunable control of the transition frequencies of a nearby quantum well, demonstrating a sharp break with the emitter-centric view. Central to this result is the large momenta of surface polaritons that can approach the momenta of electrons and impart a pronounced non-local behaviour to the quantum well. This work facilitates non-vertical optical transitions in solids and empowers ongoing efforts to access such transitions in indirect-bandgap materials, such as silicon, as well as

**Distribution Statement:** 3-Distribution authorized to U.S. Government Agencies and their contractors

Acknowledged Federal Support: Y

## RPPR Interim Progress Report as of 10-Mar-2020

**Publication Type:** Journal Article

Peer Reviewed: Y

**Publication Status:** 1-Published

**Journal:** Small

Publication Identifier Type: DOI

Publication Identifier: 10.1002/sml.201800072

Volume: 14

Issue: 22

First Page #: 1800072

Date Submitted: 8/16/18 12:00AM

Date Published: 5/1/18 4:00AM

Publication Location:

**Article Title:** Large Photothermal Effect in Sub-40 nm h-BN Nanostructures Patterned Via High-Resolution Ion Beam

**Authors:** Josué J. López, Antonio Ambrosio, Siyuan Dai, Chuong Huynh, David C. Bell, Xiao Lin, Nicholas Rivera

**Keywords:** 2D materials helium and neon ion beam fabrication hexagonal boron nitride (h-BN) near-field imaging photothermal effect

**Abstract:** The controlled nanoscale patterning of 2D materials is a promising approach for engineering the optoelectronic, thermal, and mechanical properties of these materials to achieve novel functionalities and devices. Herein, high-resolution patterning of hexagonal boron nitride (h-BN) is demonstrated via both helium and neon ion beams and an optimal dosage range for both ions that serve as a baseline for insulating 2D materials is identified. Through this nanofabrication approach, a grating with a 35 nm pitch, individual structure sizes down to 20 nm, and additional nanostructures created by patterning crystal step edges are demonstrated. Raman spectroscopy is used to study the defects induced by the ion beam patterning and is correlated to scanning probe microscopy. Photothermal and scanning near-field optical microscopy measure the resulting near-field absorption and scattering of the nanostructures. These measurements reveal a large photothermal expansion of nanostructured h-BN that is d

**Distribution Statement:** 3-Distribution authorized to U.S. Government Agencies and their contractors  
Acknowledged Federal Support: Y

**Publication Type:** Journal Article

Peer Reviewed: Y

**Publication Status:** 1-Published

**Journal:** Nature Physics

Publication Identifier Type: DOI

Publication Identifier: 10.1038/s41567-018-0138-4

Volume: 14

Issue: 8

First Page #: 816

Date Submitted: 8/16/18 12:00AM

Date Published: 5/1/18 4:00AM

Publication Location:

**Article Title:** Controlling Cherenkov angles with resonance transition radiation

**Authors:** Xiao Lin, Sajjan Easo, Yichen Shen, Hongsheng Chen, Baile Zhang, John D. Joannopoulos, Marin Solja

**Keywords:** photonic crystals

**Abstract:** Cherenkov radiation provides a valuable way to identify high-energy particles in a wide momentum range, through the relation between the particle velocity and the Cherenkov angle. However, since the Cherenkov angle depends only on the material's permittivity, the material unavoidably sets a fundamental limit to the momentum coverage and sensitivity of Cherenkov detectors. For example, ring-imaging Cherenkov detectors must employ materials transparent to the frequency of interest as well as possessing permittivities close to unity to identify particles in the multi-gigaelectronvolt range, and thus are often limited to large gas chambers. It would be extremely important, albeit challenging, to lift this fundamental limit and control Cherenkov angles at will. Here we propose a new mechanism that uses the constructive interference of resonance transition radiation from photonic crystals to generate both forward and backward effective Cherenkov radiation. This mechanism can control the radi

**Distribution Statement:** 3-Distribution authorized to U.S. Government Agencies and their contractors  
Acknowledged Federal Support: Y

## RPPR Interim Progress Report as of 10-Mar-2020

**Publication Type:** Journal Article

Peer Reviewed: Y

**Publication Status:** 1-Published

**Journal:** Physical Review B

Publication Identifier Type: DOI

Publication Identifier: 10.1103/PhysRevB.97.195435

Volume: 97

Issue: 19

First Page #:

Date Submitted: 8/16/18 12:00AM

Date Published: 5/1/18 4:00AM

Publication Location:

**Article Title:** Quantum plasmons with optical-range frequencies in doped few-layer graphene

**Authors:** Sharmila N. Shirodkar, Marios Mattheakis, Paul Cazeaux, Prineha Narang, Marin Soljačić, Efthimios Ka

**Keywords:** lithium intercalation, doped graphene, plasmons

**Abstract:** Although plasmon modes exist in doped graphene, the limited range of doping achieved by gating restricts the plasmon frequencies to a range that does not include the visible and infrared. Here we show, through the use of first-principles calculations, that the high levels of doping achieved by lithium intercalation in bilayer and trilayer graphene shift the plasmon frequencies into the visible range. To obtain physically meaningful results, we introduce a correction of the effect of plasmon interaction across the vacuum separating periodic images of the doped graphene layers, consisting of transparent boundary conditions in the direction perpendicular to the layers; this represents a significant improvement over the exact Coulomb cutoff technique employed in earlier works. The resulting plasmon modes are due to local field effects and the nonlocal response of the material to external electromagnetic fields, requiring a fully quantum mechanical treatment. We describe the features of these

**Distribution Statement:** 3-Distribution authorized to U.S. Government Agencies and their contractors

Acknowledged Federal Support: Y

**Publication Type:** Journal Article

Peer Reviewed: Y

**Publication Status:** 1-Published

**Journal:** Polymer

Publication Identifier Type: DOI

Publication Identifier: 10.1016/j.polymer.2018.05.034

Volume: 146

Issue:

First Page #: 222

Date Submitted: 8/16/18 12:00AM

Date Published: 6/1/18 4:00AM

Publication Location:

**Article Title:** Molecular influence in the glass/polymer interface design: The role of segmental dynamics

**Authors:** Alex J. Hsieh, David Veysset, Daniel F. Miranda, Steven E. Kooi, James Runt, Keith A. Nelson

**Keywords:** Dynamic impedance Shock Hugoniot Segmental dynamics Poly(urethane urea) Polyurea

Glass/polymer interface Dynamic stiffening High-rate deformation-induced glass transition Microballistics

**Abstract:** Recent observations of the high-velocity impact response in poly (urethane urea), PUU, elastomers has inspired a new inquiry on whether enabling molecular mechanisms could benefit dynamic impedance optimization at the interface of a glass/polymer bilayer, particularly at the moment of impulse interaction. In this work, we investigate the molecular influence on dynamic impedance using microballistic measurements on two bulk elastomers, a PUU and a polyurea, PU. Upon impact at strain rates  $\sim 10^8$ /s, PUU exhibits a moderate improvement in resistance against penetration than PU, that is more pronounced at higher speeds. The variation in dynamic stiffening corroborates well with the corresponding segmental dynamics data determined via broadband dielectric relaxation. Meanwhile, we calculate the shock impedance from the shock velocity data derived from the respective shock Hugoniot to discern the efficacy of dynamic impedance optimization between PUU and glass. New insight on molecular attributions

**Distribution Statement:** 3-Distribution authorized to U.S. Government Agencies and their contractors

Acknowledged Federal Support: Y

## RPPR Interim Progress Report as of 10-Mar-2020

**Publication Type:** Journal Article      Peer Reviewed: Y      **Publication Status:** 1-Published

**Journal:** Journal of Physics: Conference Series

Publication Identifier Type: DOI

Publication Identifier: 10.1088/1742-6596/1052/1/012041

Volume: 1052

Issue:

First Page #: 012041

Date Submitted: 8/17/18 12:00AM

Date Published: 7/1/18 4:00AM

Publication Location:

**Article Title:** Towards a portable mesoscale thermophotovoltaic generator

**Authors:** Walker R. Chan, Veronika Stelmakh, Sunny Karnani, Christopher M. Waits, Marin Soljacic, John D. Joannopoulos

**Keywords:** TPV, Thermophotovoltaics, photonics crystals, photovoltaics

**Abstract:** Thermophotovoltaics (TPV) is the conversion of fuel to electricity with heat and light as intermediaries, and is a promising source of high energy density power at the mesoscale. This work describes our transition from our bench-top experiments to a fully-integrated portable generator. Specifically, we redesigned the microcombustor for propane-air combustion from the previous propane-oxygen design. Next, we validated vacuum package of the microcombustor, necessary to preserve the photonic crystal, in a 50+ day experiment in which there was no degradation of vacuum level. Finally, we vacuum packaged a microcombustor with integrated photonic crystals in a housing with two infrared-transparent windows to transmit the thermal radiation to external PV cells. Although considerable challenges remain, this work demonstrates the feasibility of a mesoscale TPV system.

**Distribution Statement:** 3-Distribution authorized to U.S. Government Agencies and their contractors

Acknowledged Federal Support: Y

**Publication Type:** Journal Article      Peer Reviewed: Y      **Publication Status:** 1-Published

**Journal:** Journal of Physics: Conference Series

Publication Identifier Type: DOI

Publication Identifier: 10.1088/1742-6596/1052/1/012056

Volume: 1052

Issue:

First Page #: 012056

Date Submitted: 8/17/18 12:00AM

Date Published: 7/1/18 4:00AM

Publication Location:

**Article Title:** Improved Omnidirectional 2D Photonic Crystal Selective Emitter for Thermophotovoltaics

**Authors:** Rey Sakakibara, Veronika Stelmakh, Walker R. Chan, Michael Ghebrebrhan, John D. Joannopoulos, N. Aslamkhani

**Keywords:** Hafnia, Tantalum, Photonic crystals, thermophotovoltaic, FIB, focused ion beam, FIB

**Abstract:** Hafnia-filled, two dimensional (2D) tantalum (Ta) photonic crystals (PhCs) are promising emitters for high performance thermophotovoltaic (TPV) systems because they enable, for a wide range of incidence angles, efficient spectral tailoring of thermal radiation. However, fabricating these PhCs to the required tolerances has proven to be a challenging task. In this paper, we use both focused ion beam (FIB) imaging and simulations to investigate the effects of fabrication imperfections on the emittance of a fabricated hafnia-filled PhC and to identify critical geometric features that drive the overall PhC performance. We demonstrate that, more so than uniform cavity filling, the key to the best filled PhC performance is the precise cavity period and radius values and thickness of the top hafnia layer.

**Distribution Statement:** 3-Distribution authorized to U.S. Government Agencies and their contractors

Acknowledged Federal Support: Y

## RPPR Interim Progress Report as of 10-Mar-2020

**Publication Type:** Journal Article

Peer Reviewed: Y

**Publication Status:** 1-Published

**Journal:** Science Advances

Publication Identifier Type: DOI

Publication Identifier: 10.1126/sciadv.aau8528

Volume: 5

Issue: 1

First Page #:

Date Submitted: 8/15/19 12:00AM

Date Published: 1/1/19 5:00AM

Publication Location:

**Article Title:** Anti-fatigue-fracture hydrogels

**Authors:** Shaoting Lin, Xinyue Liu, Ji Liu, Hyunwoo Yuk, Hyun-Chae Loh, German A. Parada, Charles Settens, Jr

**Keywords:** hydrogel, fracture, fatigue

**Abstract:** The emerging applications of hydrogels in devices and machines require hydrogels to maintain robustness under cyclic mechanical loads. Whereas hydrogels have been made tough to resist fracture under a single cycle of mechanical load, these toughened gels still suffer from fatigue fracture under multiple cycles of loads. The reported fatigue threshold for synthetic hydrogels is on the order of 1 to 100 J/m<sup>2</sup>. We propose that designing anti-fatigue-fracture hydrogels requires making the fatigue crack encounter and fracture objects with energies per unit area much higher than that for fracturing a single layer of polymer chains. We demonstrate that the controlled introduction of crystallinity in hydrogels can substantially enhance their anti-fatigue-fracture properties. The fatigue threshold of polyvinyl alcohol (PVA) with a crystallinity of 18.9 weight % in the swollen state can exceed 1000 J/m<sup>2</sup>.

**Distribution Statement:** 3-Distribution authorized to U.S. Government Agencies and their contractors

Acknowledged Federal Support: Y

**Publication Type:** Journal Article

Peer Reviewed: Y

**Publication Status:** 1-Published

**Journal:** Proceedings of the National Academy of Sciences

Publication Identifier Type: DOI

Publication Identifier: 10.1073/pnas.1903019116

Volume: 116

Issue: 21

First Page #: 10244

Date Submitted: 8/16/19 12:00AM

Date Published: 5/1/19 4:00AM

Publication Location:

**Article Title:** Muscle-like fatigue-resistant hydrogels by mechanical training

**Authors:** Shaoting Lin, Ji Liu, Xinyue Liu, Xuanhe Zhao

**Keywords:** polyvinyl alcohol | anti-fatigue-fracture | freeze-thaw | prestretch | 3D printing

**Abstract:** Skeletal muscles possess the combinational properties of high fatigue resistance (1,000 J/m<sup>2</sup>), high strength (1 MPa), low Young's modulus (100 kPa), and high water content (70 to 80 wt %), which have not been achieved in synthetic hydrogels. The muscle-like properties are highly desirable for hydrogels' nascent applications in load-bearing artificial tissues and soft devices. Here, we propose a strategy of mechanical training to achieve the aligned nanofibrillar architectures of skeletal muscles in synthetic hydrogels, resulting in the combinational muscle-like properties. These properties are obtained through the training-induced alignment of nanofibrils, without additional chemical modifications or additives. In situ confocal microscopy of the hydrogels' fracturing processes reveals that the fatigue resistance results from the crack pinning by the aligned nanofibrils, which require much higher energy to fracture than the corresponding amorphous polymer chains. This strategy i

**Distribution Statement:** 3-Distribution authorized to U.S. Government Agencies and their contractors

Acknowledged Federal Support: Y

## RPPR Interim Progress Report as of 10-Mar-2020

**Publication Type:** Journal Article      Peer Reviewed: Y      **Publication Status:** 1-Published

**Journal:** Journal of the Mechanics and Physics of Solids

Publication Identifier Type: DOI

Publication Identifier: 10.1016/j.jmps.2019.06.020

Volume: 131

Issue:

First Page #: 252

Date Submitted: 8/15/19 12:00AM

Date Published: 10/1/19 8:00AM

Publication Location:

**Article Title:** A path-following simulation-based study of elastic instabilities in nearly-incompressible confined cylinders under tension

**Authors:** Bianca Giovanardi, Adam A. Sliwiak, Anwar Koshakji, Shaoting Lin, Xuanhe Zhao, Raúl Radovitzky

**Keywords:** Elastic instabilities; Soft materials; Arc-length nonlinear solver; Fringe and fingering in solids; Large-scale simulation

**Abstract:** Recent experiments on hydrogels subjected to large elongations have shown elastic instabilities resulting in the formation of geometrically intricate fringe and fingering deformation patterns. In this paper, we present a robust numerical framework addressing the challenges that emerge in the simulation of this complex material response from the onset of instability to the post-bifurcation behavior. We observe that the numerical difficulties stem from the non-convexity of the strain energy density in the near-incompressible, large-deformation regime, which is responsible for the coexistence of multiple equilibrium paths with vastly-different, sinuous deformation patterns immediately after bifurcation. We show that these numerical challenges can be overcome by using sufficiently-high order of interpolation in the finite element approximation, an arc-length-based nonlinear solution procedure that follows the entire equilibrium path of the system, and an implementation enabling

**Distribution Statement:** 3-Distribution authorized to U.S. Government Agencies and their contractors

Acknowledged Federal Support: Y

**Publication Type:** Journal Article

Peer Reviewed: Y

**Publication Status:** 1-Published

**Journal:** Nature Materials

Publication Identifier Type: DOI

Publication Identifier: 10.1038/s41563-018-0258-3

Volume: 18

Issue: 2

First Page #: 129

Date Submitted: 8/15/19 12:00AM

Date Published: 1/1/19 5:00AM

Publication Location:

**Article Title:** Addressing the isomer cataloguing problem for nanopores in two-dimensional materials

**Authors:** Ananth Govind Rajan, Kevin S. Silmore, Jacob Swett, Alex W. Robertson, Jamie H. Warner, Daniel Blar

**Keywords:** isomer cataloguing problem, nanopore, graphene, hBN

**Abstract:** The presence of extended defects or nanopores in two-dimensional (2D) materials can change the electronic, magnetic and barrier membrane properties of the materials. However, the large number of possible lattice isomers of nanopores makes their quantitative study a seemingly intractable problem, confounding the interpretation of experimental and simulated data. Here we formulate a solution to this isomer cataloguing problem (ICP), combining electronic-structure calculations, kinetic Monte Carlo simulations, and chemical graph theory, to generate a catalogue of unique, most-probable isomers of 2D lattice nanopores. The results demonstrate remarkable agreement with precise nanopore shapes observed experimentally in graphene and show that the thermodynamic stability of a nanopore is distinct from its kinetic stability. Triangular nanopores prevalent in hexagonal boron nitride are also predicted, extending this approach to other 2D lattices. The proposed method should accelerate the...

**Distribution Statement:** 3-Distribution authorized to U.S. Government Agencies and their contractors

Acknowledged Federal Support: Y



## RPPR Interim Progress Report as of 10-Mar-2020

**Publication Type:** Journal Article      Peer Reviewed: Y      **Publication Status:** 1-Published  
**Journal:** Nanoscale  
**Publication Identifier Type:** DOI      **Publication Identifier:** 10.1039/C8NR10366F  
**Volume:** 11      **Issue:** 6      **First Page #:** 2925  
**Date Submitted:** 8/16/19 12:00AM      **Date Published:**  
**Publication Location:**

**Article Title:** Fundamental scaling laws for the direct-write chemical vapor deposition of nanoscale features: modeling mass transport around a translating nanonozzle

**Authors:** Lee W. Drahushuk, Ananth Govind Rajan, Michael S. Strano

**Keywords:** atomically precise manufacturing (APM), CVD, Buckingham ? analysis

**Abstract:** The nanometer placement of nanomaterials, such as nanoribbons and nanotubes, at a specific pitch and orientation on a surface, remains an unsolved fundamental problem in nanotechnology. In this work, we introduce and analyze the concept of a direct-write chemical vapor deposition (CVD) system that enables the in-place synthesis of such structures with control over orientation and characteristic features. A nanometer scale pore or conduit, called the nanonozzle, delivers precursor gases for CVD locally on a substrate, with spatial translation of either the nozzle or the substrate to enable a novel direct write (DW) tool. We analyze the nozzle under conditions where it delivers reactants to a substrate while translating at a constant velocity over the surface at a fixed reaction temperature. We formulate and solve a multi-phase three-dimensional reaction and diffusion model of the direct-write operation, and evaluate specific analytically-solvable limits to determine the allowable...

**Distribution Statement:** 3-Distribution authorized to U.S. Government Agencies and their contractors  
**Acknowledged Federal Support:** Y

**Publication Type:** Journal Article      Peer Reviewed: Y      **Publication Status:** 1-Published  
**Journal:** The Journal of Physical Chemistry Letters  
**Publication Identifier Type:** DOI      **Publication Identifier:** 10.1021/acs.jpcllett.7b03443  
**Volume:** 9      **Issue:** 7      **First Page #:** 1584  
**Date Submitted:** 8/15/19 12:00AM      **Date Published:** 3/1/18 5:00AM  
**Publication Location:**

**Article Title:** Ab Initio Molecular Dynamics and Lattice Dynamics-Based Force Field for Modeling Hexagonal Boron Nitride in Mechanical and Interfacial Applications

**Authors:** Ananth Govind Rajan, Michael S. Strano, Daniel Blankschtein

**Keywords:** hBN, density-functional-theory-based ab initio molecular dynamics (MD) simulation; lattice dynamics calculations; classical force field (FF); modeling

**Abstract:** Hexagonal boron nitride (hBN) is an up-and-coming two-dimensional material, with applications in electronic devices, tribology, and separation membranes. Herein, we utilize density-functional-theory-based ab initio molecular dynamics (MD) simulations and lattice dynamics calculations to develop a classical force field (FF) for modeling hBN. The FF predicts the crystal structure, elastic constants, and phonon dispersion relation of hBN with good accuracy and exhibits remarkable agreement with the interlayer binding energy predicted by random phase approximation calculations. We demonstrate the importance of including Coulombic interactions but excluding 1–4 intrasheet interactions to obtain the correct phonon dispersion relation. We find that improper dihedrals do not modify the bulk mechanical properties and the extent of thermal vibrations in hBN, although they impact its flexural rigidity. Combining the FF with the accurate TIP4P/Ice water model yields excellent agreement with intera

**Distribution Statement:** 3-Distribution authorized to U.S. Government Agencies and their contractors  
**Acknowledged Federal Support:** Y

## RPPR Interim Progress Report as of 10-Mar-2020

**Publication Type:** Journal Article

Peer Reviewed: Y

**Publication Status:** 1-Published

**Journal:** Nature Materials

Publication Identifier Type: DOI

Publication Identifier: 10.1038/s41563-018-0197-z

Volume: 17 Issue: 11

First Page #: 1005

Date Submitted: 8/15/19 12:00AM

Date Published: 10/1/18 4:00AM

Publication Location:

**Article Title:** Autoperforation of 2D materials for generating two-terminal memristive Janus particles

**Authors:** Pingwei Liu, Albert Tianxiang Liu, Daichi Kozawa, Juyao Dong, Jing Fan Yang, Volodymyr B. Koman, M

**Keywords:** autoperforation, Janus, CVD

**Abstract:** Graphene and other two-dimensional materials possess desirable mechanical, electrical and chemical properties for incorporation into or onto colloidal particles, potentially granting them unique electronic functions. However, this application has not yet been realized, because conventional top-down lithography scales poorly for producing colloidal solutions. Here, we develop an 'autoperforation' technique that provides a means of spontaneous assembly for surfaces composed of two-dimensional molecular scaffolds. Chemical vapour deposited two-dimensional sheets can autoperforate into circular envelopes when sandwiching a microprinted polymer composite disk of nanoparticle ink, allowing liftoff into solution and simultaneous assembly. The resulting colloidal microparticles have two independently addressable, external Janus faces that we show can function as an intraparticle array of vertically aligned, two-terminal electronic devices. Such particles demonstrate remarkable chemical and

**Distribution Statement:** 3-Distribution authorized to U.S. Government Agencies and their contractors

Acknowledged Federal Support: Y

**Publication Type:** Journal Article

Peer Reviewed: Y

**Publication Status:** 1-Published

**Journal:** Small

Publication Identifier Type: DOI

Publication Identifier: 10.1002/smll.201703727

Volume: 14 Issue: 13

First Page #: 1703727

Date Submitted: 8/15/19 12:00AM

Date Published: 3/1/18 5:00AM

Publication Location:

**Article Title:** Determining the Optimized Interlayer Separation Distance in Vertical Stacked 2D WS<sub>2</sub>:hBN:MoS<sub>2</sub> Heterostructures for Exciton Energy Transfer

**Authors:** Wenshuo Xu, Daichi Kozawa, Yu Liu, Yuewen Sheng, Ke Wei, Volodymyr B. Koman, Shanshan Wang,

**Keywords:** 2D heterostructures energy transfer hexagonal boron nitride photoluminescence transition metal dichalcogenides

**Abstract:** The 2D semiconductor monolayer transition metal dichalcogenides, WS<sub>2</sub> and MoS<sub>2</sub>, are grown by chemical vapor deposition (CVD) and assembled by sequential transfer into vertical layered heterostructures (VLHs). Insulating hBN, also produced by CVD, is utilized to control the separation between WS<sub>2</sub> and MoS<sub>2</sub> by adjusting the layer number, leading to fine-scale tuning of the interlayer interactions within the VLHs. The interlayer interactions are studied by photoluminescence (PL) spectroscopy and are demonstrated to be highly sensitive to the input excitation power. For thin hBN separators (one to two layers), the total PL emission switches from quenching to enhancement by increasing the laser power. Femtosecond broadband transient absorption measurements demonstrate that the increase in PL quantum yield results from Förster energy transfer from MoS<sub>2</sub> to WS<sub>2</sub>. The PL signal is further enhanced at cryogenic temperatures due to the suppressed nonradiative decay channels. It is shown that  $(4 \pm 1)$

**Distribution Statement:** 3-Distribution authorized to U.S. Government Agencies and their contractors

Acknowledged Federal Support: N

## RPPR Interim Progress Report as of 10-Mar-2020

**Publication Type:** Journal Article      Peer Reviewed: Y      **Publication Status:** 1-Published

**Journal:** Polymer

Publication Identifier Type: DOI

Publication Identifier: 10.1016/j.polymer.2019.02.038

Volume: 168

Issue:

First Page #: 218

Date Submitted: 8/16/19 12:00AM

Date Published: 4/1/19 4:00AM

Publication Location:

**Article Title:** Unraveling the high strain-rate dynamic stiffening in select model polyurethanes ? the role of intermolecular hydrogen bonding

**Authors:** You-Chi Mason Wu, Weiguo Hu, Yuchen Sun, David Veyssset, Steven E. Kooi, Keith A. Nelson, Timothy

**Keywords:** Polyurethane elastomers; High strain-rate deformation; Dynamic stiffening; Laser-induced micro-particle impact test; Intermolecular hydrogen bonding; Attenuated total reflectance–Fourier transform infrared (ATR–FTIR) spectroscopy; Solid-state nuclear magnetic resonance (ssNMR) spectroscopy; Dynamics at the molecular level; Coefficient of restitution

**Abstract:** This study elucidates the influence of molecular attributes on the observed dynamic stiffening in select two-component polyurethanes upon high strain-rate impact. Unlike typical segmented elastomers, polyurethanes consisting of poly(tetramethylene oxide), PTMO, and a diisocyanate, but without a chain extender, are investigated. The hexamethylenediisocyanate (HDI)-based polyurethane, HDI?PU, exhibits crystallinity and a much higher ambient storage modulus, as determined by dynamic mechanical analysis at 1 Hz, than that of 4,4'-methylenebis(phenyldiisocyanate) (MDI)-based polyurethane, MDI?PU. In contrast, MDI?PU exhibits a higher glass transition temperature than that of HDI?PU, and a greater dynamic stiffening against silica micro-particle impacts at strain rates between 10<sup>7</sup> and 10<sup>8</sup> s<sup>-1</sup>. The variation in dynamic stiffening corroborates well the observed dynamics at the molecular level, as determined via solid-state nuclear magnetic resonance (ssNMR) spectroscopy. The presence of a slower-dynamic

**Distribution Statement:** 3-Distribution authorized to U.S. Government Agencies and their contractors

Acknowledged Federal Support: Y

**Publication Type:** Journal Article      Peer Reviewed: Y      **Publication Status:** 1-Published

**Journal:** Journal of the American Chemical Society

Publication Identifier Type: DOI

Publication Identifier: 10.1021/jacs.9b06009

Volume: 141

Issue: 32

First Page #: 12498

Date Submitted: 8/16/19 12:00AM

Date Published: 7/1/19 4:00AM

Publication Location:

**Article Title:** Living Polymerization of 2-Ethylthio-2-oxazoline and Postpolymerization Diversification

**Authors:** You-Chi Mason Wu, Timothy M. Swager

**Keywords:** polymers, monomers, functionalization, block copolymers

**Abstract:** The postpolymerization modification of polymers produced by living polymerization is an attractive method to create precision nanomaterials. We describe the living cationic ring-opening polymerization of a 2-alkylthio-2-oxazoline to furnish a polythiocarbamate. The polythiocarbamate is activated toward substitution by N- and S-nucleophiles via oxidation of the S to an SO<sub>2</sub>. Mild substitution conditions provide broad functional group tolerance, constituting a versatile postpolymerization modification platform with access to a diversity of polyureas and polythiocarbamates. We further demonstrate the utility of this strategy by synthesizing and functionalizing block copolymers.

**Distribution Statement:** 3-Distribution authorized to U.S. Government Agencies and their contractors

Acknowledged Federal Support: Y

## RPPR Interim Progress Report as of 10-Mar-2020

**Publication Type:** Journal Article      Peer Reviewed: Y      **Publication Status:** 1-Published

**Journal:** Acta Materialia

Publication Identifier Type: DOI

Publication Identifier: 10.1016/j.actamat.2019.07.028

Volume: 177

Issue:

First Page #: 230

Date Submitted: 8/16/19 12:00AM

Date Published: 9/1/19 4:00AM

Publication Location:

**Article Title:** Reduced cracking in polycrystalline ZrO<sub>2</sub>-CeO<sub>2</sub> shape-memory ceramics by meeting the cofactor conditions

**Authors:** Edward L. Pang, Caitlin A. McCandler, Christopher A. Schuh

**Keywords:** Shape memory; Ceramics; Zirconia; Cracking; Compatibility

**Abstract:** Cracking is generally regarded as an unavoidable consequence of martensitic transformation in polycrystalline ZrO<sub>2</sub>-based ceramics. This shortcoming has limited ZrO<sub>2</sub>-based shape-memory ceramics (SMCs) to micron-sized single- or oligo-crystals to reduce bulk transformation stresses. In this paper we explore an alternate approach to reduce transformation-induced cracking by manipulating the crystallographic phase compatibility in polycrystalline ZrO<sub>2</sub>-CeO<sub>2</sub> ceramics. For a range of compositions 12.5e15 mol% CeO<sub>2</sub>, we present lattice parameter measurements for the tetragonal and monoclinic phases from in situ X-ray diffraction, direct observation of lattice correspondences by electron backscatter diffraction, and calculations of interface and bulk compatibility. We identify ZrO<sub>2</sub>-13.5 mol% CeO<sub>2</sub> as having preferred interface compatibility in that it closely meets the crystallographic cofactor conditions. This composition resists cracking through 10 thermal cycles, whereas other compositions all...

**Distribution Statement:** 3-Distribution authorized to U.S. Government Agencies and their contractors

Acknowledged Federal Support: Y

**Publication Type:** Journal Article      Peer Reviewed: Y      **Publication Status:** 1-Published

**Journal:** ACS Biomaterials Science & Engineering

Publication Identifier Type: DOI

Publication Identifier: 10.1021/acsbiomaterials.9b00054

Volume: 5

Issue: 5

First Page #: 2563

Date Submitted: 8/16/19 12:00AM

Date Published: 5/1/19 4:00AM

Publication Location:

**Article Title:** Systemically Administered Hemostatic Nanoparticles for Identification and Treatment of Internal Bleeding

**Authors:** Manos Gkikas, Thomas Peponis, Tomaz Mesar, Celestine Hong, Reginald K. Avery, Emmanuel Rousseau

**Keywords:** hemostasis, imaging, theranostic, bleeding, internal injuries, injectable, nanoparticle

**Abstract:** Internal bleeding is an injury that can be difficult to localize and effectively treat without invasive surgeries. Injectable polymeric nanoparticles have been developed that can reduce clotting times and blood loss, but they have yet to incorporate sufficient diagnostic capabilities to assist in identifying bleeding sources. Herein, polymeric nanoparticles were developed to simultaneously treat internal bleeding while incorporating tracers for visualization of the nanoparticles by standard clinical imaging modalities. Addition of 1,1'-dioctadecyl-3,3',3'-tetramethylindodicarbocyanine perchlorate (DiD; a fluorescent dye), biotin functionality, and gold nanoparticles to hemostatic polymeric nanoparticles resulted in nanoparticles amenable to imaging with near-infrared (NIR) imaging, immunohistochemistry, and X-ray computed tomography (CT), respectively. Following a lethal liver resection injury, visualization of accumulated nanoparticles by multiple imaging methods was achieved in...

**Distribution Statement:** 3-Distribution authorized to U.S. Government Agencies and their contractors

Acknowledged Federal Support: Y

## RPPR Interim Progress Report as of 10-Mar-2020

**Publication Type:** Journal Article      Peer Reviewed: Y      **Publication Status:** 1-Published

**Journal:** Science Advances

Publication Identifier Type: DOI

Publication Identifier: 10.1126/sciadv.aav2252

Volume: 5

Issue: 5

First Page #:

Date Submitted: 8/16/19 12:00AM

Date Published: 5/1/19 4:00AM

Publication Location:

**Article Title:** Engineering single-atom dynamics with electron irradiation

**Authors:** Cong Su, Mukesh Tripathi, Qing-Bo Yan, Zegao Wang, Zihan Zhang, Christoph Hofer, Haozhe Wang, L

**Keywords:** single-step dynamics of graphene dopants, electron irradiation

**Abstract:** Atomic engineering is envisioned to involve selectively inducing the desired dynamics of single atoms and combining these steps for larger-scale assemblies. Here, we focus on the first part by surveying the single-step dynamics of graphene dopants, primarily phosphorus, caused by electron irradiation both in experiment and simulation, and develop a theory for describing the probabilities of competing configurational outcomes depending on the postcollision momentum vector of the primary knock-on atom. The predicted branching ratio of configurational transformations agrees well with our atomically resolved experiments. This suggests a way for biasing the dynamics toward desired outcomes, paving the road for designing and further upscaling atomic engineering using electron irradiation.

**Distribution Statement:** 3-Distribution authorized to U.S. Government Agencies and their contractors

Acknowledged Federal Support: Y

**Publication Type:** Journal Article      Peer Reviewed: Y      **Publication Status:** 1-Published

**Journal:** Science Advances

Publication Identifier Type: DOI

Publication Identifier: 10.1126/sciadv.aav1493

Volume: 5

Issue: 6

First Page #:

Date Submitted: 8/15/19 12:00AM

Date Published: 6/1/19 4:00AM

Publication Location:

**Article Title:** Asymmetric hot-carrier thermalization and broadband photoresponse in graphene-2D semiconductor lateral heterojunctions

**Authors:** Yuxuan Lin, Qiong Ma, Pin-Chun Shen, Batyr Ilyas, Yaqing Bie, Albert Liao, Emre Ergeçen, Bingnan Ha

**Keywords:** Dirac electron transport, light-matter interaction, optoelectronic devices

**Abstract:** The massless Dirac electron transport in graphene has led to a variety of unique light-matter interaction phenomena, which promise many novel optoelectronic applications. Most of the effects are only accessible by breaking the spatial symmetry, through introducing edges, p-n junctions, or heterogeneous interfaces. The recent development of direct synthesis of lateral heterostructures offers new opportunities to achieve the desired asymmetry. As a proof of concept, we study the photothermoelectric effect in an asymmetric lateral heterojunction between the Dirac semimetallic monolayer graphene and the parabolic semiconducting monolayer MoS<sub>2</sub>. Very different hot-carrier cooling mechanisms on the graphene and the MoS<sub>2</sub> sides allow us to resolve the asymmetric thermalization pathways of photoinduced hot carriers spatially with electrostatic gate tunability. We also demonstrate the potential of graphene-2D semiconductor lateral heterojunctions as broadband infrared photodetectors. The proposed

**Distribution Statement:** 3-Distribution authorized to U.S. Government Agencies and their contractors

Acknowledged Federal Support: Y

## RPPR Interim Progress Report as of 10-Mar-2020

**Publication Type:** Journal Article      Peer Reviewed: Y      **Publication Status:** 1-Published

**Journal:** Proceedings of the National Academy of Sciences

Publication Identifier Type: DOI

Publication Identifier: 10.1073/pnas.1816197116

Volume: 116

Issue: 9

First Page #: 3437

Date Submitted: 8/15/19 12:00AM

Date Published: 2/1/19 5:00AM

Publication Location:

**Article Title:** Additive manufacturing of patterned 2D semiconductor through recyclable masked growth

**Authors:** Yunfan Guo, Pin-Chun Shen, Cong Su, Ang-Yu Lu, Marek Hempel, Yimo Han, Qingqing Ji, Yuxuan Lin,

**Keywords:** 2D semiconductor | monolayer MoS<sub>2</sub> | patterned growth | growth mechanism | recyclable masked growth

**Abstract:** The 2D van der Waals crystals have shown great promise as potential future electronic materials due to their atomically thin and smooth nature, highly tailorable electronic structure, and mass production compatibility through chemical synthesis. Electronic devices, such as field effect transistors (FETs), from these materials require patterning and fabrication into desired structures. Specifically, the scale up and future development of "2D"-based electronics will inevitably require large numbers of fabrication steps in the patterning of 2D semiconductors, such as transition metal dichalcogenides (TMDs). This is currently carried out via multiple steps of lithography, etching, and transfer. As 2D devices become more complex (e.g., numerous 2D materials, more layers, specific shapes, etc.), the patterning steps can become economically costly and time consuming. Here, we developed a method to directly synthesize a 2D semiconductor, monolayer molybdenum disulfide (MoS<sub>2</sub>), in air.

**Distribution Statement:** 3-Distribution authorized to U.S. Government Agencies and their contractors

Acknowledged Federal Support: Y

**Publication Type:** Journal Article

Peer Reviewed: Y

**Publication Status:** 1-Published

**Journal:** Advanced Functional Materials

Publication Identifier Type: DOI

Publication Identifier: 10.1002/adfm.201902538

Volume: 29

Issue: 28

First Page #: 1902538

Date Submitted: 8/16/19 12:00AM

Date Published: 5/1/19 4:00AM

Publication Location:

**Article Title:** Photoelectric Synaptic Plasticity Realized by 2D Perovskite

**Authors:** Yilin Sun, Liu Qian, Dan Xie, Yuxuan Lin, Mengxing Sun, Weiwei Li, Liming Ding, Tianling Ren, Tomás F

**Keywords:** perovskite, neuromorphic computing, long-term plasticity (LTP), short-term plasticity (STP)

**Abstract:** Recently, several light-stimulated artificial synaptic devices have been proposed to mimic photonic synaptic plasticity for neuromorphic computing. Here, the photoelectric synaptic plasticity based on 2D lead-free perovskite ((PEA)<sub>2</sub>SnI<sub>4</sub>) is demonstrated. The devices show a photocurrent activation in response to a light stimulus in a neuron-like way and exhibit several essential synaptic functions such as short-term plasticity (STP) and long-term plasticity (LTP) as well as their transmission based on spike frequency control. The strength of synaptic connectivity can be effectively modulated by the duration, irradiance, and wavelength of light spikes. The ternary structure of (PEA)<sub>2</sub>SnI<sub>4</sub> causes it to possess varied photoelectric properties by composition control, which enhances the complexity and freedoms required by neuromorphic computing. The physical mechanisms of the memory effect are attributed to two distinct lifetimes of photogenerated carrier trapping/detrapping processes...

**Distribution Statement:** 3-Distribution authorized to U.S. Government Agencies and their contractors

Acknowledged Federal Support: Y

## RPPR Interim Progress Report as of 10-Mar-2020

**Publication Type:** Journal Article

Peer Reviewed: Y

**Publication Status:** 1-Published

**Journal:** Nature Nanotechnology

Publication Identifier Type: DOI

Publication Identifier: 10.1038/s41565-018-0323-8

Volume: 14

Issue: 2

First Page #: 145

Date Submitted: 8/16/19 12:00AM

Date Published: 12/1/18 5:00AM

Publication Location:

**Article Title:** Giant intrinsic photoresponse in pristine graphene

**Authors:** Qiong Ma, Chun Hung Lui, Justin C. W. Song, Yuxuan Lin, Jian Feng Kong, Yuan Cao, Thao H. Dinh, N

**Keywords:** Dirac point, Fermi Level, electron scattering, fermions

**Abstract:** When the Fermi level is aligned with the Dirac point of gra- phene, reduced charge screening greatly enhances electron– electron scattering<sup>1–5</sup>. In an optically excited system, the kinematics of electron–electron scattering in Dirac fermions is predicted to give rise to novel optoelectronic phenomena<sup>6–11</sup>. In this paper, we report on the observation of an intrinsic pho- tocurrent in graphene, which occurs in a different parameter regime from all the previously observed photothermoelectric or photovoltaic photocurrents in graphene<sup>12–20</sup>: the photo- current emerges exclusively at the charge neutrality point, requiring no finite doping. Unlike other photocurrent types that are enhanced near p–n or contact junctions, the photo- current observed in our work arises near the edges/corners. By systematic data analyses, we show that the phenomenon stems from the unique electron– electron scattering kinemat- ics in charge-neutral graphene. Our results not only high- light the intriguing electron...

**Distribution Statement:** 3-Distribution authorized to U.S. Government Agencies and their contractors

Acknowledged Federal Support: Y

**Publication Type:** Journal Article

Peer Reviewed: Y

**Publication Status:** 1-Published

**Journal:** Nature

Publication Identifier Type: DOI

Publication Identifier: 10.1038/s41586-019-0892-1

Volume: 566

Issue: 7744

First Page #: 368

Date Submitted: 8/16/19 12:00AM

Date Published: 1/1/19 5:00AM

Publication Location:

**Article Title:** Two-dimensional MoS<sub>2</sub>-enabled flexible rectenna for Wi-Fi-band wireless energy harvesting

**Authors:** Xu Zhang, Jesús Grajal, Jose Luis Vazquez-Roy, Ujwal Radhakrishna, Xiaoxue Wang, Winston Chern, I

**Keywords:** two-dimensional materials, rectenna, Wi-Fi harvesting

**Abstract:** The mechanical and electronic properties of two-dimensional materials make them promising for use in flexible electronics<sup>1–3</sup>. Their atomic thickness and large-scale synthesis capability could enable the development of ‘smart skin’<sup>1,3–5</sup>, which could transform ordinary objects into an intelligent distributed sensor network<sup>6</sup>. However, although many important components of such a distributed electronic system have already been demonstrated (for example, transistors, sensors and memory devices based on two-dimensional materials<sup>1, 2,4,7</sup>), an efficient, flexible and always-on energy-harvesting solution, which is indispensable for self-powered systems, is still missing. Electromagnetic radiation from Wi-Fi systems operating at 2.4 and 5.9 gigahertz<sup>8</sup> is becoming increasingly ubiquitous and would be ideal to harvest for powering future distributed electronics. However, the high frequencies used for Wi-Fi communications have remained elusive to radiofrequency harvesters (that is, rectennas) made..

**Distribution Statement:** 3-Distribution authorized to U.S. Government Agencies and their contractors

Acknowledged Federal Support: Y

## RPPR Interim Progress Report as of 10-Mar-2020

**Publication Type:** Journal Article      Peer Reviewed: Y      **Publication Status:** 1-Published

**Journal:** Laser & Photonics Reviews

Publication Identifier Type: DOI

Publication Identifier: 10.1002/lpor.201900075

Volume: 13

Issue: 7

First Page #: 1900075

Date Submitted: 8/16/19 12:00AM

Date Published: 5/1/19 8:00AM

Publication Location:

**Article Title:** Distributed Quantum Fiber Magnetometry

**Authors:** Shai Maayani, Christopher Foy, Dirk Englund, Yoel Fink

**Keywords:** distributed optical fiber sensors, fiber sensors, multifunctional fibers, nitrogen vacancies, solid-state quantum sensing

**Abstract:** Nitrogen-vacancy (NV) quantum magnetometers offer exceptional sensitivity and long-term stability. However, their use to date in distributed sensing applications, including remote detection of ferrous metals, geophysics, and biosensing, is limited due to the need to combine optical, microwave (MW), and magnetic excitations into a single system. Existing approaches have yielded localized devices but not distributed capabilities. In this study, a continuous system-in-a-fiber architecture is reported, which enables distributed magnetic sensing over extended lengths. Key to this realization is a thermally drawn fiber that has hundreds of embedded photodiodes connected in parallel and a hollow optical waveguide that contains a fluid with NV diamonds. This fiber is placed in a larger coaxial cable to deliver the required MW excitation. This distributed quantum sensor is realized in a water-immersible 90-m-long cable with 102 detection sites. A sensitivity of  $63 \pm 5$  nT Hz<sup>1/2</sup> per site....

**Distribution Statement:** 3-Distribution authorized to U.S. Government Agencies and their contractors

Acknowledged Federal Support: Y

**Publication Type:** Journal Article      Peer Reviewed: Y      **Publication Status:** 1-Published

**Journal:** Physical Review Applied

Publication Identifier Type: DOI

Publication Identifier: 10.1103/PhysRevApplied.11.034033

Volume: 11

Issue: 3

First Page #:

Date Submitted: 8/16/19 12:00AM

Date Published: 3/1/19 5:00AM

Publication Location:

**Article Title:** From Solar Cells to Ocean Buoys: Wide-Bandwidth Limits to Absorption by Metaparticle Arrays

**Authors:** Mohammed Benzaouia, Grgur Tokic, Owen D. Miller, Dick K.P. Yue, Steven G. Johnson

**Keywords:** metaparticles, Yablonovitch result, wide-bandwidth upper bound, absorption enhancement

**Abstract:** In this paper, we develop an approximate wide-bandwidth upper bound to the absorption enhancement in arrays of metaparticles, applicable to general wave-scattering problems and motivated here by ocean-buoy energy extraction. We show that general limits, including the well-known Yablonovitch result in solar cells, arise from reciprocity conditions. The use of reciprocity in the stochastic regime leads us to a corrected diffusion model from which we derive our main result: an analytical prediction of optimal array absorption that closely matches exact simulations for both random and optimized arrays under angle and frequency averaging. This result also enables us to propose and quantify approaches to increase performance through careful particle design and/or using external reflectors. We show, in particular, that the use of membranes on the water's surface allows substantial enhancement.

**Distribution Statement:** 3-Distribution authorized to U.S. Government Agencies and their contractors

Acknowledged Federal Support: Y



## RPPR Interim Progress Report as of 10-Mar-2020

**Publication Type:** Journal Article      Peer Reviewed: Y      **Publication Status:** 1-Published  
**Journal:** Physical Review X  
**Publication Identifier Type:** DOI      **Publication Identifier:** 10.1103/PhysRevX.9.011043  
**Volume:** 9      **Issue:** 1      **First Page #:**  
**Date Submitted:** 8/16/19 12:00AM      **Date Published:** 3/1/19 5:00AM  
**Publication Location:**

**Article Title:** Fundamental Limits to Near-Field Optical Response over Any Bandwidth

**Authors:** Hyunki Shim, Lingling Fan, Steven G. Johnson, Owen D. Miller

**Keywords:** light-matter interactions, optical near field, greater-than-blackbody heat transfer

**Abstract:** We develop an analytical framework to derive upper bounds to light-matter interactions in the optical near field, where applications ranging from spontaneous-emission amplification to greater-than-blackbody heat transfer show transformative potential. Our framework connects the classic complex-analytic properties of causal fields with newly developed energy-conservation principles, resulting in a new class of power-bandwidth limits. These limits demonstrate the possibility of orders-of-magnitude enhancement in near-field optical response with the right combination of material and geometry. At specific frequency and bandwidth combinations, the bounds can be closely approached by canonical plasmonic geometries, with the opportunity for new designs to emerge away from those frequency ranges. Embedded in the bounds is a material “figure of merit,” which determines the maximum response of any material (metal, dielectric, bulk, 2D, etc.), for any frequency and bandwidth. Our bounds on local

**Distribution Statement:** 3-Distribution authorized to U.S. Government Agencies and their contractors  
**Acknowledged Federal Support:** Y

**Publication Type:** Journal Article      Peer Reviewed: Y      **Publication Status:** 1-Published  
**Journal:** ACS Photonics  
**Publication Identifier Type:** DOI      **Publication Identifier:** 10.1021/acsp Photonics.8b01263  
**Volume:** 6      **Issue:** 2      **First Page #:** 395  
**Date Submitted:** 8/16/19 12:00AM      **Date Published:** 12/1/18 5:00AM  
**Publication Location:**

**Article Title:** Optimal Nanoparticle Forces, Torques, and Illumination Fields

**Authors:** Yuxiang Liu, Lingling Fan, Yoonkyung E. Lee, Nicholas X. Fang, Steven G. Johnson, Owen D. Miller

**Keywords:** optomechanics, optical force, optical torque, illumination fields, fundamental limits

**Abstract:** A universal property of resonant subwavelength scatterers is that their optical cross-sections are proportional to a square wavelength,  $\lambda^2$ , regardless of whether they are plasmonic nanoparticles, two-level quantum systems, or RF antennas. The maximum cross-section is an intrinsic property. **KEYWORDS:** optomechanics, optical force, optical torque, illumination fields, fundamental limits of the incident field: plane waves, with infinite power, can be decomposed into 2 multipolar orders with finite powers proportional to  $\lambda^2$ . In this article, we identify  $\lambda^2/c$  and  $\lambda^3/c$  as analogous force and torque constants, derived within a more general quadratic scattering-channel framework for upper bounds to optical force and torque for any illumination field. This framework also solves the reverse problem: computing globally optimal “holographic” incident beams, for a fixed collection of scatterers. We analyze structures and incident fields that approach the bounds, which for wavelength-scale bodies show

**Distribution Statement:** 3-Distribution authorized to U.S. Government Agencies and their contractors  
**Acknowledged Federal Support:** Y

## RPPR Interim Progress Report as of 10-Mar-2020

**Publication Type:** Journal Article      Peer Reviewed: Y      **Publication Status:** 1-Published  
**Journal:** Light: Science & Applications  
**Publication Identifier Type:** DOI      **Publication Identifier:** 10.1038/s41377-018-0065-2  
**Volume:** 7      **Issue:** 1      **First Page #:**  
**Date Submitted:** 8/16/19 12:00AM      **Date Published:** 9/1/18 4:00AM  
**Publication Location:**

**Article Title:** Metasurface-based multi-harmonic free-electron light source

**Authors:** Gilles Rosolen, Liang Jie Wong, Nicholas Rivera, Bjorn Maes, Marin Soljačić, Ido Kaminer

**Keywords:** light, metasurface, free-electron, x-rays

**Abstract:** Metasurfaces are subwavelength spatial variations in geometry and material where the structures are of negligible thickness compared to the wavelength of light and are optimized for far-field applications, such as controlling the wavefronts of electromagnetic waves. Here, we investigate the potential of the metasurface near-field profile, generated by an incident few-cycle pulse laser, to facilitate the generation of high-frequency light from free electrons. In particular, the metasurface near-field contains higher-order spatial harmonics that can be leveraged to generate multiple higher-harmonic X-ray frequency peaks. We show that the X-ray spectral profile can be arbitrarily shaped by controlling the metasurface geometry, the electron energy, and the incidence angle of the laser input. Using ab initio simulations, we predict bright and monoenergetic X-rays, achieving energies of 30 keV (with harmonics spaced by 3 keV) from 5-MeV electrons using 3.4-eV plasmon polaritons on a...

**Distribution Statement:** 3-Distribution authorized to U.S. Government Agencies and their contractors

**Acknowledged Federal Support:** Y

**Publication Type:** Journal Article      Peer Reviewed: Y      **Publication Status:** 1-Published  
**Journal:** Physical Review Letters  
**Publication Identifier Type:** DOI      **Publication Identifier:** 10.1103/PhysRevLett.122.053901  
**Volume:** 122      **Issue:** 5      **First Page #:**  
**Date Submitted:** 8/16/19 12:00AM      **Date Published:** 2/1/19 5:00AM  
**Publication Location:**

**Article Title:** Ultrafast Multiharmonic Plasmon Generation by Optically Dressed Electrons

**Authors:** Nicholas Rivera, Liang Jie Wong, Marin Soljacic, Ido Kaminer

**Keywords:** Plasmon Generation

**Abstract:** Interactions between electrons and photons are a source of rich physics from atomic to astronomical scales. Here, we examine a new kind of electron-photon interaction in which an electron, modulated by light, radiates multiple harmonics of plasmons. The emitted plasmons can be femtosecond in duration and nanometer in spatial scale. The extreme subwavelength nature of the plasmons lowers the necessary input light intensity by at least 4 orders of magnitude relative to state-of-the-art strong-field processes involving bound or free electrons. The results presented here reveal a new means of ultrafast (10–1000 fs) interconversion between photonic and plasmonic energy, and a general scheme for generating spatio-temporally shaped ultrashort pulses in optical materials. More generally, our results suggest a route towards realizing analogues of fascinating physical phenomena like nonlinear Compton scattering in plasmonics and nanophotonics with relatively low intensities, slow electrons...

**Distribution Statement:** 3-Distribution authorized to U.S. Government Agencies and their contractors

**Acknowledged Federal Support:** Y

## RPPR Interim Progress Report as of 10-Mar-2020

**Publication Type:** Journal Article

Peer Reviewed: Y

**Publication Status:** 1-Published

**Journal:** Nature Communications

Publication Identifier Type: DOI

Publication Identifier: 10.1038/s41467-019-11070-7

Volume: 10

Issue: 1

First Page #:

Date Submitted: 8/16/19 12:00AM

Date Published: 7/1/19 4:00AM

Publication Location:

**Article Title:** Towards integrated tunable all-silicon free-electron light sources

**Authors:** Charles Roques-Carmes, Steven E. Kooi, Yi Yang, Aviram Massuda, Phillip D. Keathley, Aun Zaidi, Yuji

**Keywords:** Tunable emission from silicon, nanograting

**Abstract:** Extracting light from silicon is a longstanding challenge in modern engineering and physics. While silicon has underpinned the past 70 years of electronics advancement, a facile tunable and efficient silicon-based light source remains elusive. Here, we experimentally demonstrate the generation of tunable radiation from a one-dimensional, all-silicon nanograting. Light is generated by the spontaneous emission from the interaction of these nanogratings with low-energy free electrons (2–20 keV) and is recorded in the wavelength range of 800–1600 nm, which includes the silicon transparency window. Tunable free-electron-based light generation from nanoscale silicon gratings with efficiencies approaching those from metallic gratings is demonstrated. We theoretically investigate the feasibility of a scalable, compact, all-silicon tunable light source comprised of a silicon Field Emitter Array integrated with a silicon nanograting that emits at telecommunication wavelengths. Our results...

**Distribution Statement:** 3-Distribution authorized to U.S. Government Agencies and their contractors

Acknowledged Federal Support: Y

**Publication Type:** Journal Article

Peer Reviewed: Y

**Publication Status:** 1-Published

**Journal:** Journal of Photonics for Energy

Publication Identifier Type: DOI

Publication Identifier: 10.1117/1.JPE.9.032713

Volume: 9

Issue: 03

First Page #: 1

Date Submitted: 8/16/19 12:00AM

Date Published: 2/1/19 5:00AM

Publication Location:

**Article Title:** Practical emitters for thermophotovoltaics: a review

**Authors:** Reyu Sakakibara, Veronika Stelmakh, Walker R. Chan, Michael Ghebrebrhan, John D. Joannopoulos, M

**Keywords:** thermophotovoltaic (TPV)

**Abstract:** Thermophotovoltaic (TPV) systems are promising for harnessing solar energy, waste heat, and heat from radioisotope decay or fuel combustion. TPV systems work by heating an emitter that emits light that is converted to electricity. One of the key challenges is designing an emitter that not only preferentially emits light in certain wavelength ranges but also simultaneously satisfies other engineering constraints. To elucidate these engineering constraints, we first provide an overview of the state of the art, by classifying emitters into three categories based on whether they have been used in prototype system demonstrations, fabricated and measured, or simulated. We then present a systematic approach for assessing emitters. This consists of five metrics: optical performance, ability to scale to large areas, stability at high temperatures, ability to integrate into the system, and cost. Using these metrics, we evaluate and discuss the reported results of emitters used in system....

**Distribution Statement:** 3-Distribution authorized to U.S. Government Agencies and their contractors

Acknowledged Federal Support: Y

## RPPR Interim Progress Report as of 10-Mar-2020

**Publication Type:** Journal Article

Peer Reviewed: Y

**Publication Status:** 1-Published

**Journal:** Science Advances

Publication Identifier Type: DOI

Publication Identifier: 10.1126/sciadv.aau0823

Volume: 5

Issue: 5

First Page #:

Date Submitted: 8/16/19 12:00AM

Date Published: 5/1/19 4:00AM

Publication Location:

**Article Title:** Experimental investigation of performance differences between coherent Ising machines and a quantum annealer

**Authors:** Ryan Hamerly, Takahiro Inagaki, Peter L. McMahon, Davide Venturelli, Alireza Marandi, Tatsuhiko Onoc

**Keywords:** Ising machines, quantum annealer, optimization

**Abstract:** Physical annealing systems provide heuristic approaches to solving combinatorial optimization problems. Here, we benchmark two types of annealing machines—a quantum annealer built by D-Wave Systems and measurement- feedback coherent Ising machines (CIMs) based on optical parametric oscillators—on two problem classes, the Sherrington-Kirkpatrick (SK) model and MAX-CUT. The D-Wave quantum annealer outperforms the CIMs on MAX-CUT on cubic graphs. On denser problems, however, we observe an exponential penalty for the quantum annealer [ $\exp(-\alpha_{\text{DWN}}N^2)$ ] relative to CIMs [ $\exp(-\alpha_{\text{CIM}}N)$ ] for fixed anneal times, both on the SK model and on 50% edge density MAX-CUT. This leads to a several orders of magnitude time-to-solution difference for instances with over 50 vertices. An optimal-annealing time analysis is also consistent with a substantial projected performance difference. The difference in performance between the sparsely connected D-Wave machine and the fully-connected CIMs provides strong...

**Distribution Statement:** 3-Distribution authorized to U.S. Government Agencies and their contractors

Acknowledged Federal Support: Y

**Publication Type:** Journal Article

Peer Reviewed: Y

**Publication Status:** 1-Published

**Journal:** Physical Review X

Publication Identifier Type: DOI

Publication Identifier: 10.1103/PhysRevX.9.021032

Volume: 9

Issue: 2

First Page #:

Date Submitted: 8/16/19 12:00AM

Date Published: 5/1/19 4:00AM

Publication Location:

**Article Title:** Large-Scale Optical Neural Networks Based on Photoelectric Multiplication

**Authors:** Ryan Hamerly, Liane Bernstein, Alexander Sludds, Marin Soljacic, Dirk Englund

**Keywords:** deep neural networks, photonic accelerator, subattojoule matrix multiplication, multiply and accumulate (MAC)

**Abstract:** Recent success in deep neural networks has generated strong interest in hardware accelerators to improve speed and energy consumption. This paper presents a new type of photonic accelerator based on coherent detection that is scalable to large ( $N \sim 10^6$ ) networks and can be operated at high (gigahertz) speeds and very low (subattojoule) energies per multiply and accumulate (MAC), using the massive spatial multiplexing enabled by standard free-space optical components. In contrast to previous approaches, both weights and inputs are optically encoded so that the network can be reprogrammed and trained on the fly. Simulations of the network using models for digit and image classification reveal a “standard quantum limit” for optical neural networks, set by photodetector shot noise. This bound, which can be as low as 50 zJ/MAC, suggests that performance below the thermodynamic (Landauer) limit for digital irreversible computation is theoretically possible in this device. The...

**Distribution Statement:** 3-Distribution authorized to U.S. Government Agencies and their contractors

Acknowledged Federal Support: Y

## RPPR Interim Progress Report as of 10-Mar-2020

**Publication Type:** Journal Article      Peer Reviewed: Y      **Publication Status:** 1-Published

**Journal:** Neural Computation

Publication Identifier Type: DOI

Publication Identifier: 10.1162/neco\_a\_01174

Volume: 31

Issue: 4

First Page #: 765

Date Submitted: 8/16/19 12:00AM

Date Published: 4/1/19 4:00AM

Publication Location:

**Article Title:** Gated Orthogonal Recurrent Units: On Learning to Forget

**Authors:** Li Jing, Caglar Gulcehre, John Peurifoy, Yichen Shen, Max Tegmark, Marin Soljacic, Yoshua Bengio

**Keywords:** recurrent neural network (RNN); unitary evolution RNN; long short-term memory

**Abstract:** We present a novel recurrent neural network (RNN)-based model that combines the remembering ability of unitary evolution RNNs with the ability of gated RNNs to effectively forget redundant or irrelevant information in its memory. We achieve this by extending restricted orthogonal evolution RNNs with a gating mechanism similar to gated recurrent unit RNNs with a reset gate and an update gate. Our model is able to outperform long short-term memory, gated recurrent units, and vanilla unitary or orthogonal RNNs on several long-term-dependency benchmark tasks. We empirically show that both orthogonal and unitary RNNs lack the ability to forget. This ability plays an important role in RNNs. We provide competitive results along with an analysis of our model on many natural sequential tasks, including question answering, speech spectrum prediction, character-level language modeling, and synthetic tasks that involve long-term dependencies such as algorithmic, denoising, and copying task

**Distribution Statement:** 3-Distribution authorized to U.S. Government Agencies and their contractors

Acknowledged Federal Support: Y

**Publication Type:** Journal Article      Peer Reviewed: Y      **Publication Status:** 1-Published

**Journal:** Transactions of the Association for Computational Linguistics

Publication Identifier Type: DOI

Publication Identifier: 10.1162/tacl\_a\_00258

Volume: 7

Issue:

First Page #: 121

Date Submitted: 8/16/19 12:00AM

Date Published: 3/1/19 5:00AM

Publication Location:

**Article Title:** Rotational Unit of Memory: A Novel Representation Unit for RNNs with Scalable Applications

**Authors:** Rumen Dangovski, Li Jing, Preslav Nakov, Mico Tatalovic, Marin Soljacic

**Keywords:** long short-term memory (LSTM) cells, gated recurrent units (GRUs), recurrent neural network (RNN), Rotational Unit of Memory (RUM)

**Abstract:** Stacking long short-term memory (LSTM) cells or gated recurrent units (GRUs) as part of a recurrent neural network (RNN) has become a standard approach to solving a number of tasks ranging from language modeling to text summarization. Although LSTMs and GRUs were designed to model long-range dependencies more accurately than conventional RNNs, they nevertheless have problems copying or recalling information from the long distant past. Here, we derive a phase-coded representation of the memory state, Rotational Unit of Memory (RUM), that unifies the concepts of unitary learning and associative memory. We show experimentally that RNNs based on RUMs can solve basic sequential tasks such as memory copying and memory recall much better than LSTMs/GRUs. We further demonstrate that by replacing LSTM/GRU with RUM units we can apply neural networks to real-world problems such as language modeling and text summarization, yielding results comparable to the state of the art.

**Distribution Statement:** 3-Distribution authorized to U.S. Government Agencies and their contractors

Acknowledged Federal Support: Y

## RPPR Interim Progress Report as of 10-Mar-2020

**Publication Type:** Journal Article      Peer Reviewed: Y      **Publication Status:** 1-Published  
**Journal:** Optics Express  
**Publication Identifier Type:** DOI      **Publication Identifier:** 10.1364/OE.27.015765  
**Volume:** 27      **Issue:** 11      **First Page #:** 15765  
**Date Submitted:** 8/16/19 12:00AM      **Date Published:** 5/1/19 4:00AM  
**Publication Location:**

**Article Title:** Topology optimization of freeform large-area metasurfaces

**Authors:** Zin Lin, Victor Liu, Raphael Pestourie, Steven G. Johnson

**Keywords:** topology optimization, metasurfaces

**Abstract:** We demonstrate optimization of optical metasurfaces over 105–106 degrees of freedom in two and three dimensions, 100–1000+ wavelengths (?) in diameter, with 100+ parameters per ?2. In particular, we show how topology optimization, with one degree of freedom per high-resolution “pixel,” can be extended to large areas with the help of a locally periodic approximation that was previously only used for a few parameters per ?2. In this way, we can computationally discover completely unexpected metasurface designs for challenging multi-frequency, multi-angle problems, including designs for fully coupled multi-layer structures with arbitrary per-layer patterns. Unlike typical metasurface designs based on subwavelength unit cells, our approach can discover both sub- and supra-wavelength patterns and can obtain both the near and far fields.

**Distribution Statement:** 3-Distribution authorized to U.S. Government Agencies and their contractors

**Acknowledged Federal Support:** Y

**Publication Type:** Journal Article      Peer Reviewed: Y      **Publication Status:** 1-Published  
**Journal:** Optics Express  
**Publication Identifier Type:** DOI      **Publication Identifier:** 10.1364/OE.26.033732  
**Volume:** 26      **Issue:** 26      **First Page #:** 33732  
**Date Submitted:** 8/16/19 12:00AM      **Date Published:** 12/1/18 5:00AM  
**Publication Location:**

**Article Title:** Inverse design of large-area metasurfaces

**Authors:** Raphaël Pestourie, Carlos Pérez-Arancibia, Zin Lin, Wonseok Shin, Federico Capasso, Steven G. Johnson

**Keywords:** inverse design, aperiodic metasurfaces, wavefront shaping

**Abstract:** We present a computational framework for efficient optimization-based “inverse design” of large-area “metasurfaces” (subwavelength-patterned surfaces) for applications such as multi-wavelength/multi-angle optimizations, and demultiplexers. To optimize surfaces that can be thousands of wavelengths in diameter, with thousands (or millions) of parameters, the key is a fast approximate solver for the scattered field. We employ a “locally periodic” approximation in which the scattering problem is approximated by a composition of periodic scattering problems from each unit cell of the surface, and validate it against brute-force Maxwell solutions. This is an extension of ideas in previous metasurface designs, but with greatly increased flexibility, e.g. to automatically balance tradeoffs between multiple frequencies or to optimize a photonic device given only partial information about the desired field. Our approach even extends beyond the metasurface regime to non-subwavelength structures..

**Distribution Statement:** 3-Distribution authorized to U.S. Government Agencies and their contractors

**Acknowledged Federal Support:** Y

## RPPR Interim Progress Report as of 10-Mar-2020

**Publication Type:** Journal Article      Peer Reviewed: Y      **Publication Status:** 1-Published

**Journal:** Optics Express

Publication Identifier Type: DOI

Publication Identifier: 10.1364/OE.26.030202

Volume: 26

Issue: 23

First Page #: 30202

Date Submitted: 8/16/19 12:00AM

Date Published: 11/1/18 4:00AM

Publication Location:

**Article Title:** Sideways adiabaticity: beyond ray optics for slowly varying metasurfaces

**Authors:** Carlos Pérez-Arancibia, Raphaël Pestourie, Steven G. Johnson

**Keywords:** Computational electromagnetic methods; Diffraction theory; Diffractive optics; Metamaterials

**Abstract:** Optical metasurfaces (subwavelength-patterned surfaces typically described by variable effective surface impedances) are typically modeled by an approximation akin to ray optics: the reflection or transmission of an incident wave at each point of the surface is computed as if the surface were “locally uniform,” and then the total field is obtained by summing all of these local scattered fields via a Huygens principle. (Similar approximations are found in scalar diffraction theory and in ray optics for curved surfaces.) In this paper, we develop a precise theory of such approximations for variable-impedance surfaces. Not only do we obtain a type of adiabatic theorem showing that the “zeroth-order” locally uniform approximation converges in the limit as the surface varies more and more slowly, including a way to quantify the rate of convergence, but we also obtain an infinite series of higher-order corrections. These corrections, which can be computed to any desired order by performing..

**Distribution Statement:** 3-Distribution authorized to U.S. Government Agencies and their contractors

Acknowledged Federal Support: Y

**Publication Type:** Journal Article

Peer Reviewed: Y

**Publication Status:** 1-Published

**Journal:** Optica

Publication Identifier Type: DOI

Publication Identifier: 10.1364/OPTICA.5.001046

Volume: 5

Issue: 9

First Page #: 1046

Date Submitted: 8/15/19 12:00AM

Date Published: 8/1/18 4:00AM

Publication Location:

**Article Title:** Are slot and sub-wavelength grating waveguides better than strip waveguides for sensing?

**Authors:** Derek M. Kita, Jérôme Michon, Steven G. Johnson, Juejun Hu

**Keywords:** slot and sub-wavelength grating (SWG), waveguides, light, sensing

**Abstract:** The unique ability of slot and sub-wavelength grating (SWG) waveguides to confine light outside of the waveguide core material has attracted significant interest in their application to chemical and biological sensing. However, a high sensitivity to sidewall-roughness-induced scattering loss in these structures compared with strip waveguides casts doubt on their efficacy. In this article, we seek to settle the controversy for silicon-on-insulator (SOI) photonic devices by quantitatively comparing the sensing performance of various waveguide geometries through figures of merit that we derive for each mode of sensing. These methods (which may be readily applied to other material systems) take into account both modal confinement and roughness scattering loss, the latter of which is computed using a volume-current (Green's function) method with a first Born approximation. For devices based on the standard 220 nm SOI platform at telecommunication wavelengths ( $\lambda=1550$  nm)...

**Distribution Statement:** 3-Distribution authorized to U.S. Government Agencies and their contractors

Acknowledged Federal Support: Y

## RPPR Interim Progress Report as of 10-Mar-2020

**Publication Type:** Journal Article      Peer Reviewed: Y      **Publication Status:** 1-Published

**Journal:** Journal of the Optical Society of America B

Publication Identifier Type: DOI

Publication Identifier: 10.1364/JOSAB.36.000C22

Volume: 36

Issue: 4

First Page #:

Date Submitted: 8/15/19 12:00AM

Date Published: 2/1/19 5:00AM

Publication Location:

**Article Title:** Ab initio theory of quantum fluctuations and relaxation oscillations in multimode lasers

**Authors:** Adi Pick, Alexander Cerjan, Steven G. Johnson

**Keywords:** multimode lasers, quantum fluctuations, relaxation oscillations

**Abstract:** We present an ab initio semi-analytical solution for the noise spectrum of complex-cavity microstructured lasers, including central Lorentzian peaks at the multimode lasing frequencies and additional sidepeaks due to relaxation-oscillation (RO) dynamics. In Phys. Rev. A 91, 063806 (2015), we computed the central-peak linewidths by solving generalized laser rate equations, which we derived from the Maxwell–Bloch equations by invoking the fluctuation–dissipation theorem to relate the noise correlations to the steady-state lasing properties. Here, we generalize this approach and obtain the entire laser spectrum, focusing on the RO sidepeaks. Our formulation treats inhomogeneity, cavity openness, nonlinearity, and multimode effects accurately. We find a number of new effects, including new multimode RO sidepeaks and three generalized  $Q$  factors. Last, we apply our formulas to compute the noise spectrum of single-mode and multimode photonic-crystal lasers.

**Distribution Statement:** 3-Distribution authorized to U.S. Government Agencies and their contractors

Acknowledged Federal Support: Y

**Publication Type:** Journal Article

Peer Reviewed: Y

**Publication Status:** 1-Published

**Journal:** ACS Photonics

Publication Identifier Type: DOI

Publication Identifier: 10.1021/acsp Photonics.8b01526

Volume: 6

Issue: 5

First Page #: 1168

Date Submitted: 8/16/19 12:00AM

Date Published: 5/1/19 4:00AM

Publication Location:

**Article Title:** Migrating Knowledge between Physical Scenarios Based on Artificial Neural Networks

**Authors:** Yurui Qu, Li Jing, Yichen Shen, Min Qiu, Marin Soljačić

**Keywords:** artificial neural networks, deep learning, transfer learning, physical scenarios, multilayer films, nanoparticles

**Abstract:** Deep learning is known to be data-hungry, which hinders its application in many areas of science when data sets are small. Here, we propose to use transfer learning methods to migrate knowledge between different physical scenarios and significantly improve the prediction accuracy of artificial neural networks trained on a small data set. This method can help reduce the demand for expensive data by making use of additional inexpensive data. First, we demonstrate that, in predicting the transmission from multilayer photonic film, the relative error rate is reduced by 50.5% (23.7%) when the source data comes from 10-layer (8-layer) films and the target data comes from 8-layer (10-layer) films. Second, we show that the relative error rate is decreased by 19.7% when knowledge is transferred between two very different physical scenarios: transmission from multilayer films and scattering from multilayer nanoparticles. Next, we propose a multitask learning method to improve the performance of

**Distribution Statement:** 3-Distribution authorized to U.S. Government Agencies and their contractors

Acknowledged Federal Support: Y



## RPPR Interim Progress Report as of 10-Mar-2020

**Publication Type:** Journal Article      Peer Reviewed: Y      **Publication Status:** 1-Published  
**Journal:** Advanced Materials  
**Publication Identifier Type:** DOI      **Publication Identifier:** 10.1002/adma.201902021  
**Volume:** 31      **Issue:** 30      **First Page #:** 1902021  
**Date Submitted:** 8/16/19 12:00AM      **Date Published:** 6/1/19 4:00AM  
**Publication Location:**

**Article Title:** Scalable Fabrication of Porous Microchannel Nerve Guidance Scaffolds with Complex Geometries

**Authors:** Dena Shahriari, Gabriel Loke, Ian Tafel, Seongjun Park, Po-Han Chiang, Yoel Fink, Polina Anikeeva

**Keywords:** nerve repair, microchannel scaffold, injury, fiber drawing

**Abstract:** Microchannel scaffolds accelerate nerve repair by guiding growing neu-ronal processes across injury sites. Although geometry, materials chemistry, stiffness, and porosity have been shown to influence nerve growth within nerve guidance scaffolds, independent tuning of these properties in a high-throughput manner remains a challenge. Here, fiber drawing is combined with salt leaching to produce microchannels with tunable cross sections and porosity. This technique is applicable to an array of biochemically inert polymers, and it delivers hundreds of meters of porous microchannel fibers. Employing these fibers as filaments during 3D printing enables the production of microchannel scaffolds with geometries matching those of biological nerves, including branched topographies. Applied to sensory neurons, fiber-based porous microchannels enhance growth as compared to non-porous channels with matching materials and geometries. The combinatorial scaffold fabrication approach may advance the...

**Distribution Statement:** 3-Distribution authorized to U.S. Government Agencies and their contractors  
**Acknowledged Federal Support:** Y

**Publication Type:** Journal Article      Peer Reviewed: Y      **Publication Status:** 1-Published  
**Journal:** Optical Materials Express  
**Publication Identifier Type:** DOI      **Publication Identifier:** 10.1364/OME.9.003432  
**Volume:** 9      **Issue:** 8      **First Page #:** 3432  
**Date Submitted:** 8/16/19 12:00AM      **Date Published:** 7/1/19 4:00AM  
**Publication Location:**

**Article Title:** Fabrication and measurement of 3D printed retroreflective fibers

**Authors:** Michael Ghebrebrhan, Gabriel Z. J. Loke, Yoel Fink

**Keywords:** retroreflectors, thermal drawing, preform, Additive manufacturing, 3D-printing-derived fiber, optical scattering

**Abstract:** Additive manufacturing enables new fiber preform geometries to be built that were either impossible or extremely difficult with traditional subtractive manufacturing methods. Additionally fiber thermal drawing is undergoing an explosion of interest due to new materials and fiber functions. We fabricate a retroreflective fiber that possesses a complex cross-section and material combination not achievable with other textile fiber fabrication methods such melt extrusion. This is the first such 3D-printing-derived fiber to demonstrate optical scattering properties with a non-circular, non-convex cross-section.

**Distribution Statement:** 3-Distribution authorized to U.S. Government Agencies and their contractors  
**Acknowledged Federal Support:** Y

### BOOKS:

**Publication Type:** Book      Peer Reviewed: Y      **Publication Status:** 1-Published  
**Publication Identifier Type:** DOI      **Publication Identifier:** 10.1016/C2016-0-01129-4  
**Book Edition:**      **Volume:**      **Publication Year:** 2019      **Date Received:** 15-Aug-2019  
**Publication Location:**  
**Publisher:** Elsevier

**Book Title:** Robotic Systems and Autonomous Platforms

**Authors:** Shawn M. Walsh, Michael S. Strano (editors)

**Editor:**

**Acknowledged Federal Support:** Y

# RPPR Interim Progress Report

## as of 10-Mar-2020

### CONFERENCE PAPERS:

**Publication Type:** Conference Paper or Presentation **Publication Status:** 1-Published  
**Conference Name:** CLEO: QELS\_Fundamental Science  
Date Received: 16-Aug-2019 Conference Date: 10-May-2019 Date Published:  
Conference Location: San Jose, California  
**Paper Title:** Photonic Recurrent Ising Sampler  
**Authors:** Charles Roques-Carmes, Yichen Shen, Cristian Zanolini, Mihika Prabhu, Fadi Atieh, Li Jing, Tena Dubc?  
Acknowledged Federal Support: **Y**

**Publication Type:** Conference Paper or Presentation **Publication Status:** 1-Published  
**Conference Name:** CLEO: Science and Innovations  
Date Received: 16-Aug-2019 Conference Date: 10-May-2019 Date Published:  
Conference Location: San Jose, California  
**Paper Title:** Luneburg Lens for Wide-Angle Chip-Scale Optical Beam Steering  
**Authors:** Samuel Kim, Jamison Sloan, Josue J Lopez, Dave Kharas, Jeffrey Herd, Suraj Bramhavar, Paul Juodav  
Acknowledged Federal Support: **N**

### PATENTS:

**Intellectual Property Type:** Patent Date Received: **17-Aug-2018**  
**Patent Title:** Systems and methods for particle guiding  
**Patent Abstract:** A technique to guide a micro- or nano-scale particle uses the wavelengths of light beams to con  
**Patent Number:** 10,004,135  
Patent Country: USA  
Application Date: 24-Aug-2016 Application Status: 3  
Date Issued: 06-Aug-2019

**Intellectual Property Type:** Patent Date Received: **17-Aug-2018**  
**Patent Title:** Methods and apparatus for transparent display using scattering nanoparticles  
**Patent Abstract:** Transparent displays enable many useful applications, including heads-up displays for cars and  
**Patent Number:** US9927616B2  
Patent Country: USA  
Application Date: 29-Jun-2017 Application Status: 3  
Date Issued: 27-Mar-2018

**Intellectual Property Type:** Patent Date Received: **17-Aug-2018**  
**Patent Title:** Spectrally-engineered solar thermal photovoltaic devices  
**Patent Abstract:** A solar thermal photovoltaic device, and method of forming same, includes a solar absorber and  
**Patent Number:** US9929690B2  
Patent Country: USA  
Application Date: 09-Jun-2016 Application Status: 3  
Date Issued: 27-Mar-2018

**Intellectual Property Type:** Patent Date Received: **19-Aug-2019**  
**Patent Title:** Efficient Weakly-Radiative Wireless Energy Transfer: An EIT-Like Approach  
**Patent Abstract:** Disclosed is a method for transferring energy wirelessly. The method includes i) transferring ene  
**Patent Number:** 2345100  
Patent Country: DEU

**RPPR Interim Progress Report**  
as of 10-Mar-2020

Application Date: 01-Oct-2009  
Date Issued: 05-Dec-2018

Application Status: 3

**Intellectual Property Type:** Patent

Date Received: **19-Aug-2019**

**Patent Title:** Electrodeposited alloys and methods of making same using power pulses

**Patent Abstract:** Power pulsing, such as current pulsing, is used to control the structures of metals and alloys ele

**Patent Number:** 2488681

Patent Country: DEU

Application Date: 06-Oct-2010

Application Status: 3

Date Issued: 15-Aug-2018

**Intellectual Property Type:** Patent

Date Received: **19-Aug-2019**

**Patent Title:** Discriminating electromagnetic radiation based on angle of incidence

**Patent Abstract:** The present invention provides systems, articles, and methods for discriminating electromagneti

**Patent Number:** RE47157

Patent Country: USA

Application Date: 12-Jun-2017

Application Status: 3

Date Issued: 11-Dec-2018

**Intellectual Property Type:** Patent

Date Received: **19-Aug-2019**

**Patent Title:** Stable binary nanocrystalline alloys and methods of identifying same

**Patent Abstract:** Identifying a stable phase of a binary alloy comprising a solute element and a solvent element. I

**Patent Number:** 10234410

Patent Country: USA

Application Date: 11-Sep-2014

Application Status: 3

Date Issued: 19-Aug-2019

**Intellectual Property Type:** Patent

Date Received: **19-Aug-2019**

**Patent Title:** METHOD FOR CONTROLLING THE ENERGY DAMPING OF A SHAPE MEMORY ALLOY WITH SURFACE ROUGHNESS

**Patent Abstract:** A method for producing an energy damping-controlled shape memory alloy wire comprising:form

**Patent Number:** 10,214,798

Patent Country: USA

Application Date: 03-Dec-2012

Application Status: 3

Date Issued: 19-Mar-2019

**Intellectual Property Type:** Patent

Date Received: **19-Aug-2019**

**Patent Title:** Stable nanocrystalline ordering alloy systems and methods of identifying same

**Patent Abstract:** Provided in one embodiment is a method of identifying a stable phase of an ordering binary allo

**Patent Number:** US10209208

Patent Country: USA

Application Date: 21-May-2013

Application Status: 3

Date Issued: 19-Feb-2019

**Intellectual Property Type:** Patent

Date Received: **19-Aug-2019**

**Patent Title:** Developer Free Positive Tone Lithography by Thermal Direct Write

**Patent Abstract:** A method for lithographic patterning of thin films. A thin film is deposited on a substrate and the

**Patent Number:** US10074544

Patent Country: USA

Application Date: 18-Apr-2014

Application Status: 3

Date Issued: 08-Aug-2019

# RPPR Interim Progress Report

as of 10-Mar-2020

<b>Intellectual Property Type:</b> Patent	Date Received: <b>19-Aug-2019</b>
<b>Patent Title:</b> Chemical and physical sensing with a reader and RFID tags	
<b>Patent Abstract:</b> A method of detecting a stimulus can include detecting an output from a radio frequency identifier	
<b>Patent Number:</b> US10157340	
Patent Country: USA	
Application Date: 17-Feb-2017	Application Status: 3
Date Issued: 18-Dec-2018	

<b>Intellectual Property Type:</b> Patent	Date Received: <b>19-Aug-2019</b>
<b>Patent Title:</b> High-pressure in-fiber particle production with precise dimensional control	
<b>Patent Abstract:</b> Herein is provided a fiber that includes a cladding material disposed along a longitudinal-axis fib	
<b>Patent Number:</b> US10112321	
Patent Country: USA	
Application Date: 13-Mar-2014	Application Status: 3
Date Issued: 30-Oct-2018	

<b>Intellectual Property Type:</b> Patent	Date Received: <b>19-Aug-2019</b>
<b>Patent Title:</b> Nanoparticles for magnetic resonance imaging applications	
<b>Patent Abstract:</b> A method of preparing a coated nanoparticle can include decomposing a compound to produce	
<b>Patent Number:</b> US10086094	
Patent Country: USA	
Application Date: 11-Sep-2015	Application Status: 3
Date Issued: 02-Oct-2018	

<b>Intellectual Property Type:</b> Patent	Date Received: <b>19-Aug-2019</b>
<b>Patent Title:</b> Methods and apparatus for broadband angular selectivity of electromagnetic waves	
<b>Patent Abstract:</b> A filter to transmit incident radiation at a predetermined incidence angle includes a plurality of ph	
<b>Patent Number:</b> US10073191	
Patent Country: USA	
Application Date: 24-Feb-2015	Application Status: 3
Date Issued: 11-Sep-2018	

<b>Intellectual Property Type:</b> Patent	Date Received: <b>19-Aug-2019</b>
<b>Patent Title:</b> Continuous oligocrystalline shape memory alloy wire produced by melt spinning	
<b>Patent Abstract:</b> There is provided herein a shape memory alloy wire that includes an alloy composition of CuAlNi	
<b>Patent Number:</b> us10167540	
Patent Country: USA	
Application Date: 06-May-2015	Application Status: 3
Date Issued: 01-Jan-2019	

<b>Intellectual Property Type:</b> Patent	Date Received: <b>19-Aug-2019</b>
<b>Patent Title:</b> Artificially engineered protein hydrogels to mimic nucleoporin selective gating	
<b>Patent Abstract:</b> Disclosed are synthetic polypeptides modeled after Nspl nucleoporin which are useful for formin	
<b>Patent Number:</b> US10220098	
Patent Country: USA	
Application Date: 19-Jun-2015	Application Status: 3
Date Issued: 05-Mar-2019	

**Intellectual Property Type:** Patent  
**Patent Title:** Systems, methods, and apparatus for in vitro single-cell identification and recovery  
**Patent Abstract:** Described herein are systems, methods, and apparatus for automatically identifying and recovering single cells from a sample of cells.  
**Patent Number:** US10078778  
**Patent Country:** USA

## RPPR Interim Progress Report as of 10-Mar-2020

Application Date: 15-Jan-2015  
Date Issued: 18-Sep-2018

Application Status: 3

**Intellectual Property Type:** Patent

Date Received: **19-Aug-2019**

**Patent Title:** Eliminating emissive sub-bandgap states in nanocrystals

**Patent Abstract:** The size-dependent band-gap tunability and solution processability of nanocrystals (NCs) make

**Patent Number:** US10109760

Patent Country: USA

Application Date: 08-Apr-2016

Application Status: 3

Date Issued: 23-Oct-2018

**Intellectual Property Type:** Patent

Date Received: **19-Aug-2019**

**Patent Title:** Apparatus and methods for optical neural network

**Patent Abstract:** An optical neural network is constructed based on photonic integrated circuits to perform neuror

**Patent Number:** US10268232

Patent Country: USA

Application Date: 02-Jun-2017

Application Status: 3

Date Issued: 23-Apr-2019

**Intellectual Property Type:** Patent

Date Received: **19-Aug-2019**

**Patent Title:** Systems including janus droplets capable of binding an analyte and changing orientation to provide a detectable change

**Patent Abstract:** Embodiments described herein may be useful in the detection of analytes. The systems and me

**Patent Number:** US10060913

Patent Country: USA

Application Date: 19-Sep-2016

Application Status: 3

Date Issued: 28-Aug-2018

**Intellectual Property Type:** Patent

Date Received: **19-Aug-2019**

**Patent Title:** CHEMICAL AND PHYSICAL SENSING WITH A READER AND RFID TAGS

**Patent Abstract:** A method of detecting a stimulus can include detecting an output from a radio frequency identifi

**Patent Number:** 20180107909

Patent Country: USA

Application Date: 19-Apr-2018

Application Status: 2

Date Issued:

**Intellectual Property Type:** Patent

Date Received: **20-Aug-2019**

**Patent Title:** DURABLE WATER RESISTANT COATINGS

**Patent Abstract:** Polymers comprising fluorinated side chains that can be used for water resistance coatings on s

**Patent Number:** WO/2019/028271

Patent Country: USA

Application Date: 02-Aug-2018

Application Status: 1

Date Issued:

**Intellectual Property Type:** Patent

Date Received: **20-Aug-2019**

**Patent Title:** SINGLE CELL ANALYSES

**Patent Abstract:** This disclosure describes improvements to both hardware and enzymatic reactions used in sing

**Patent Number:** WO2019113457

Patent Country: USA

Application Date: 08-Dec-2018

Application Status: 1

Date Issued:

**RPPR Interim Progress Report**  
as of 10-Mar-2020

**Intellectual Property Type:** Patent

Date Received: **20-Aug-2019**

**Patent Title:** SINGLE CELL ANALYSES

**Patent Abstract:** This disclosure describes improvements to both hardware and enzymatic reactions used in sing

**Patent Number:** WO2019113457

Patent Country: USA

Application Date: 08-Dec-2018

Application Status: 1

Date Issued:

**Intellectual Property Type:** Patent

Date Received: **20-Aug-2019**

**Patent Title:** SINGLE CELL ANALYSES

**Patent Abstract:** This disclosure describes improvements to both hardware and enzymatic reactions used in sing

**Patent Number:** WO2019113457

Patent Country: USA

Application Date: 08-Dec-2018

Application Status: 1

Date Issued:



Institute for Soldier  
Nanotechnologies



# CA Interim Progress Report

## Jan 1 to Jul 31, 2018



## Table of Contents

<b>Introduction</b>		<i>i</i>
<b>Strategic Area 1:</b>	<b>Soldier Protection, Battlefield Care, and Sensing</b>	<b>1</b>
Project 1.1	<i>Advanced Multiscale Methods for Modelling of Fracture in Novel Nanomaterials</i>	2
Project 1.2	<i>Shock Mitigating and Reinforcing Molecular Nanocomposites</i>	7
Project 1.3	<i>Design &amp; Testing of Polymers for Improved Soldier Protection</i>	11
Project 1.4	<i>Superelastic Granular Materials for Impact Absorption</i>	15
Project 1.5	<i>Rapid Hemostasis for the Treatment of Incompressible Wounds</i>	19
Project 1.6	<i>Empowering Future Vaccines &amp; Immunotherapies with Nanotech-Based Adjuvants</i>	23
<b>Strategic Area 2:</b>	<b>Augmenting Situational Awareness</b>	<b>28</b>
Project 2.1	<i>Uncovering Chemical Stability &amp; Charge Transfer Mechanisms at Electrode-Electrolyte Interfaces</i>	29
Project 2.2	<i>Mid- &amp; LW-Infrared Detector Arrays on Flexible Substrates</i>	34
Project 2.3	<i>Room Temperature LWIR-THz Detection via E-Field Enhancement-Induced Quantum Dot Upconversion</i>	38
Project 2.4	<i>Particulate Fluid Fiber Processing for Novel Fabric Architectures</i>	42
Project 2.5	<i>Nano-Plasmonics for Soldier Applications</i>	45
<b>Strategic Area 3:</b>	<b>Transformational Nano-Optoelectronic Soldier Capabilities</b>	<b>49</b>
Project 3.1	<i>Solid State Power Generation at Millimeter Scales</i>	50
Project 3.2	<i>Photonic Integrated Circuits for LIDARS, Displays &amp; Low-Power Computing</i>	55
Project 3.3	<i>Nanophotonics Enhanced Systems for the Soldier</i>	59
Project 3.4	<i>Applications of Novel Topological Phenomena</i>	63
Project 3.5	<i>Novel Multimaterial Inks for Multiscale 3D Device Printing</i>	66



## Introduction

Each summer, the Institute for Soldier Nanotechnologies (ISN) at the Massachusetts Institute of Technology (MIT) submits to the U.S. Army an Interim Progress Report (IPR) detailing ISN research activities under its current contract for the preceding year. This report is subsequently reviewed by Army subject matter experts and thereafter used with the results of those reviews to inform the ISN's Technical Assessment Board (TAB) co-chaired by the Director of the U.S. Army Research Laboratory (ARL) and the Assistant Secretary of the Army for Acquisition Logistics and Technology's Director for Basic Research.

Because in the summer of 2018, the ISN-4 research portfolio funded under Cooperative Agreement Number W911NF-18-2-0048 had only recently begun, it was determined by the ISN's Army Research Office (ARO) program manager, Dr. Aura Gimm, that neither a full-length IPR nor a meeting of the TAB were necessary. Instead, in addition to a substantially foreshortened IPR, to which these paragraphs provide an introduction, Dr. Gimm requested that the ISN organize for her a series of meetings at MIT during which she could become more familiar not only with the technical aspects of each ISN-4 project but also with the research teams performing them.

The ISN arranged the requested meetings for the weeks of Monday, April 30 through Friday May 4, 2018 and Monday, July 9 through Friday, July 13, 2018. The complete meeting schedule is included as Figure 1. Through these meetings, Dr. Gimm was introduced to the principal investigators for each of the 16 core 6.1 research projects, as well as many of the graduate students and postdoctoral associates whose work supports them.

The following pages comprise the aforementioned shortened IPR, which includes brief summaries of each project in the ISN-4 core 6.1 research portfolio.

Week of April 30 – May 4, 2018

	Monday (4/30/2018)	Tuesday (5/1/18)	Wednesday (5/2/18)	Thursday (5/3/18)	Friday (5/4/18)
9am					Project 2.1: Yildiz (9-10am) 24-213
10am		Project 3.2: Englund/Soljagic (10am-Noon) 26-142	Project 3.1: Celanovic (10am-Noon) NE47-479	Project 1.3: Swager/Rutledge/ Nelson (10am-Noon) NE47-479	Project 1.1: Radovitzky/Zhao/ Nelson (10:30am-12:30pm) NE47-479
11am					
12noon					
1pm		Project 2.5: Johnson/Soljagic/Kong (1-3pm) Includes a working lunch NE47-479	Project 1.4: Schuh/Radovitzky/ Kamrin (1-3pm) NE47-407	Project 1.5: Olsen/Hammond (1-3pm) 66-350	
2pm	Project 3.1: Fisher (1:30-2:30pm) E14-674				
3pm		Project 3.3: Johnson/Soljagic (3-4pm) NE47-479			
4pm					
5pm				Project 1.2: Strano (4-5pm) 66-570	

Week of July 9-13, 2018

	Monday (7/9/18)	Tuesday (7/10/18)	Wednesday (7/11/18)	Thursday (7/12/18)	Friday (7/13/18)
9am		Project 1.6: Irvine (9-10am) (76-261)			
10am		Palacios (10-10:15am) (NE47-479)	Project 3.4: Fu/Gedik/Soljagic (Thomas Christensen for Soljagic) (10am-Noon) (4-331)	Project 2.3: Bawendi/Nelson/ Willard/Bulovic (10:30am-12:30pm) (6-233)	
11am		Projects 2.4 + 3.5: Fink/Stolyarov/ Joannopoulos (10:30am-1:30pm) (NE47-479)			
12noon		Includes working lunch (NE47-479)			
1pm			2.2: Palacios/Englund/ Kong (rep for Palacios) (1-3pm) (26-201)		
2pm					
3pm					
4pm					
5pm					

**Figure 1:** The schedule for the ISN-4 project meetings with Dr. Aura Gimm, the ISN's Army Research Office program manager. Meetings related to projects in SRA1 are in blue, SRA2 are in red, and SRA3 are in purple; one meeting, which related both to projects in SRA1 and SRA2, is in purple.

# Strategic Research Area 1

## Soldier Protection, Battlefield Care and Sensing

---

**SRA-1** focuses on studies to develop lighter weight, stronger materials to protect the Soldier and Soldier-augmenting platforms and systems from mechanical damage owing to blast waves, ballistic impacts, and mechanical vibrations, using various mechanisms of energy absorption including phase transitions and materials deformation. Specific materials to be studied include molecular composites, organic polymers, superelastic metal alloys and ultrahigh strength ceramic formulations. This SRA includes studies to elucidate how materials fail and thus will provide guidance to test materials under battlefield simulation conditions and on how to interpret the test results, as well as insights on how to improve the strength and durability of these materials. One project will study the use of packed granular particles of shape memory *ceramic materials* to dissipate energy through *inter*-particle friction and *intra*-particle martensitic phase transformations with interest in applications to vibrational damping. Another project features basic research on three different nanomaterials to arrest bleeding in battlefield wounds that cannot be treated by traditional methods of macro-compression, including use of injectable hemostats to counter the vexing problem of internal bleeding. Also proposed are novel means to safely intervene in the human immune system to protect the Soldier against infections through design of novel lymphoid- and leukocyte-targeting nanomaterials that concentrate adjuvant compounds and immunomodulators in immune cell populations to respectively enhance prophylactic vaccines and anti-microbial therapies.

---

**ISN Project Number: 1.1**

**Project Title: Advanced Multiscale Methods for Modeling of Fracture in Novel Nanomaterials**

**Principal Investigator(s): Raúl Radovitzky, Keith Nelson, Xuanhe Zhao**

**Summary of Accomplishments:**

We performed tensile tests on pock-chip hydrogel layers for exploring failure and damage mechanisms in adhesive layers. The hydrogels consist of polyacrylamide network with varying concentrations for tunable modulus ranging from 1-15 kPa. The elastic instabilities arising in these material systems are notoriously difficult to describe analytically or numerically due to the extreme nonlinearity combined with the incompressible material response

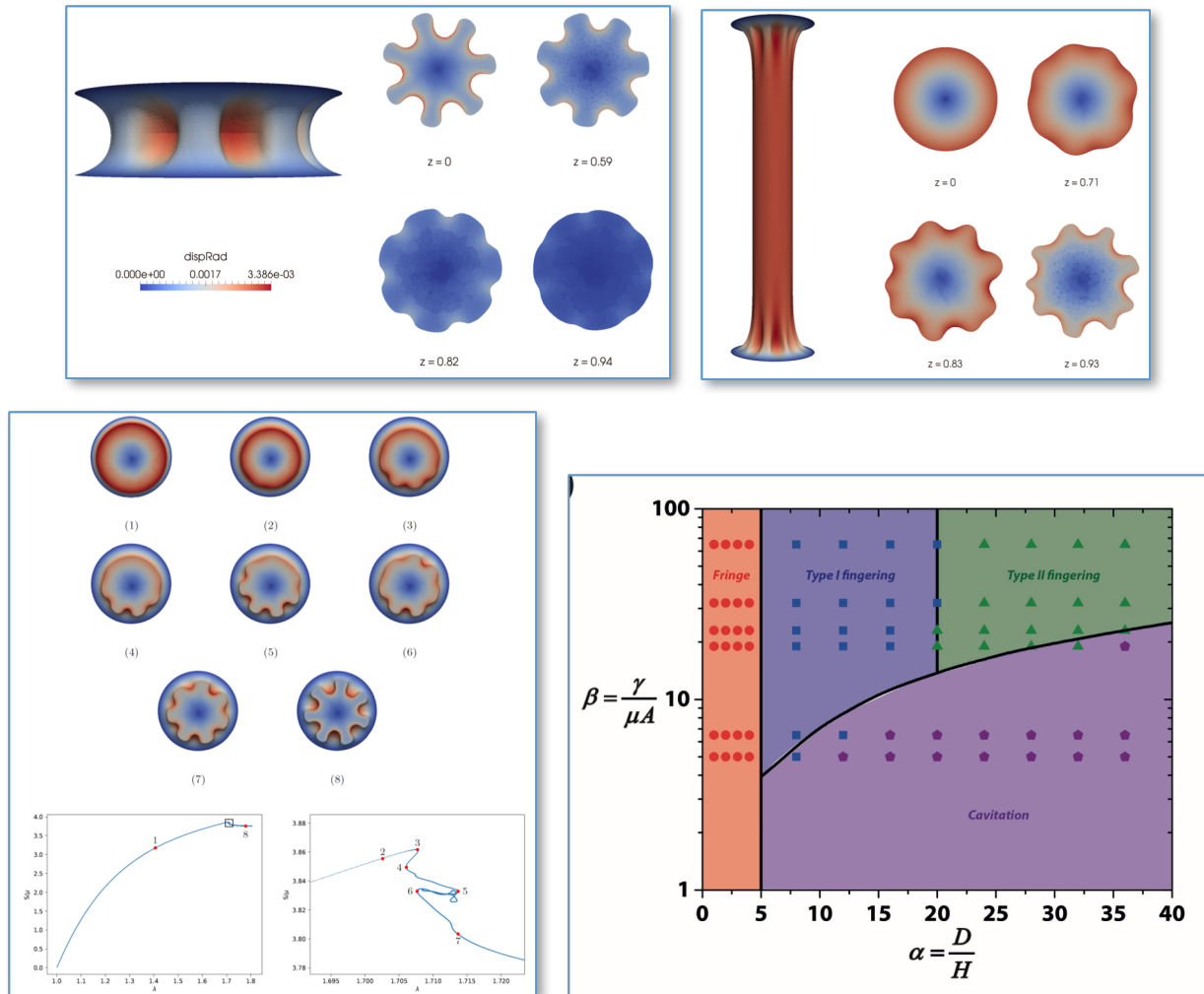


**Figure 1:** Simulations and experiments of elastic instabilities in confined hydrogel layers under tension: fingering instability (top left), fringe instabilities (top right). Complex evolution of fingers at instability point with multiple snap-backs (bottom left). Calculated phase diagram for the prediction of the initial occurrence mode of mechanical instabilities. Dots represent the experimental results and the solid lines represent theoretical calculations.

and the inherently three dimensional character of the observed bifurcation modes. We developed, implemented and tested in our ISN platform SumMIT, a large-scale computational framework for the simulation of elastic instabilities in soft materials containing all the essential ingredients to address these challenges: 1) high-order interpolation tetrahedral finite elements that do not exhibit incompressibility locking, and 2) scalable and robust nonlinear static solution algorithms. We find that the mode of instability is determined by both geometry and mechanical properties of the elastic layer through two non-dimensional parameters: layer's lateral dimension over its thickness and elastocapillary length over the defect size. We also calculate a phase diagram to predict the occurrence of any mode of instability **Figure 1**. The current findings can help the design of robust adhesives by rationally harnessing the desired mode of instabilities while suppressing the other modes.

In addition, we fabricated hydrogel samples with varying modulus and toughness for shock experiments on hydrogels conducted in Nelson group. We fabricate an interpenetrating network, which consists of one elastic network polyacrylamide and one dissipative network alginate. By varying the amount of calcium ions, the fracture energies of the hydrogel samples can be tuned across wide range from 10 to 10,000 J/m<sup>2</sup>.

We performed impact experiments on gels provided by ARL collaborators. The gels consist of poly(styrene-b-

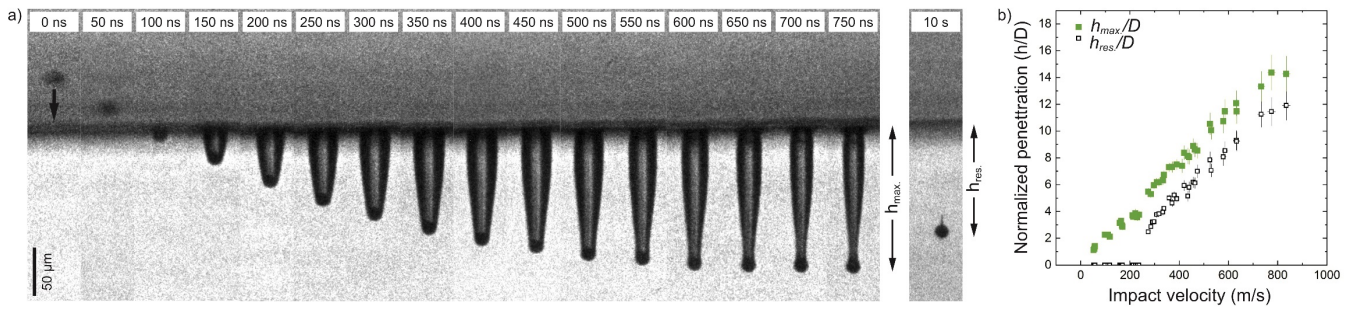


**Figure 2:** (a) Image sequence recorded using a high-speed camera showing a particle impact on a 40vol% SEBS sample. A 13-μm steel micro-particle impacts with a speed of 630 m/s. The time stamps, shown at the tops of the frames, indicate the delay in acquisition time relative to the first frame of the sequence. (b) Normalized penetrations (maximum and residual) as a function of impact velocity.

ethylene-co-butylene-b-styrene) triblock copolymer (SEBS) in mineral oil with varying concentrations. We aimed at comparing macroscopic impact results, which used 5.56-mm diameter steel balls launched at 100-500 m/s. In our laser-induced particle impact test (LIPIT), we launched steel particles (diameter  $D=17\pm4$  μm) at speeds varying from 50 m/s to 800 m/s. An exemplary impact of a steel particle launched at 630 m/s on a SEBS-mineral oil sample (40vol%-60vol%) is shown in **Figure 2**. The particle penetrates to a maximum penetration depth  $h_{max}=150$  μm before resting at a residual penetration depth of  $h_{res}=120$  μm. As observed in macroscopic and microscopic impact experiments, a large cavity opens behind the particle before eventually fully closing.

We have additionally conducted shock experiments using an in-house-designed laser-induced micro-shock platform, on samples provided by the Zhao group. A series of high frame rate (3 ns interframe) images are recorded and allow the direct visualization of cavitation events that occur in the gel **Figure 3**. These measurements have shown that for a given shock energy, the “toughness” (as tuned by the Zhao group) can dictate whether or not cavitation will occur.

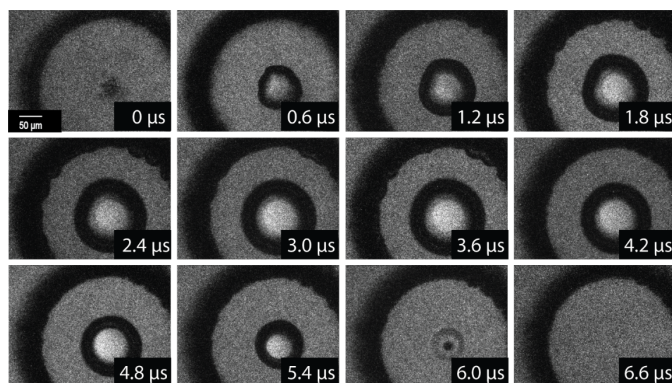


**Figure 3:** Image sequence recorded using a high-speed camera showing gel response following a converging shock wave. Microbubbles form within the first 10 ns and coalesce into a larger cavitation bubble which persists for approximately 6  $\mu$ s before collapse.

### Research Plans for Next Year:

We will continue the development of the computational framework as described in the proposal with special emphasis on understanding the competing mechanisms of deformation and failure: e.g. elastic instabilities vs adhesion failure and fracture.

We will further provide hydrogels samples with tunable modulus and fracture energies for exploring impact behavior of hydrogels by shock experiments. In addition, we will further perform tensile tests on pock-chip hydrogel layers, that will increase of our understanding of other types of instabilities and provide data for validating the computational models.

We are recently developing anti-fatigue hydrogels that have the potential to be applied to various engineering applications. One interesting yet challenging point is the mechanism for fatigue performance in hydrogels, which is not explored yet. The micro-shock setup in Nelson group allows us to explore the fatigue mechanisms of hydrogels using cyclic laser loadings.

Further impact and shock experiments will be performed on the SEBS gels with varying concentration (15, 20, 25, 30, 35, 40 vol%) provided by ARL. The impact behavior of gels synthesized by the Zhao group will also be investigated under LIPIT.

We have recently begun and will continue testing fatigue in the hydrogels provided by the Zhao group. The micro-shock setup allows us to shock-compress the samples up to 100 times per second, which will allow us to study the gel's response after many load/unload cycles.



## Representative Image and Caption:

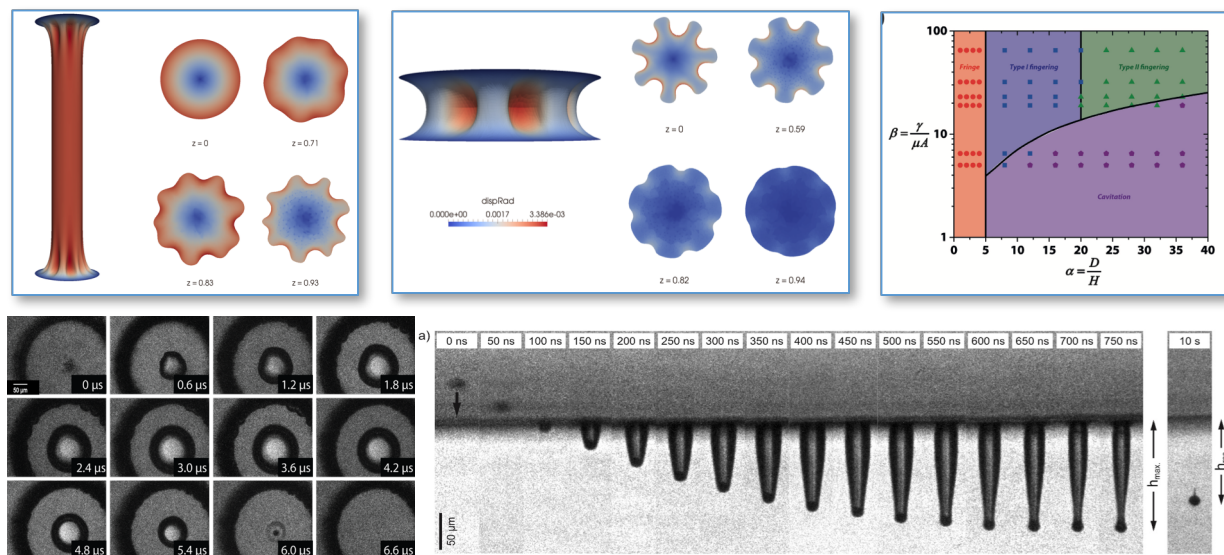


**Figure 4:** Complex response of soft hydrogels to static and dynamic loading. The material exhibits nonlinear elastic instabilities under quasistatic tension: fringe (top left), fingering (top center); cavitation under converging shock loading (bottom left); and deep cratering followed by self-healing in micro-sphere impact penetration.

## Papers Published in Peer-reviewed Journals (Full citation required. Please include DOI if available):

- 1) Lin, S., Mao, Y., Radovitzky R., Zhao X. (May 2017), Instabilities in confined elastic layers under tension: Fringe, fingering and cavitation. *J. Mech. Phys. Solids*. 106, 229-256. doi: 10.1016/j.jmps.2017.05.011.
- 2) Kim, Y., Yuk, H., Zhao, R., Chester S.A., Zhao X. (June 2018), Printing ferromagnetic domains for untethered fast-transforming soft materials. *Nature*. 558, 274-279. doi: 10.1038/s41586-018-0185-0.
- 3) Veysset, D., Kooi, S.E., Maznev, A.A., Tang, S., Mijailovic, A.S., Yang, Y.J., Geiser, K., Van Vliet, K.J., Olsen, B.D., Nelson, K.A. (14 June 2018), High-velocity micro-particle impact on gelatin and synthetic hydrogel. *J. Mech. Behav. Biomed. Mater.* 86, 71-79. doi:10.1016/j.jmbbm.2018.06.016.

## Peer-Reviewed Conference Proceeding Publications (Full citation required. Please include DOI if available):

None

## Books and Book Chapters:

None



---

***Presentations at Meetings, but not Published in Conference Proceedings:***

- 1) Lin, S. (2017, Dec). Elastic instabilities in confined layers under tension. Oral presentation at International Mechanical Engineering Congress & Exposition 2018, Tampa, Florida (USA)
- 2) Veysset, D. (2018, June). Advances in laser-induced microparticle impact experiments. Poster session presented at the Forum Lasers et Plasmas 2018, Saint-Pierre d'Oléron (France).

***Patents, Patent Applications, and IP Disclosures:***

None

***Doctoral Degrees Awarded During Reporting Period (First and Last Name):***

None

***Master's Degrees Awarded During Reporting Period (First and Last Name):***

None

ISN Project Number: 1.2

Project Title: **Shock Mitigating and Reinforcing Molecular Nanocomposites**

Principal Investigator(s): **Michael Strano, (K. Nelson as adviser)**

### Summary of Accomplishments:

#### Autoperforation of graphene as a fabrication technique to fabricate colloidal electronics

Extending nanoelectronics into traditionally inaccessible locations using devices with form factors of a colloidal microparticle represent an emerging field in materials science and semiconductor physics. Herein we developed a nanofabrication technique called *autoperforation* to make colloidal electronic devices. Usually, large-area graphene prepared by the chemical vapor deposition (CVD) method carry intrinsic nanometer-sized defects originating from the CVD growth as well as subsequent transfer processes. However, the seed crack formation from these randomly orientated defects is stochastic, prevents the brittle fracture from being used as a controlled nanofabrication technique. We found that according to the numerical simulation of the graphene fracture, a heterogeneous strain field imposed on the 2D material is predicted to both attract crack growth and guide the crack trajectory along the path of maximum hoop strain (**Figure 1A**). In particular, one can establish such a hoop strain within a thin sheet by conforming/folding it over either a rigid substrate with Gaussian curvature<sup>11</sup> or disk-shaped polymer protrusions used in this study (Thin film A of **Figure 1B-C**). Such folding and stretching, together, can afford lattice strains up to 1% at a disk aspect ratio (radius versus height) of 100:1 (**Figure 1A**), large enough to reduce the 2D material's local Griffith length ( $a_c$ ) down to several nanometers. With an  $a_c$  on the same order of magnitude with the length scales of the intrinsic defects, the seed cracks in 2D sheets can grow spontaneously, generating circular particulates (**Figure 1A&D**). Thus in our experiment, after stacking and annealing, the sandwiched structure is lifted off by selectively dissolving away the PMMA layer, hatching the microdisks with a perfect yield. During the fracture course, the microdisk array guides the crack path of the conformed graphene sheets along the disk edges during this liftoff (**Figure 1D**), that is why we term this process as “*autoperforation*”.

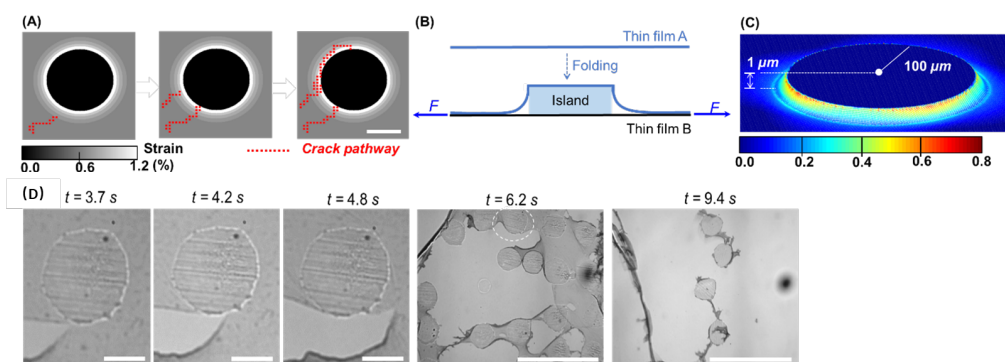


**Figure 1.** Autoperforation of 2D materials for microparticles with 2D surface. (A) Simulation of the fracture propagation of the graphene with an encapsulated polystyrene spot ( $h = 1 \mu\text{m}$ ). Scale bar,  $100 \mu\text{m}$ . (B) Schematic illustration of folding thin film A on to an island and stretching thin film B covered by the same island under force  $F$  to create local strain field synergistically. (C) The local strain field after stacking/folding a thin polymer film ( $200 \text{ nm}$ ) onto a microspot (radius/height =  $100/1$ ) based on finite element analysis. (D) Fracture and crack propagation of graphene layers around a single spot ( $t = 3.7\text{-}4.8\text{ s}$ . Scale bars,  $100 \mu\text{m}$ ) and multiple spots ( $t = 6.2\text{-}9.4 \text{ s}$ . Scale bars,  $1 \text{ mm}$ ) during the liftoff observed under an optical microscope.

#### Optically Active Archimedean Scroll Fibers of MoS<sub>2</sub>/PMMA Composites

The use of polymers as matrices can provide MoS<sub>2</sub> or other 2D sheets the mechanical strength and flexibility to become a free-standing structure, which may allow the device applications of the composite bodies. Herein, we created the layered planar composite and Archimedean scroll fiber consisting of monolayer MoS<sub>2</sub> and PMMA matrix. We studied the Raman shifts of the scroll fiber under uniaxial strain in range of 0-4%, which was applied



along the longitudinal axis of the fiber using a motorized translation stage. We mapped the Raman spectra continuously during the stretching process (Figure 2A). In  $E_{2g}$  mode under stretching, the Raman peaks shift downward up to 0.25% strain (Figure 2B), in consistent with the reported experiment. Interestingly, Raman peaks shift upward at 0.25-1% strain. The peak wavenumber becomes a constant at strain > 2%. The Raman spectra under relaxing show little hysteresis compared to the stretching one. These results suggest that the larger strain may cause in-plane slippage between MoS<sub>2</sub> and PMMA. In our previous work, we have observed such slippage at strain higher than 0.5% in graphene/polycarbonate nanocomposites.

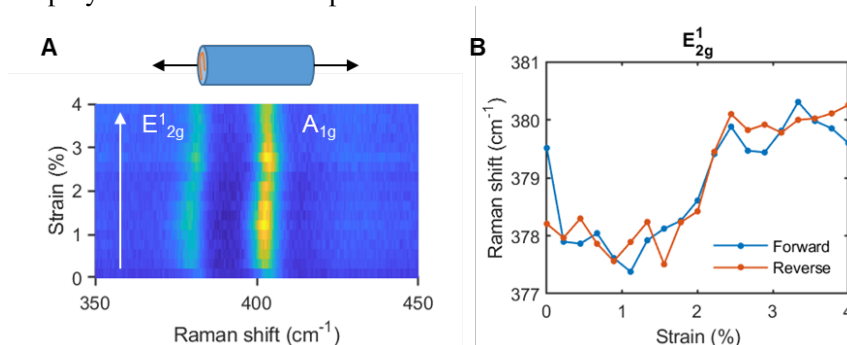


**Figure 2.** (A) Intensity map of Raman spectra of MoS<sub>2</sub>/PMMA scroll fiber under uniaxial strain. (B) Peak wavenumber of Raman  $E'_{2g}$  modes.

### Observation and Spectral Assignment of a Family of Hexagonal Boron Nitride Lattice Defects

Defects in 2D materials initiate fractures of the layers and affect their mechanical properties. Hexagonal boron nitride (hBN) allows us to detect photoluminescence (PL) even from a single defect. The challenge originates from multi-color PL peaks that have not been assigned to their chemical and electronic structures. To address the problem, Strano Research Group has developed a powerful tool to investigate the liquid-phase exfoliation of hBN nanosheets, where the instrument is based on conductive and photocurrent spectral atomic force microscopy (C- and PCS-AFM) combined with a spectrometer. This is called Scanning Probe Imaging for Chemical, Impedance, and Electro-optical Reconstruction (SPICIER). This technique allows correlating multiple aspects of material from topography, electrical and optical viewpoints in a single platform. Accessing individual defects in hBN, we can characterized their fundamental optical properties. Incorporating PL excitation (PLE) spectroscopy, time-resolved PL (TRPL), and hyperspectral mapping on the instrument enables to describe the photophysical properties of hBN color center. This characterization technique may be applicable not only to defects of hBN structure, but also to the other nanoparticles and nanosheets.

### Formation of nanometer-sized defects in single-layer graphene and their gas permeation properties

Defects in single-layer graphene affect its mechanical strength and its performance as a filter material. We found that that defects in graphene forms during the chemical vapor deposition (CVD) growth and this process is related to the oxidation treatment of the Cu substrate before the graphene growth process. Specifically, we studied the defect formation by introducing 0-10  $\mu\text{mol}$  of oxygen into the CVD furnace at 1077  $^{\circ}\text{C}$  before the carbon source ( $\text{CH}_4$ ) was fed. We concluded that due to the formation of copper oxide nanoparticles (NPs) on the Cu surface, the oxidation treatment introduces topographical heterogeneity which increases the number of active sites for graphene nucleation surrounding the NPs. On the other hand, graphene growth is prohibited on top of these oxide NPs, leading to the defect formation. As shown in Figure 3, the D peak in the Raman spectrum (indicating the formation of graphene defects) emerges only when a moderate amount of  $\text{O}_2$  (3  $\mu\text{mol}$ ) is introduced. When the oxidation is excessive (9  $\mu\text{mol}$   $\text{O}_2$ ), the copper oxide nanoparticles coalesces and forms a flat  $\text{Cu}_2\text{O}$  film, removing the

topographical heterogeneity and eliminating defect formation in graphene. This finding is noteworthy because it suggests that the homogeneity of CVD-grown graphene is dependent on the  $O_2$  level of the CVD furnace, which should be treated carefully.

On the other hand, this pre-oxidation strategy can provide us with porous graphene membranes with controlled gas separation abilities. The gas permeation measurements constitute a powerful tool for not only characterizing nanometer-scale pores created in graphenes but also reflecting the existence of micron or larger size defects. For those membranes with large pore size, the gas permeance did not vary substantially as a function of temperature. However, when the pore size is comparable to the gas molecules, an energy barrier is observed, supported by the dramatic increase of gas permeance from 27 to 100 °C.

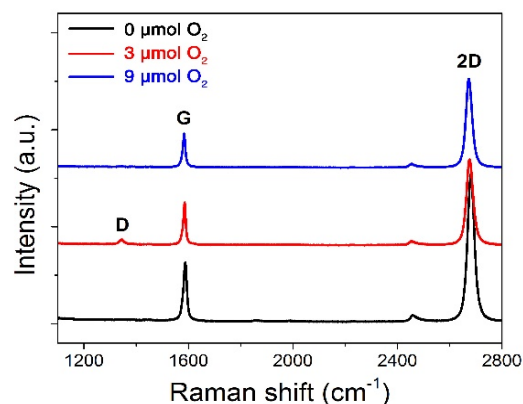
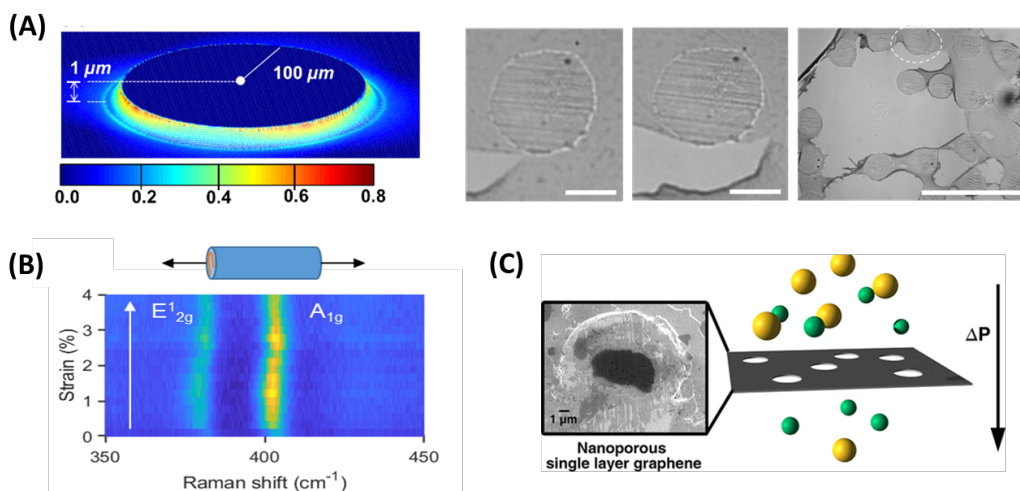


**Figure 3.** Raman spectra of single layer graphene grown on Cu substrates oxidized by different amount of  $O_2$ .

### Research Plans for Next Year:

1. The autoperforation technique should in principle scales to all length scales as well as to fabricate composite particles of all shapes. In the next year, we plan to explore this potential by making particles of many shapes and many sizes next year.
2. Generate 4 stacks and shear scrolling fibers with different 2D materials such as MoS<sub>2</sub> and hBN, and test mechanical properties at ARL Aberdeen. Correlate optical characterization of hBN defects with their mechanical properties in 4 stacks and shear scrolling fibers under force fields.
3. We will calibrate the correlation between the nanopore size and the  $O_2$  dosage for better control over the defects. We will also test the nanoporous membrane for other separation problems, such as C1-C4 alkanes and linear/branched alkanes.

### Representative Image and Caption:



**Rep. Image:** (A) Autoperforation to fabricate colloidal electronics. (B) Optically active Archimedean scroll MoS<sub>2</sub>/PMMA fibers. (C) Gas permeation properties of single-layer graphene with nanometer-sized defects.

***Papers Published in Peer-reviewed Journals:***

- 1) Yuan, Z.; Benck, J. D.; Eatmon, Y.; Blankschtein, D.; Strano, M. S. (Date of publication). Stable, Temperature-Dependent Gas Mixture Permeation and Separation through Suspended Nanoporous Single-Layer Graphene Membranes. *Nano Lett*, **2018**, 18 (8), 5057–5069. doi: 10.1021/acs.nanolett.8b01866
- 2) Liu, P.; Cottrill, A. L.; Kozawa, D.; Koman, V. B.; Parviz, D.; Liu, A. T.; Yang, J.; Tran, T. Q.; Wong, M. H.; Wang, S.; Strano, M. S. Emerging trends in 2D nanotechnology that are redefining our understanding of “Nanocomposites”. *Nano Today*, **2018**, doi.org/10.1016/j.nantod.2018.04.012.

***Peer-Reviewed Conference Proceeding Publications:***

- 1) none

***Books and Book Chapters:***

- 1) none

***Presentations at Meetings, but not Published in Conference Proceedings:***

- 1) (Invited) Autoperforation of 2D Materials for Generating Two Terminal Memresistive Janus Particles, oral presentation, **233rd ECS Meeting**, Seattle, WA.
- 2) Synthetic electronic cells: distributed, modular, particulate electronic devices as a platform for emergent intelligence, poster, **MIT Intelligence Quest 2018**, Boston, MA.

***Patents, Patent Applications, and IP Disclosures:***

- 1) Liu, A. T.; Liu, P.; Koman, V.; Kozawa, D.; Strano, M. S. 2D Electronic Microparticles. (2017) US 62/525,752.

***Doctoral Degrees Awarded During Reporting Period (First and Last Name):***

none

***Master's Degrees Awarded During Reporting Period (First and Last Name):***

none

ISN Project Number: 1.3

Project Title: **Design and Testing of Polymers for Improved Soldier Protection**

Principal Investigator(s): **Keith Nelson, Tim Swager, Greg Rutledge**

### Summary of Accomplishments:

The overall goal of this project is to investigate the fundamental mechanisms that govern the high-rate mechanical response of polymers through an integrated effort including material synthesis, material characterization and modeling (Fig. 1). We aim at identifying the key attributes for energy absorption and dissipation, including the role of hydrogen bonding, to guide the synthesis of novel materials with improved performance. The PI groups work with ARL collaborators, Alex Hsieh, Jan Andzelm and In-Chul Yeh, who interact closely at MIT (Hsieh) and participate remotely in our monthly team meetings.

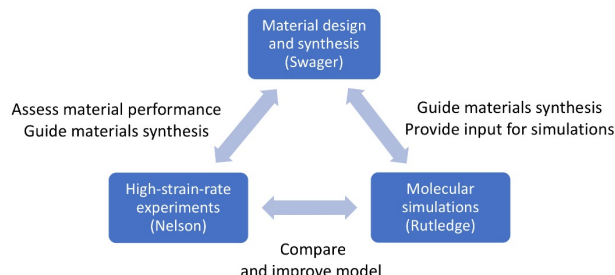
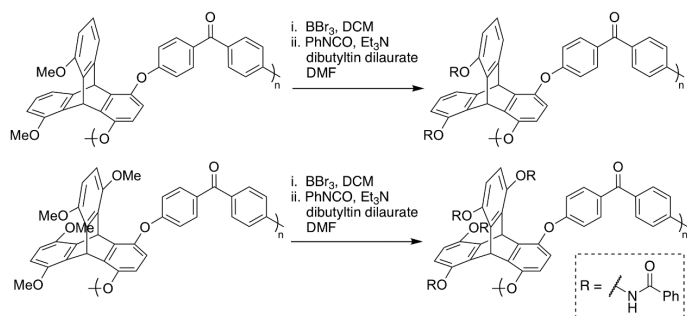


**Figure 1.** Integrated efforts to develop new materials with improved performance in ISN.

In our design and synthesis of novel polymers, we sought to incorporate triptycene-based poly(ether ether ketone)s and poly(ether ether sulfone)s (TripPEEKs and TripPEESs) into materials with enhanced strength, toughness, and energy dissipation. As hydrogen bonding (H-bonding) is key to such properties in thermoplastic polyurethanes (TPUs), we set out to produce TripPEEKs and TripPEESs functionalized with H-bonding groups. In addition to the high strength afforded by the high- $T_g$  backbone polymer, such materials could demonstrate improved flexibility and ductility owing to interpenetration of soft segments (SSs) within the free volume of the triptycene moiety [1]. H-bond donor and acceptor properties can be used to direct novel assemblies and phase segregation behavior.

Initial efforts focused on appending simple H-bonding groups to TripPEEK to enhance compatibility with conventional TPUs. Based on methoxy-substituted TripPEEKs developed in the Swager lab, we successfully

**Scheme 1.** Synthesis of carbamate-functionalized TripPEEK.



synthesized TripPEEKs functionalized with carbamate groups (Scheme 1). We envisioned that blending these materials with TPUs could provide enhanced modulus. Solution-cast blends with a conventional poly(urethane urea) (PUU) were subject to dynamic mechanical analysis (DMA), which revealed a significant decrease in storage moduli as compared to the unblended PUU. We hypothesize that this could be attributed to the disruption of H-bonding associated with the bidentate urea-urea and urea-urethane linkages of the PUU upon blending with the TripPEEK derivatives.

To address compatibility issues and enhance phase mixing with TPUs, we envisioned a rigid TripPEEK or TripPEES backbone grafted with flexible H-bonding polymers. Such brush architecture is also known to give rise to self-healing behavior [2]. We selected cationic ring-opening polymerization of oxazolines as a promising route, which should provide efficient reactivity due to its living character. Hydroxymethyl-TripPEES was converted to the mesylate to serve as the macroinitiator, from which we have grafted poly(2-ethyl-2-oxazoline) and poly(2-pyrrolidino-2-oxazoline) (see Representative Image, a). Both polymers are H-bond acceptors only, with the pyrrolidine substituent producing a tertiary urea, a very strong acceptor. Based on such H-bonding properties, we anticipated that these polymer brushes would strongly interact and phase mix with H-bond-donating polymers. Taking the brushes as the hard segment, we blended TripPEES-*g*-poly(ethyl oxazoline) with a SS-only PU made from poly(tetrahydrofuran) (PTHF) and hexamethylene diisocyanate (HDI), where the use of HDI produced a

semicrystalline PU. DMA revealed a moderate increase in storage modulus across the rubbery plateau with increasing amount of TripPEES brush polymer in the blends, in contrast to the aforementioned TripPEEK blends; meanwhile, a large drop of storage modulus was noted at temperatures above the melting point of HDI (47 °C) and the glass transition of pEtOx grafts (56-60 °C). Encouraged by the robust synthesis and good mechanical properties of the TripPEES-g-poly(ethyl oxazoline) brush polymers, we will continue to explore synthetic derivatives of this system.

Two TripPEES-g-poly(ethyl oxazoline) blended with PU (20wt% and 40wt%) were tested under the laser-induced particle impact test (LIPIT) and compared with PU. The LIPIT is a table-top all-optical platform that enables real-time visualization of micro-scale high-velocity impacts (see Representative Image, b). Using this platform, we could directly compare the impact response of the samples prepared by the Swager. The rebound velocity  $V_r$  of solid silica spheres (7.4- $\mu$ m diameter) impacting those samples was measured as a function of impact speed  $V_i$ . The coefficient of restitution ( $V_r/V_i$ ) data first reveal that SS-only PU behaves under impact similarly to a previously-tested poly(urethane urea) 211-2000 elastomer (Fig. 2) [3]. Secondly, increasing the TripPEES-g-pEtOx content tends to increase the rebound velocity similar to what was observed for poly(urethane urea) elastomers where the coefficient of restitution at a given speed was shown to be a function of the hard segment content, increasing from 26% for 211-2000 to 44% for the 431-2000 [3]. These observations are indicative of the molecular influence on the dynamic stiffening upon high-velocity impact, as demonstrated with the hierarchical PUU elastomers [3] and now in the case of the TripPEES-g-pEtOx polyurethane blends. In parallel, thin polyethylene (MW 4000 g/mol) films (50- $\mu$ m thick) were impacted using LIPIT with 20- $\mu$ m steel particles. We determined that steel particles rebounded at impact velocities up to 250 m/s, penetrated and remained embedded in the film between 250 m/s and 400 m/s, and perforated at velocities above 400 m/s.

Over the past seven months, the Rutledge group has tested several approaches for the molecular level simulation of polymeric materials under shock deformation conditions. The main effort thus far has been on application of the constant uniaxial stress Hugoniotstat, as developed by Ravelo *et al.* [4] and implemented in the molecular dynamics software LAMMPS [5]. We have tested this method on a system of amorphous polyethylene consisting of several  $C_{100}$  chains equilibrated under ambient conditions. Results from these simulations compare favorably with experimental data published by Agrawal *et al.* for semicrystalline polyethylene (see Reference Image, c) [6]). These data contain trends for several important and measurable parameters, such as specific volume, shock velocity, and particle velocity, and can be simply extended to incorporate other statistical mechanical parameters. We have also generated a model semicrystalline polyethylene system and are currently running shock deformations of this system.

### Research Plans for Next Year:

We will continue to explore synthetic derivatives of the TripPEES-g-poly(ethyl oxazoline) system, focusing on the hydrolysis of the polyoxazoline amides, which will reveal secondary amines that can be further functionalized. Methylation produces poly(methyl ethylene imine), a low- $T_g$  material that can serve as a SS, while reaction with isocyanates and isothiocyanates affords ureas and thioureas, which are H-bonding-active, expanding upon the microphase separation and H-bonding properties of PU. These materials will be tested for improved mechanical properties as well as self-healing behavior. Guided by DMA results, we will continue to explore polymer blends with varying components. We will expand the scope of diols and diisocyanates in the PU, such as using HMDI to

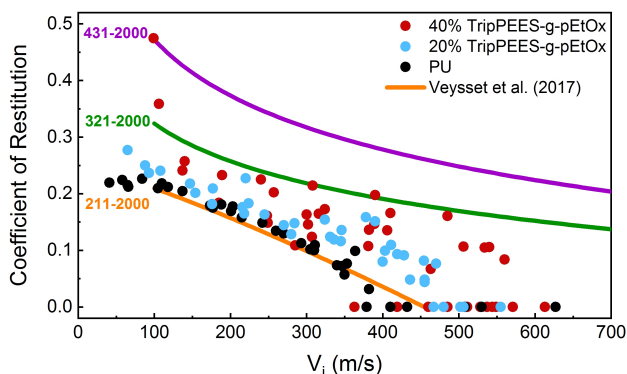


**Figure 2.** Coefficient of restitution as a function of impact speed for TripPEES-g-pEtOx and previously-tested poly(urethane urea) elastomers [1].



decrease crystallinity. Derivatives of TripPEES-g-poly(ethyl oxazoline) with varying H-bonding properties will be incorporated in order to modulate interactions with the PU and thus the microphase structure.

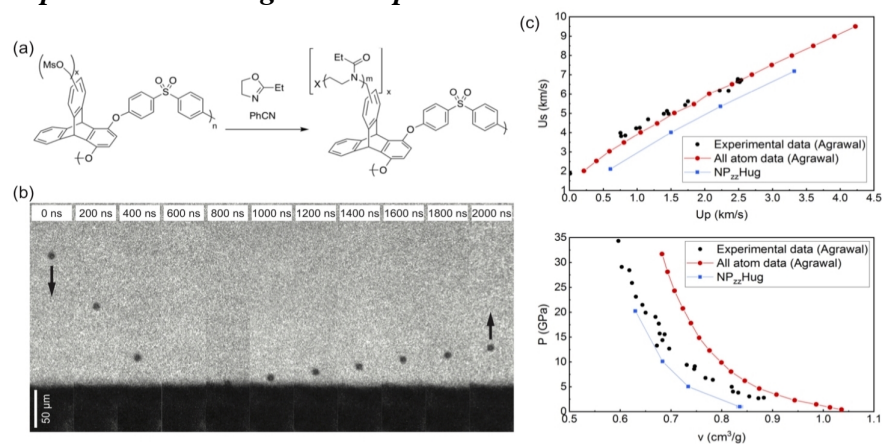
Impact experiments will be conducted on the different samples provided by the Swager group to assess impact performance and guide further material synthesis. We will continue to impact polyethylene films and study the influence of the molecular weight on the impact behavior. We also plan to conduct shock experiments using an in-house-designed laser-induced micro-shock platform [7]. Efforts are underway to implement femtosecond stimulated Raman scattering (FSRS) [8] into the existing micro-shock platform. FSRS measurements on shock-compressed samples provided by the Swager group will help elucidate the role and extent of H-bonding in the material's shock response. Results from both *in situ* spectroscopy and imaging (index of refraction) will be compared with Rutledge group results to help guide both the experimental and modeling efforts.

On the molecular simulation front, we plan to conduct further analysis of our current systems, including possible identification of a Hugoniot elastic limit (HEL) [4]. We will also expand our material search space to examine other complex and heterogeneous materials, in particular semicrystalline polyethylene and a thermoplastic polyurethanes (TPUs), both of which have been simulated previously in the group under isothermal high strain rate conditions [9], [10]. Our main interest lies in understanding how the shock wave changes as it navigates the interface between domains of mismatched compliance. In the case of semicrystalline polyethylene, we plan to contrast the mechanisms of response for shock deformation with those for isothermal deformation, and to simulate deformations parallel and perpendicular to the crystalline-amorphous interface, to understand the anisotropy of response. For these complex materials, it may be necessary to implement a more rigorous method of inducing shockwaves or nonequilibrium (e.g. piston) methods of deformation. We will also conduct vibrational analysis on the materials [11], including characterization of optical properties of the polymers (e.g., index of refraction), for comparison to experimental measurements by the Nelson group.

## References

- [1] N. T. Tsui, A. J. Paraskos, L. Torun, T. M. Swager, and E. L. Thomas, *Macromolecules* **39**, 3350 (2006).
- [2] Y. Chen, A. M. Kushner, G. A. Williams, and Z. Guan, *Nat. Chem.* **4**, 467 (2012).
- [3] D. Veysset, A. J. Hsieh, S. E. Kooi, and K. A. Nelson, *Polymer* **123**, 30 (2017).
- [4] R. Ravelo, B. Holian, T. Germann, and P. Lomdahl, *Phys. Rev. B* **70**, 014103 (2004).
- [5] S. Plimpton, *J. Comput. Phys.* **117**, 1 (1995).
- [6] V. Agrawal, P. Peralta, Y. Li, and J. Oswald, *J. Chem. Phys.* **145**, 104903 (2016).
- [7] T. Pezeril et al. *Phys. Rev. Lett.* **106**, 214503 (2011).
- [8] D. W. McCamant, P. Kukura, S. Yoon, and R. A. Mathies, *Rev. Sci. Instrum.* **75**, 4971 (2004).
- [9] S. Lee and G. C. Rutledge, *Macromolecules* **44**, 3096 (2011).
- [10] S. Zhu, N. Lempeis, P. J. in 't Veld, and G. C. Rutledge, *Macromolecules* **51**, 1850 (2018).
- [11] A. L. Brayton, I.-C. Yeh, J. W. Andzelm, and G. C. Rutledge, *Macromolecules* **50**, 6690 (2017).

## Representative Image and Caption



**Rep. Image:** (a) Synthesis of TripPEES-g-poly(ethyl oxazoline). (b) Image sequence recorded showing silica particle impact on a TripPEES-g-poly(ethyl oxazoline) – PU blend sample. at 330 m/s. The time stamps, shown at the top of the frames, indicate the delay in acquisition time relative to the first frame. (c) Results from constant uniaxial stress Hugoniot (NP<sub>xx</sub>Hug) simulations at four different uniaxial stress ( $P_{xx}$ ) values, plotted along with data from Agrawal et al. (top) Shock velocity vs. particle velocity, and (bottom) pressure vs. specific volume.

***Papers Published in Peer-reviewed Journals*** (Full citation required. Please include DOI if available):

- 1) Hsieh, A. J., Veyssset, D., Miranda, D. F., Kooi, S. E., Runt, J., Nelson, K. A. (15 May 2018), Molecular influence in the glass/polymer interface design: The role of segmental dynamics. *Polymer*, 146, 222-229. doi: 10.1016/j.polymer.2018.05.034. Army collaborator: Alex J. Hsieh.

***Peer-Reviewed Conference Proceeding Publications*** (Full citation required. Please include DOI if available):

None

***Books and Book Chapters:***

None

***Presentations at Meetings, but not Published in Conference Proceedings:***

- 1) Veyssset, D. (2018, June). Advances in laser-induced microparticle impact experiments. Poster session presented at the Forum Lasers et Plasmas 2018, Saint-Pierre d'Oléron (France).

***Patents, Patent Applications, and IP Disclosures:***

None

***Doctoral Degrees Awarded During Reporting Period (First and Last Name):***

None

***Master's Degrees Awarded During Reporting Period (First and Last Name):***

None

**ISN Project Number: 1.4**

**Project Title: Superelastic Granular Materials for Impact Absorption**

**Principal Investigator(s): Chris Schuh, Raúl Radovitzky, Kenneth Kamrin**

### ***Summary of Accomplishments:***

The overarching goal of this project is to understand and quantify the dissipation of mechanical energy by granular superelastic ceramics. From small size scales like single particles or micropillars all the way to granular packings of thousands of particles, we intend to understand energy dissipation in superelastic zirconia by designing and executing mechanical tests over a wide range of strain rates, ranging from quasi-static to impact events. In parallel, we will develop a modeling capability for these new functional granular materials that spans scales from the individual particle level to the full granular scale. This includes a constitutive framework describing the mechanical response of the superelastic ceramic constituent at the single-crystal micrometer level, and a Discrete Element Method (DEM) able to model interactions between contacting oligocrystalline particles. These will then be used to validate constitutive models in the future that represent large systems of particles.

#### **Experimental – Team Schuh**

The experimental work to this point has focused on the fabrication and characterization of ceria doped zirconia, the design and implementation of a compression test for granular packings, and the fabrication of superelastic zirconia composites. A modified Pechini method is used to fabricate ceria doped zirconia powder, which is then characterized using laser particle size analysis to determine particle size distribution, electron microscopy to understand particle morphology, and x-ray diffraction to quantify the amount of each phase in the zirconia powder. In order to probe the mechanical response of a granular packing (about 300 mg of ceria doped zirconia powder at a time), a die compression rig is presently being validated. In addition to the granular packings tests, ceramic-polymer composites are being investigated in collaboration with Dr. Alex Hsieh of ARL, who specializes in energy absorbing polymeric materials, with whom we have fabricated composites using our powders and his polymers.

#### **Single-crystal Modeling – Team Radovitzky**

We have developed a micromechanics-based anisotropic constitutive model for single-crystal zirconia built upon the continuum mechanics framework of previously developed models for shape memory alloys. An important feature of the model is that it captures the formation of martensite microstructure during phase transformation by adopting the geometrically nonlinear theory of phase transformation to account for transformation strains of different martensitic variants. In the model, the flow rule of the phase transformation is adopted from that in crystal plasticity theory, assuming similarity in the inelastic deformation between phase twinning and crystallographic slip. Thus, the concept of a ‘transformation system’ is introduced to describe the geometrical configuration of martensite-austenite interfaces. The phase transformation condition is then modified to include rate-dependence with two additional material parameters, which facilitates the development of a robust explicit algorithm for updating the constitutive law. The model is implemented in SUMMIT, a scalable finite element solver developed by Radovitzky's research group. Using this constitutive model, we have performed preliminary numerical tests on the stress-strain response and evolution of martensite volume fraction of a single-crystal zirconia specimen subjected to cyclic loading in isothermal conditions. Our model successfully captures the temperature-dependence and orientation-dependence, as well as the strain rate-dependence of phase transformation in single-crystal zirconia. Our continuing effort is to calibrate the material parameters in the constitutive model using the compression tests conducted by the Schuh group.

#### **Multi-particle Modeling – Team Kamrin**

An oligocrystalline particle is composed of a small number of crystalline grains, and is therefore characteristically anisotropic in its mechanical response. Likewise, a fundamental ingredient of any successful DEM representation of such systems is the ability to represent particle anisotropy through contact laws that correctly account for the anisotropy of the particle pair. To this aim, as a key first step, we have developed a novel DEM that allows each



particle to have anisotropy in its elastic response. Achieving this requires the addition of a tensorial orientation variable within each particle, which rotates with the particle. When particles come in contact, an effective contact modulus is calculated based on resolving the Young's moduli of each particle onto the contact normal. The analysis is similar to that of the classical Hertz derivation but with anisotropy. We tested the method on a polydisperse system of 10,000 anisotropic particles, with moduli and anisotropy selected to be similar to experimental particles. The test geometry was one of downward impact of a plate onto a bin of particles. By considering systems in which the major anisotropy direction of all grains is orthogonal to the impact direction vs. aligned with the impact vs. random, we successfully found that the bulk wave speed changes as expected, with faster wave speeds occurring when the particle anisotropies are more aligned with the impact direction.

### ***Research Plans for Next Year:***

#### **Experimental – Team Schuh**

We will continue the fabrication and characterization of ceria doped zirconia powder that will be used in the compression testing of granular packings. In addition, we will pursue drop weight testing of the superelastic powders, which is also a compression test but is conducted at a greater strain rate. These results will be compared to the quasi-static compression test to determine the effect of strain rate on superelastic behavior. The results of these tests will also be incorporated into the modeling efforts of our collaborators on this project. A study of the size effect on phase transformation of the superelastic ceramics is also underway. The composites research with Dr. Hsieh will also continue to determine the high strain rate response of these materials.

#### **Single-crystal Modeling – Team Radovitzky**

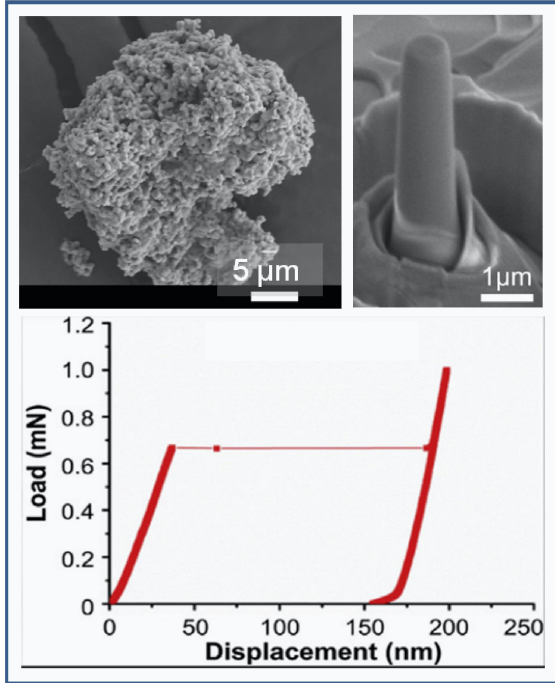
Our next step is to continue to validate the constitutive model against micro-pillar compression tests. The validation of the constitutive model requires experimental data as input and the Schuh group is providing data from micro-pillar testing, such as transformation stresses and strains, elastic constants, and sample orientations. We will also incorporate size-dependency into the constitutive model to account for the size effects in zirconia observed by the Schuh group. With the validated model, we can perform large-scale finite element simulations in SUMMIT to simulate the oligocrystal particle experiments conducted by the Schuh group and to study the interactions among crystalline grains in the oligocrystal particles. We can also utilize the discontinuous Galerkin formulation in SUMMIT to investigate the possibility of inter- and intra-grain cracking in the oligocrystal particle due to stress concentrations.

#### **Multi-particle Modeling – Team Kamrin**

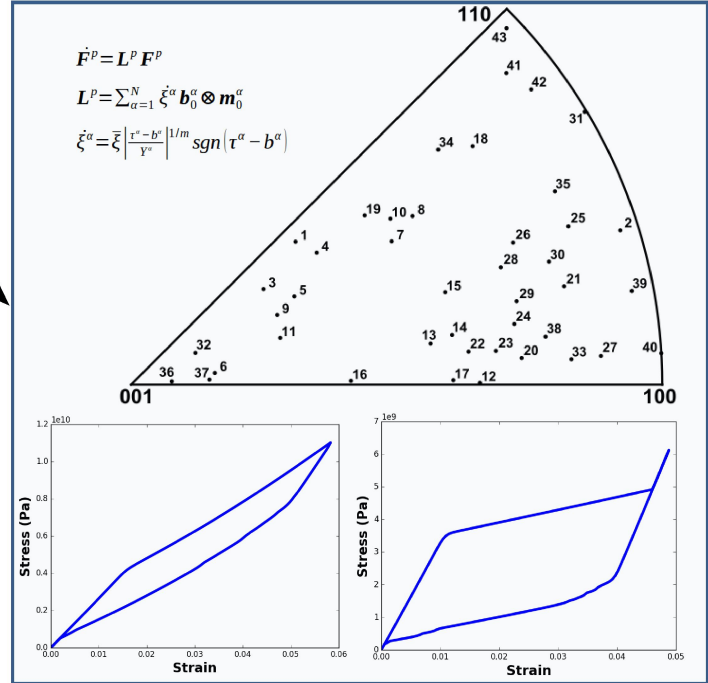
As new experimental data on the mechanical response of oligocrystalline particles is obtained, as well as information on shape distributions, and statistical variation of mechanical behaviors, we will continuously fine-tune and expand the DEM capability so as to best represent the real particles. Our plan is to work with the other PI's to extract key ingredients from their new mechanical tests to obtain a homogenized constitutive model within each particle. Once an accurate, homogenized model of a single particle is complete, it becomes the key piece to calculating the improved contact interaction between particle pairs.

**Representative Image and Caption:**

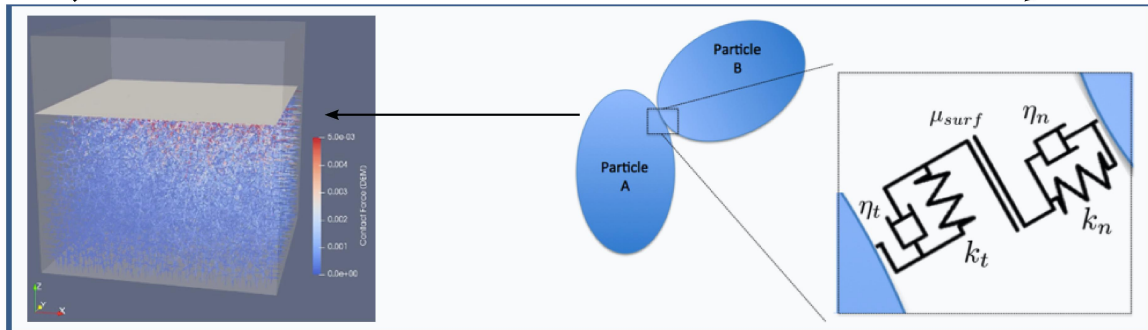
**A) Experimental Data Collection**



**B) Single-Crystal Modeling**



**C) Multi-Particle Modeling**



**A)** Experimental - Compression tests on single particles and micropillars result in characteristic load vs. displacement curves showing superelastic behavior. **B)** Single-Crystal Modeling - Using the micromechanics based constitutive model, we show the orientation dependence of the stress-strain response in single-crystal zirconia. **C)** Multi-Particle Modeling - A discrete element method was used to model the interactions between contacting oligocrystalline particles. This method was tested on a polydisperse system of 10,000 particles.



***Papers Published in Peer-reviewed Journals*** (Full citation required. Please include DOI if available):

None

***Peer-Reviewed Conference Proceeding Publications*** (Full citation required. Please include DOI if available):

None

***Books and Book Chapters:***

None

***Presentations at Meetings, but not Published in Conference Proceedings:***

- 1) Zhiyi Wang, 2018.5. “Computational Framework for Simulating the Deformation and Fracture Response of Oligocrystalline Shape Memory Alloy”, Engineering Mechanics Institute Conference 2018, MIT.
- 2) Zhiyi Wang, 2018.7. “Numerical Modeling of Oligocrystalline Shape Memory Alloys”, 2018 13<sup>th</sup> World Congress on Computational Mechanics & 2nd Pan American Congress on Applied Mechanics, New York City.
- 3) Christopher Schuh, 2018.1, “Evaluation of Crystallographic Matching in ZrO<sub>2</sub>-CeO<sub>2</sub> Shape-Memory Ceramics”, 42<sup>nd</sup> International Conference on Advanced Ceramics and Composites, Daytona Beach, FL

***Patents, Patent Applications, and IP Disclosures:***

None

***Doctoral Degrees Awarded During Reporting Period (First and Last Name):***

Tyler Olsen

***Master’s Degrees Awarded During Reporting Period (First and Last Name):***

Zhiyi Wang



**ISN Project Number: 1.5**

**Project Title: *Rapid Hemostasis for the Treatment of Incompressible Wounds***

**Principal Investigator(s): *Bradley Olsen, Paula Hammond, Shuguang Zhang***

***Summary of Accomplishments:***

**Aim 1: Develop fully resorbable sponges to treat open wounds.** Sponges will be developed that are shelf-stable and coated with biomimetic self-assembling peptides and/or clotting proteins at very high loadings using alternating electrostatic assembly to build ultrathin film nanolayers with high amounts of drugs. These dry, lightweight packs will be designed to enable rapid release in plasma with *minimal pressure placement* to address the large number of areas not amenable to tourniquets, significant compression and similar approaches.

***Accomplishments:*** Work has progressed on the optimization of the reproducibility and peptide loading in LbL films. Large variance between peptide solutions led to the need for a more consistent and optimized sample preparation prior to layering in films. This optimization was done through the use of transmission electron microscopy to observe the change in fiber length and structure with time after sonication. In addition to this a quartz crystal microbalance with dissipation was used to select optimal solution contact times for LbL film growth. Film growth and peptide release has been evaluated using these new sample preparation protocols. The work to develop this standard method will help improve reproducibility of future experiments as well as the efficacy of our LbL systems.

**Aim 2: Engineer shear-thinning injectable protein gels based on fibrin-mimetic proteins to treat deep penetrating wounds.** Gels will be designed that can be delivered from a pre-packed syringe directly into a deep penetrating wound, forming a durable solid that induces contact clotting of blood and stays in the wound site. The bioresorbable gels will be developed by engineering fibrin-mimetic biosynthetic protein polymers that contain structural and functional mimetics of natural clotting proteins, allowing the hemostatic gel to integrate with and supplement natural clotting mechanisms.

***Accomplishments:*** In this work, a panel of multifunctional fibrinogen like proteins (MFLP) were designed, expressed, and assessed for hemostatic activity in a series of *in vitro* assays. The primary approach of designing hemostatic materials is the incorporation of biomimetic moieties that can interact with various pathways within the coagulation cascade. Using a telechelic protein sequence as a scaffold, sequences known to interact with blood components (clot interacting peptides, CIPs) were inserted within the protein sequence at the N-terminus when necessary for its function. In total, 14 different proteins of varying molecular weight and CIP functionality. The second approach was to develop a modular plasmid design of  $\alpha$ C proteins that will interact directly with the fibrin network in the clot.  $\alpha$ C proteins act as self-associating hands of fibrin monomers that offer additional structural reinforcement of fibrin polymers. In our work, we expressed both whole and truncated versions of human  $\alpha$ C proteins and inserted coiled coil proteins to the truncated  $\alpha$ C proteins for enhanced self-assembly. Among the selected CIPs, those mimicking enzyme-reactive sequences on fibrinogen were most active. These included a transglutaminase reactive sequence and a knob A mimetic sequence that, when included in a protein sequence, reduced clotting times by 40%, from 9 to 5 minutes, in plasma samples. Clot magnitudes, a measure of the turbidity of the clot using a plate reader, were increased up to 150% when MFLPs were added, relative to control samples. These improvements in clot network stability also led to improved resistance to lysis by plasmin, an enzyme naturally used to lyse fibrin clots which can be present in hemorrhaging patients, and can weaken clots. New manuscripts describing this work are currently in preparation and are anticipated to be submitted soon to peer reviewed journals.

**Aim 3: Design intravenously administered hemostats to target hidden wounds.** In some cases, the source of bleeding is not identifiable on the battlefield. To address these types of injuries, we will design targeted nanoparticles that can be intravenously administered, homing to a wound site and promoting clotting.

Bioorthogonal click crosslinking will be developed to reinforce the clot to prevent re-bleeding, and controlled release from the particles will be used to further promote hemostasis, prevent infection, and aid wound healing.

**Accomplishments:** Poly(ethylene glycol)-block-poly(lactide-co-glycolide) (PEG-b-PLGA) polymers of various PEG and PLGA block lengths were synthesized using ring-opening polymerization or conjugation through NHS/EDC chemistry and screened to select a single formulation for nanoparticle synthesis. Nanoparticles over a hydrodynamic size range of approximately 60 nm to 600 nm were synthesized using the selected polymer in a 5:1 ratio with pure PLGA through a variety of methods, including nanoprecipitation (dropwise addition of polymer in dimethylformamide, tetrahydrofuran, or acetonitrile), dialysis, and oil-in-water emulsion. Following conjugation of the GRGDS peptide, these particles will be tested in a variety of *in vitro* assays to determine an adequate concentration for *in vivo* experiments.

One of the *in vitro* assays mentioned in the previous paragraphs involves the coating of a surface with activated platelets in a recreation of the wound environment. Various coating and activation conditions were investigated, including several combinations of poly-L-lysine and collagen to create a robust collagen surface, a range of platelet concentrations, and agonists such as ADP and soluble collagen to activate the cells. Each component was labeled with a different fluorophore, and the conditions were optimized sequentially to yield the final binding/ activation conditions. Comparison of the various agonists was done through immunostaining of activated platelets

***Additional Accomplishments: Methods and Mechanistic Studies***

To enhance the understanding of materials efficacy and design for each of Aims 1 through 3, a series of imaging assays were also developed to characterize hemostat-clot interactions, providing more *in vitro* methods to characterize established and novel hemostatic materials. A lack of techniques to characterize solid or gel-based hemostats *in vitro*, beyond basic clotting time tests, necessitate that *in vivo* studies be used as a screening method for new hemostats. Developing alternative *in vitro* assays can reduce the time and cost associated with screening potential hemostat candidates and provide new insight into the best design features for a hemostat. Fluorescent and brightfield techniques were used to image the area surrounding a hemostatic material, commonly the first 2-3 mm, in contact with blood components and plasma clots. Modulated distributions of blood components like fibrin, platelets, and red blood cells were observed that were hemostat dependent. A manuscript describing these approaches is currently in preparation for submission to a peer reviewed journal.

***Research Plans for Next Year:***

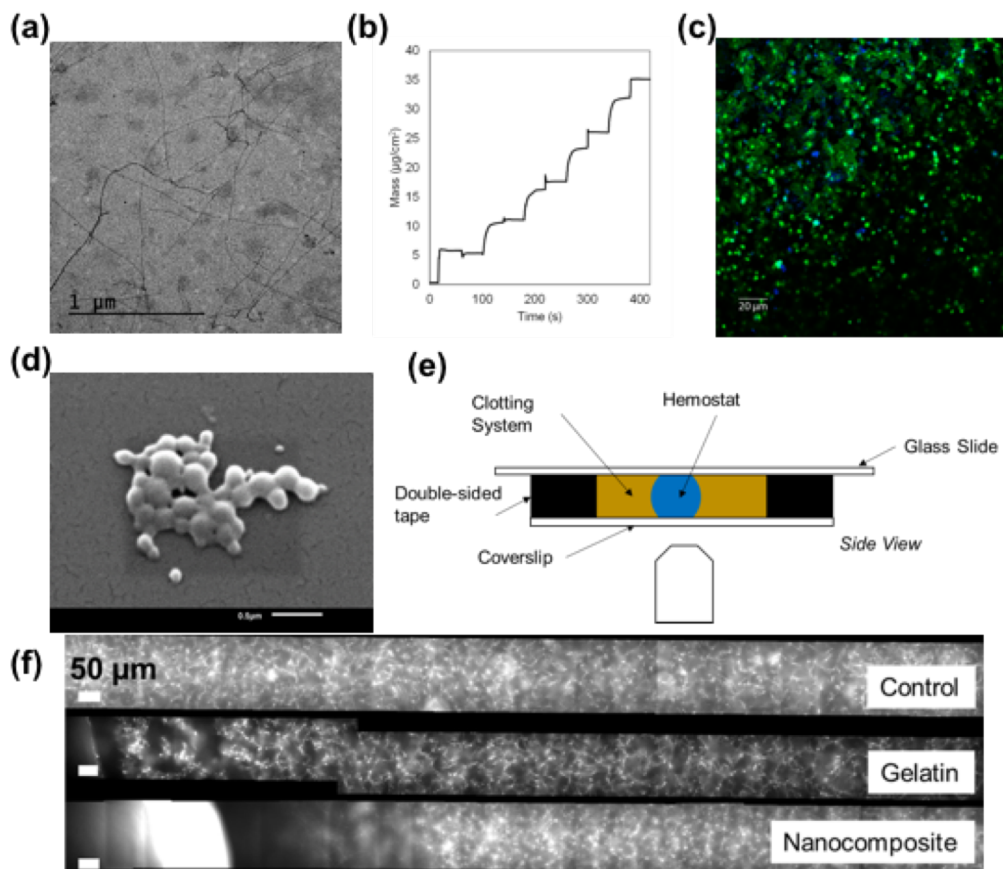
**Aim 1:** Most work will primarily be focused on tasks 1.1 and 1.3. For Task 1.1, approval is currently being obtained for small animal testing here at MIT. Once this approval is obtained, it will be possible to more rapidly screen LbL formulations for rough hemostatic efficacy and tissue interactions in rats. Additionally, we will test for interactions between the self-assembling peptides and different blood components to better understand the mechanism of action these peptides use to aid hemostasis, and whether these mechanisms are altered following release from an LbL film. Finally we will also begin work to address task 1.3 by developing films that contain both hemostats and other functionalities such as antibiotics or oxygen carriers.

**Aim 2:** Future work in the upcoming year include validation of the efficacy of clot enhancement of the protein hemostats. Enhancement of clotting will be measured by 1) platelet rich plasma (PRP) clotting kinetics to determine the speed and magnitude of clot formation, 2) PRP lysis kinetics to determine the stability of the formed clot against the natural lysing mechanism at the site of injury, and 3) determine the mechanical strength of the PRP clot. The best performing proteins can be further optimized for easy delivery and storage.

**Aim 3:** An animal protocol has been submitted to study the biodistribution and circulation time of the nanoparticle size range, which will allow us to eliminate particles that concentrate in organs at a higher risk for fatal embolisms, such as the lungs. In the meantime, the aggregation and coagulation capabilities of the particles in human plasma

will be tested in a well-plate format to optimize for concentration, and the binding capabilities of particles to activated platelets will be evaluated with flow cytometry and the assay described above.

**Representative Image and Caption:**



**Representative Image** (a) Negative Staining TEM imaging of self-assembling peptide nanofibers. (b) QCM data showing mass buildup of a RADA16 LbL film. (c) Platelets (green) immunostained for activation marker P-selectin (blue) and coated on collagen. (d) PEG-b-PLGA nanoparticles imaged via scanning electron microscopy. (e) Schematic of in vitro clot imaging assay. (f) Images showing different responses in clot structure to various hemostats in the clot imaging assay.



---

***Papers Published in Peer-reviewed Journals*** (Full citation required. Please include DOI if available):

- 1) none

***Peer-Reviewed Conference Proceeding Publications*** (Full citation required. Please include DOI if available):

- 1) none

***Books and Book Chapters:***

- 1) none

***Presentations at Meetings, but not Published in Conference Proceedings:***

- 1) none

***Patents, Patent Applications, and IP Disclosures:***

- 1) none

***Doctoral Degrees Awarded During Reporting Period (First and Last Name):***

- **Reginald Avery**, *Design and Performance of Hemostatic Biomaterials for Managing Hemorrhaging*. 2018. MIT, PhD dissertation.

***Master's Degrees Awarded During Reporting Period (First and Last Name):***

None



**ISN Project Number: 1.6**

**Project Title: *Empowering Future Vaccines and Immunotherapies with Nanotechnology-based Adjuvants***

**Principal Investigator(s): Darrell Irvine**

### **Summary of Accomplishments:**

Vaccines are a powerful defense against infectious diseases, and the advent of successful vaccines against diverse pathogens has saved millions of lives to date. However, a number of diseases relevant to the military have remained unsolved challenges for vaccine development, including malaria, tuberculosis, HIV, and ebola. Protein vaccines do not typically elicit an immune response on their own, and must be combined with adjuvants, compounds that provide inflammatory cues or promote the immune response to a co-administered antigen. Adjuvant design is made challenging by the need to strongly drive specific aspects of the immune response while maintaining a rigorous safety profile for administration to healthy recipients. Nanotechnology-based approaches that target vaccine adjuvants or immunomodulators to lymph nodes have the capacity to enhance both the potency and safety of vaccines, by focusing adjuvant activity in tissues where immune responses are initiated and avoiding systemic exposure. We are developing two distinct nano-adjuvant strategies to augment these vaccines, using self-assembling STING agonist amphiphile-adjuvants and saponin nanoparticles (see “Representative image” and caption below).

### **STING agonist amphiphile-adjuvants**

As described in our original proposal, within Aim 1 our main goal is to use self-assembling peptide nucleic acid (PNA) amphiphiles to efficiently deliver a STING agonist (STimulator of INterferon Genes) to the immune cell populations that promote a robust protective immunity to the co-administered antigen, with the additional benefits of avoiding undesired systemic side-effects and minimizing the required dose. The amphiphiles we have synthesized have a peptide nucleic acid (PNA) headgroup designed to reversibly complex the STING agonist cyclic di-guanine monophosphate (cdGMP). Incorporation of these PNA amphiphiles into appropriate nanostructures will promote drainage from the injection site via the lymph and uptake by antigen-presenting cells, such as dendritic cells. At the same time, favoring lymphatic drainage will limit diffusion into the vasculature, which can lead to both rapid excretion and unproductive systemic inflammation.

We first synthesized a number of PNA amphiphile structures, as shown in Figure 1A, and examined how changing aspects of the chemical structure affect their self-association behavior in aqueous solution. For example, the PNA amphiphiles with structures **1** and **2**, which vary only in that **1** has a hydrophobic tail derived from palmitic acid ( $C_{16}$ ) and **2** has a hydrophobic tail derived from stearic acid ( $C_{18}$ ), form long worm-like micelles that appear to be well dispersed and flexible by TEM (Fig. 1B). Amphiphiles **3** and **4** form a mixture of long, relatively straight worm-like micelles and smaller structures which may be spherical micelles (Fig. 1C). We suspect that the increased length and greater flexibility of the linking group in **3** and **4** allows for tighter packing of the amphiphiles and thus promotes greater association between the headgroups. In all of the amphiphiles, the addition of cdGMP leads to formation of extensive networks of nanofiber bundles (Fig. 1D). The increased association between nanofibers is likely a result of the nanofibers having a surface charge closer to zero as the negatively-charged cdGMP binds to the positively-charged headgroups. These nanofiber networks have shown the ability to potentially increase STING signaling *in vitro* using a RAW mouse macrophage STING reporter cell line (not shown). However, these nanofiber networks are both too large and too variable in size to be considered optimal structures for the delivery of adjuvant to the lymph node. Therefore, we began to investigate other self-assembling structures to target the nanoscale sizes (10-100 nm) that we anticipate are best suited for increasing trafficking to the lymph node.

These considerations led us to explore lipid nanodiscs (LNDs) (Fig. 1E) composed of high- $T_m$  phospholipids co-mixed with pegylated phospholipids that stabilize the areas of high curvature at the rim of the discs. We prepared them by adapting the method of Johnson and Edwards (Biophysical J. **2003**, 85 3839-3847) and formulated our



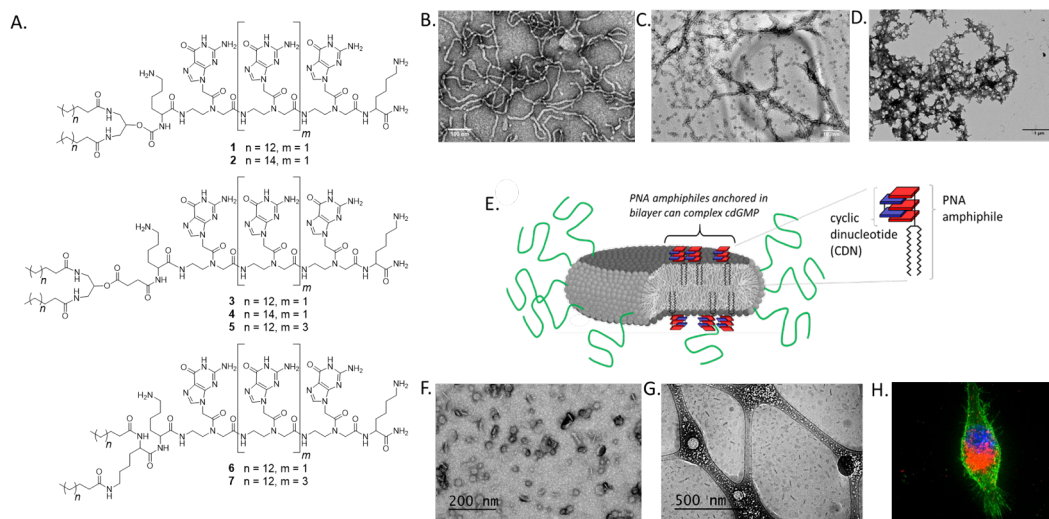


**Figure 1.** A. Chemical structures of PNA amphiphiles. B-D. TEM images of the worm-like micelles formed by amphiphile 2 (B) and amphiphile 4 (C) and the aggregated structures formed by addition of cdGMP (D). E. Schematic illustration of pegylated LNDs incorporating PNA amphiphiles. F. Negative stain TEM of LNDs. G. Hydrated LNDs visualized by cryo-EM. H. Mouse RAW macrophage showing extensive punctate fluorescence from internalized fluorescently labeled LNDs (Blue, DAPI nuclear stain; Green, Concanavalin-A FITC membrane stain; Red, Cy5-labeled LND).

discs with 40 mol% of a high- $T_m$  phospholipid (HSPC), 20 mol% of a pegylated lipid (DSPE-PEG5000), 20 mol% a cationic lipid (16:0 TAP), and 20 mol% of PNA amphiphile. The PNA lipid nanodiscs were formed by thin-film hydration followed by thermal annealing and loaded with cdGMP in high potassium buffer before buffer exchanging with PBS. Both by standard TEM with negative staining (Fig. 1F) and by cryo-EM (Fig. 1G) we observe relatively uniform nanodiscs with an average diameter of 40-50 nm and a membrane thickness of approximately 10 nm, which corresponds well with the expected width of a phospholipid bilayer. Initial *in vitro* studies suggest that the LNDs are readily taken up by immune cells, as shown by fluorescence microscopy of a Cy5-labeled LND incubated with RAW macrophages (Fig. 1H). Because of the homogeneity and desirable size of the LNDs we are currently focused on characterizing their binding and release properties, as well as testing them *in vitro* and *in vivo*.

## Saponin nanoparticles

Saponin nanoparticle (NP) adjuvants, a potent and clinically relevant class of adjuvants, are thought to function via canonical inflammasome activation and subsequent release of pro-inflammatory cytokines such as IL-18 and IL-1 $\beta$ . This mechanism is at least in part thought to be mediated by endosomal disruption and the release of NRLP3-activating cathepsin proteases into the cytosol. To explore whether we could take advantage of this endosomal disruption mechanism to also deliver activators of cytosolic danger associated molecular pattern (DAMP) receptors, we synthesized saponin nanoparticles incorporating the synthetic LPS derivative monophosphoryl lipid A (MPLA, Fig. 2A). LPS and its lipid A derivatives have been demonstrated to directly

activate cytosolic caspase 11 (human caspase4/5) and trigger non-canonical inflammasome signaling and pyroptosis, a potent immune stimulating form of program cell death. These saponin-MPLA NP triggered even strong inflammatory cytokine production in lymph nodes following vaccination compared to saponin NP, and primed much greater antibody responses in vivo in pilot studies (Fig. 2B-C). Encouraged by these preliminary findings, we are embarking on detailed structure-function studies of these novel NP adjuvants.

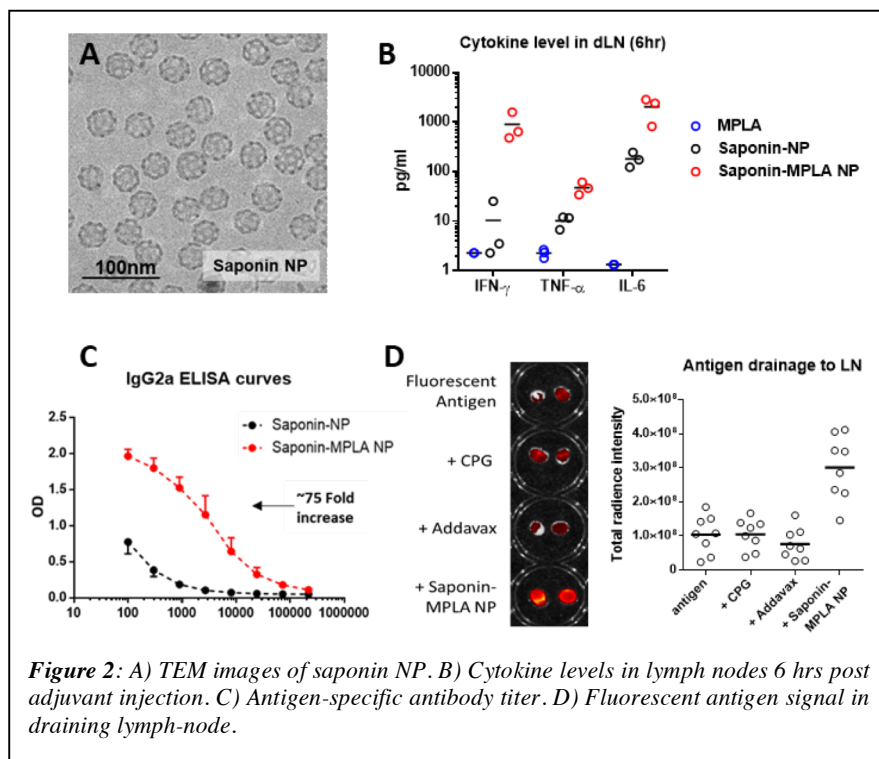


**Figure 2:** A) TEM images of saponin NP. B) Cytokine levels in lymph nodes 6 hrs post adjuvant injection. C) Antigen-specific antibody titer. D) Fluorescent antigen signal in draining lymph-node.

## Research Plans for Next Year:

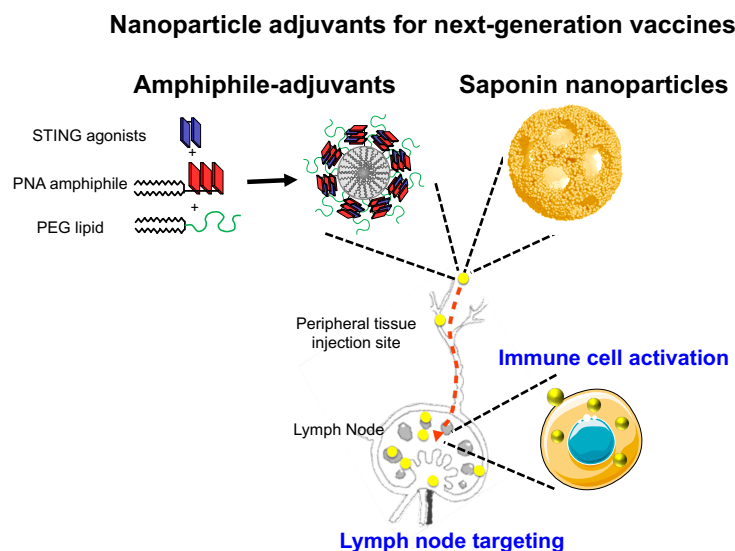
### STING agonist amphiphile-adjuvants

In the next year we will characterize the binding of cdGMP to PNA LNDs and quantify release under a range of relevant conditions. We will also begin to investigate the effectiveness of PNA LNDs at promoting drainage to the lymph node and shuttling cdGMP to relevant immune cells by quantifying trafficking and measuring the types and levels of cytokines produced. Based on these results, we will strategize on how to improve performance. For example, if we find that the release of cdGMP out-paces lymph node drainage we will work towards formulating a slower releasing nanostructure. Replacing the lysine residues with arginine residues may improve the binding, as the guanidinium base on the side-chain of arginine is known to have more favorable interactions with phosphate groups compared to the lysine side-chain due in part to its ability to interact through hydrogen-bonding with more than one phosphate oxygen.

### Saponin nanoparticles

Our preliminary data suggests that saponin-MPLA NPs may be able to promote lymphatic drainage and/or antigen retention in the draining lymph node (Fig. 2 D). In the following year we will use intra-vital microscopy to further characterize the dynamics of lymphatic flow and antigen penetration into the lymph node. These data will help us optimize both the efficacy and safety profile of our nano-adjuvants.

## Representative Image and Caption:



**Caption:** ISN project 1.6 is studying novel self-assembling amphiphiles as next-generation vaccine adjuvants for subunit vaccines. Two classes of materials are under study: (1) Amphiphile-adjuvants, based on peptide nucleic acid (PNA)-lipid and polymer-lipid conjugates, noncovalently bind to potent small molecule immunostimulators (STING agonists) and self-assemble into wormlike micelles, spherical micelles, or nanodiscs. (2) Saponin nanoparticles are formed by self-assembly of phospholipids and the glycolipid saponin, forming ~40 nm diam. porous nanoparticles. Both of these classes of nano-adjuvants have an ideal size for efficient convection through lymph to target lymph nodes following injection, are efficiently taken up by antigen presenting cells in lymph nodes, and activate these cells through multiple pathways to promote the immune response. We are studying the structure-function relationships governing the activity of these nano-adjuvants with the goal of defining their mechanisms of action and optimizing their capacity to safely and potently stimulate cellular and humoral immunity.

## Papers Published in Peer-reviewed Journals (Full citation required. Please include DOI if available):

- 1) none

## Peer-Reviewed Conference Proceeding Publications (Full citation required. Please include DOI if available):

- 1) none

## Books and Book Chapters:

- 1) none

## Presentations at Meetings, but not Published in Conference Proceedings:

- 1) none

## Patents, Patent Applications, and IP Disclosures:



1) none

***Doctoral Degrees Awarded During Reporting Period (First and Last Name):***

none

***Master's Degrees Awarded During Reporting Period (First and Last Name):***

none

## Strategic Research Area 2

### Augmenting Situational Awareness

---

**SRA-2** concentrates on providing the Soldier and Soldier platforms with the next level of capabilities for secure communications, multi-faceted situational cognition and visualization, and invulnerability to enemy detection and potentially for some cases, immunity to enemy EMP and spoofing technologies. The approach is a full frontal attack on diverse segments of the EM spectrum currently under-exploited owing to inadequate scientific understanding of the basic physics of novel electronic, optical, and electromagnetic phenomena or the unavailability of efficacious materials and devices to capitalize on recent progress in this understanding. For example, one project will perform experimental and modeling studies to develop materials and devices that will bring hyperspectral resolution to thermal- and mid-IR imagers based on graphene and thereby produce a fully functional hyperspectral focal plane array. To tackle a longer wavelength domain a different project will provide fundamental understanding of field-enhanced electroluminescence in quantum dots to enable upconversion of LWIR and THz radiation to emissions in the visible. A third project features systematic studies of nano-plasmonic phenomena that enable non-intuitive shrinking of light waves with potential applications to compact radiation sources from THz to X-rays, secure communications, and more powerful obscurant particles. Another project seeks to synthesize novel mechano-optic, electro-optic and thermo-optic fibers that can be used to enable high bandwidth communications and reflectivity management of Soldier clothing and platforms. Finally SRA-2 includes *in situ* studies of electrode-electrolyte interfaces of an operating solid state lithium ion battery to gain new fundamental understanding of the battery chemistry to improve the power density and shelf life (stability) of these power sources used in diverse equipment for Soldier communications, ISR etc.

---

**ISN Project Number: 2.1**

**Project Title: *Uncovering Chemical Stability & Charge Transfer Mechanisms at Electrode-Electrolyte Interfaces of Li-ion Batteries***

**Principal Investigator(s): Bilge Yildiz**

***Summary of Accomplishments:***

Solid-state lithium-ion batteries (SLIBs) hold great promise for obtaining high energy densities but their power density is currently limited by the inferior charge transfer properties and chemical instability of the electrode-electrolyte interfaces. The goal of this research is to advance our fundamental understanding of the solid electrolyte interfaces with Li metal anode and with high-voltage cathodes. The results obtained from this project will give us scientific insights into how solid-solid interfaces in SLIBs evolve chemically and structurally when driven by temperature and electrochemical potential, and what the electron and Li<sup>+</sup> transfer properties of the interfaces are. Such understanding is necessary for providing physically-based breakthroughs in the development of SLIB technology. The work includes *in operando* interface sensitive X-ray spectroscopy and specialized scanning-probe measurements on thin-film electrode-electrolyte systems as a function of temperature and applied voltage. Ac and dc electrochemical measurements concurrent with the X-ray measurements correlate electrochemical performance to interface chemistry.

Since the initiation of the project during last 7 months, we focused on unraveling the phase stability and cation diffusion near the interface of a high-voltage cathode and a solid electrolyte. Al<sup>3+</sup> doped Li<sub>1-x</sub>La<sub>x</sub>ZrO<sub>3</sub> (LLZO) was chosen as the electrolyte, and LiNi<sub>0.8</sub>Mn<sub>0.1</sub>Co<sub>0.1</sub>O<sub>2</sub> (NMC 622) was chosen as a state of the art high-voltage cathode. LLZO was made in the form of polycrystalline pellets, and the NMC cathodes were sputtered onto LLZO in the form of dense thin films. The interface stability was assessed as a function of annealing conditions to resolve the onset of reactions at this interface during ceramic interface sintering. Electrochemical Impedance Spectroscopy (EIS) and synchrotron X-ray absorption spectroscopy (XAS) were performed. According to the data obtained, XAS can be used to trace the oxidation state possible phase transformations during annealing.

Fabricating phase pure and highly dense LLZO pellets is essential at the onset of all our studies. During the process of making a pellet from Al<sup>3+</sup> doped LLZO powder, by pressing and sintering, cubic LLZO may decompose to secondary phases or to tetragonal LLZO. Within the resolution of X-ray diffraction, the pressed and sintered pellets in our current work were found to be fully cubic without an impurity phase. Al<sup>3+</sup> doping on the LLZO stabilizes cubic phase, thus as Al<sup>3+</sup> doping concentration increases, the pellet can be sintered at lower temperature. This will be helpful since sintering at lower temperature decreases the amount of Li that is lost at elevated temperatures. It should also be noted that Li<sub>2</sub>CO<sub>3</sub> forms spontaneously at the surface when LLZO is subjected to atmosphere. The polishing process removes this carbonate layer, as well as ensures a smoother interface. Therefore, time between the finishing time of polishing with grit paper and getting vacuum in a sputtering chamber was minimized.

EIS experiment was done on polished LLZO pellet with 100nm gold deposited on each side. Voltage amplitude was 500 mV, and frequency range was 4MHz-1Hz. As shown in Figure 1(a), data consisted of a semicircle which appears above 100kHz, and a sharp increase below 100kHz. Since there are no additional arcs, this shows that there is no additional phase boundary apart from gold-LLZO. Fitting the semicircle with an RC element gives the bulk resistance of the LLZO pellet [1]. As a result, we found that the Li-ion conductivity is 8.20×10<sup>-4</sup> S/cm, which is consistent with the range of conductivities found in literature for LLZO dependent on sintering conditions.

XAS experiments to resolve the LLZO-NMC622 interface chemistry were performed at NSLS-II, beamline 23-ID-2. Spectra for Ni L-edge, Co L-edge, Mn L-edge, O K-edge were measured. Reference spectra were taken from polished LLZO pellet, NMC 622 powder, and Co<sub>2</sub>O<sub>3</sub> powder. Samples were prepared by sputtering NMC 622 dense

thin films on a polished LLZO pellet with different thicknesses (5nm, 20nm, 100nm). After the sputtering, the samples were annealed at different temperatures (300°C, 500°C, 700°C for 4 hours each).

Analysis of the XAS data indicated cation inter-diffusion and secondary phase formation during annealing at 500°C and 700°C. Highest quality data was obtained from LLZO pellet coated with 100nm NMC 622. Change of chemical environment of Ni becomes prominent in the sample that was annealed at 500 °C for 4 hours. The area ratio between high energy peak and low energy peak of Ni L<sub>2</sub> edge shows the oxidation state of Ni inside the material. When the sample is annealed at 500°C, low energy peak noticeably decreases compared to high energy peak as shown in the figure (c). This indicates reduction of Ni<sup>3+</sup> ion to Ni<sup>2+</sup> ion [2]. This effect is more clearly seen in 700°C annealed sample. In addition, magnitude of La M<sub>5</sub> edge is comparable to Ni L<sub>2</sub> edge in 700°C annealed sample. This shows increase of La/Ni element ratio in the detection range, indicating out-diffusion of La from LLZO into the NMC cathode layer upon annealing.

Analysis of Co L-edge reveals an interesting change in the Co oxidation as annealing temperature increase. As shown in the Figure (d), High energy shoulder of Co L<sub>2</sub> edge increases as annealing temperature increase up to 500°C. This represents oxidation of the Co ion in NMC cathode. In contrast, the shape of Co L-edge changes drastically when the sample was annealed at 700°C. Low energy shoulder of Co L<sub>2</sub> edge increases, and low energy part of Co L<sub>2</sub> edge decreases compared to the high energy part. Comparing with the reference data taken from Co<sub>3</sub>O<sub>4</sub> powder, this indicates reduction of Co<sup>3+</sup> ion to Co<sup>2+</sup> ion. No distinct change in shape of Mn L-edge was found as shown in the Figure 1(b).

It is known that transition metals in delithiated NMC are reduced when it is annealed in inert gas environment [3]. Crystal structure of NMC changes to spinel and rock salt due to this process. Moreover, reduction of transition metals in NMC was claimed as a driving force for interphase formation between NMC and liquid electrolyte [4]. Because of the drastically different chemical environment of a solid electrolyte versus a liquid electrolyte, we can't conclude whether the same interpretations can be made here (i.e. reduction of Ni drives reactions with the LLZO cathode), and we're in the process of collecting and analyzing more structural data at this LLZO-NMC interface.

[1] Wachter-Welzl, A. et al. The origin of conductivity variations in Al-stabilized Li<sub>1-x</sub>La<sub>x</sub>Zr<sub>2</sub>O<sub>7</sub> ceramics. *Solid State Ionics* 319, 203–208 (2018).

[2] Tian, C. et al. Depth-Dependent Redox Behavior of LiNi<sub>0.6</sub>Mn<sub>0.2</sub>Co<sub>0.2</sub>O<sub>2</sub>. *Journal of The Electrochemical Society* 165, A696–A704 (2018).

[3] Bak, S.-M. et al. Structural Changes and Thermal Stability of Charged LiNi<sub>0.6</sub>Mn<sub>0.2</sub>Co<sub>0.2</sub>O<sub>2</sub> Cathode Materials Studied by Combined In Situ Time-Resolved XRD and Mass Spectroscopy. *ACS Applied Materials & Interfaces* 6, 22594–22601 (2014).

[4] Cherkashinin, G., Motzko, M., Schulz, N., Späth, T. & Jaegermann, W. Electron Spectroscopy Study of Li[Ni,Co,Mn]O<sub>2</sub>/Electrolyte Interface: Electronic Structure, Interface Composition, and Device Implications. *Chemistry of Materials* 27, 2875–2887 (2015).

### ***Research Plans for Next Year:***

During the next year, effect of depositing an interlayer between NMC622 and LLZO on prohibiting the growth of unwanted interphase chemistry will be investigated. Former researchers claimed that, depositing a Nb-containing layer as an interlayer between LiCoO<sub>2</sub> (LCO) and LLZO gives lower interfacial resistance compared to the one that has no Nb deposited after heat treatment [5]. After the heat treatment (600°C, 2h in O<sub>2</sub> environment), amorphous Li-Nb-O compound forms due to reaction of Nb with Li. Authors hypothesized that this layer contains LiNb<sub>2</sub>O<sub>7</sub> and LiNbO<sub>3</sub>, based on the XRD experiment done on mixed powder of LLZO and Nb annealed at 600°C. The arguments in literature for the protective role of this interface coating include the possible avoidance of a blocking space charge layer, or the avoidance of interface reactions between LLZO and LCO. However, previous research does not present



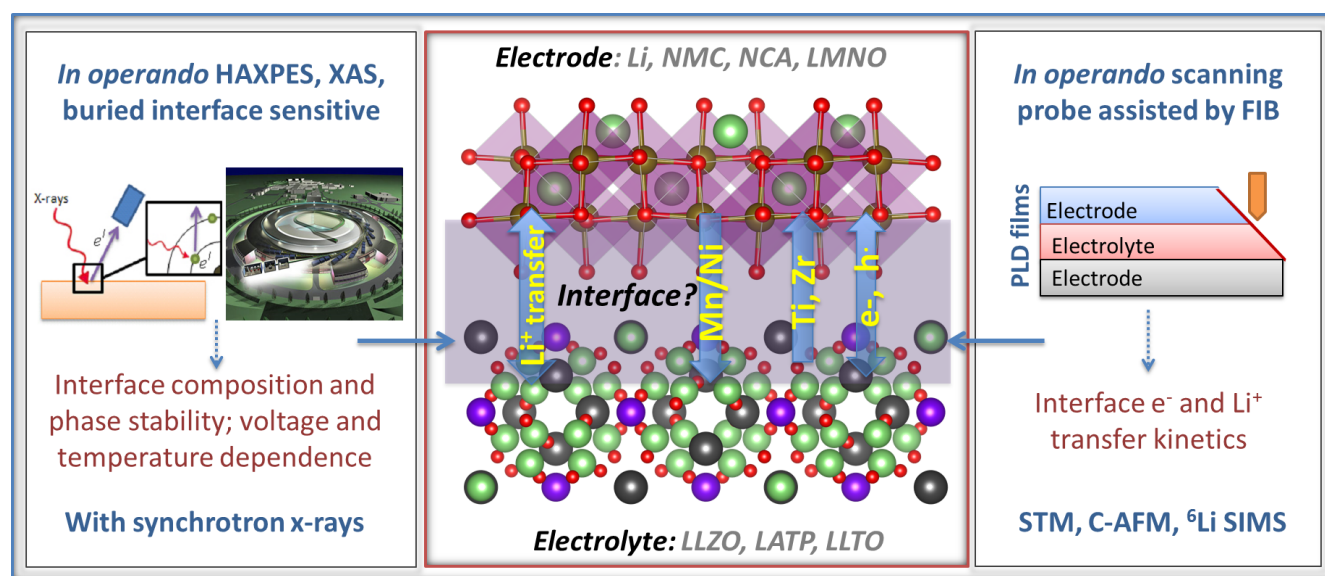
any quantitative proof in the form of a cation profile after the annealing or detailed chemical analysis of the oxidation state of each element.

In our upcoming research,  $\text{LiNbO}_3$  will be directly deposited by RF sputtering. This will give better control on the thickness of the interphase coating between cathode and electrolyte layer. Secondary Ion Mass Spectroscopy (SIMS) will be used to get cation profile before and after annealing. XAS and EIS will be done to figure out whether chemical environment changed or secondary phase formed. Thickness of  $\text{LiNbO}_3$  and annealing conditions will be changed, and the effect of those factors will be analyzed. In addition, symmetric or half cells will be polarized, and the effect of such electrochemical potential at the cathode-electrolyte interface will be assessed. In addition, formation of possible space charge layer between NMC622 and LLZO will be investigated by using Kelvin Probe Force Microscopy (KPFM) to identify possible potential build-up and Li depletion layer. This will be used to calculate charge carrier concentration, which will reveal whether space charge layer exists at the interface [6].

[5] Kato, T. et al. In-situ  $\text{Li}_x\text{La}_y\text{Zr}_z\text{O}_w/\text{LiCoO}_2$  interface modification for advanced all-solid-state battery. *Journal of Power Sources* 260, 292–298 (2014).

[6] Maier, J. Ionic conduction in space charge regions. *Progress in Solid State Chemistry* 23, 171–263 (1995).

### Representative Image and Caption:



**Repres. Image.** Graphical summary of the project research objectives and methods for probing the stability and charge transfer properties of solid electrolyte interfaces with Li and with cathodes. We focus on interface evolution because of (1) formation of a space-charge zone or cation inter-diffusion, (2) phase instability and secondary phase formation, (3)  $e^-$  and  $\text{Li}^+$  transfer/transport properties of the interface, with implications for performance of the interface and for the stabilization of the phases at the interface. Methods include interface sensitive, in operando synchrotron X-ray spectroscopy and scanning probe experiments on model nano-scale thin film structures. The results from this project provide insights to guide physically-based breakthroughs in the development of solid state battery technology.



### Optional Image (Technical Figure)

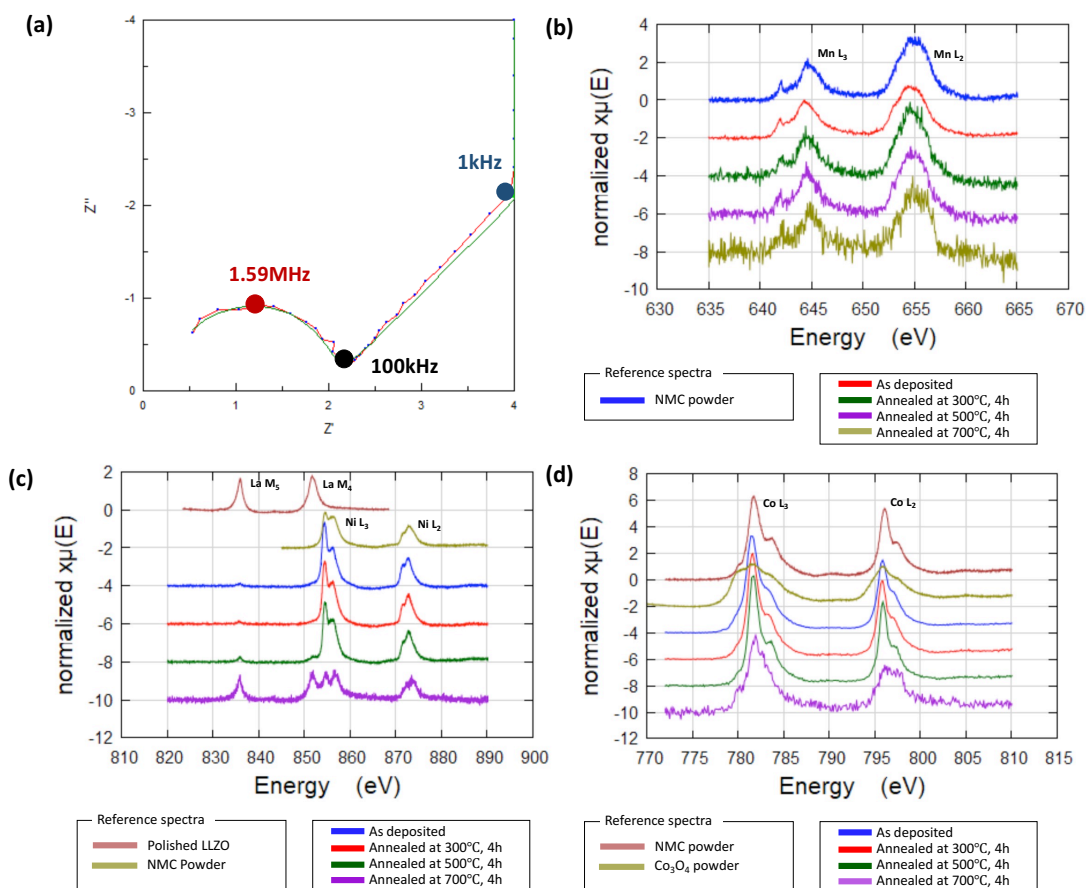


Figure 1:

(a) Electrochemical impedance spectra taken on polished LLZO pellet. Frequency range: 4MHz-1kHz, Voltage Amplitude: 500mV

(b) Normalized X-ray absorption spectra (XAS) for Mn  $L_{2,3}$ -edge

(c) Normalized XAS signal for La  $M_{4,5}$ -edge and Ni  $L_{2,3}$ -edge

(d) Normalized XAS signal for Co  $L_{2,3}$ -edge

### Papers Published in Peer-reviewed Journals (Full citation required. Please include DOI if available):

1) none

### Peer-Reviewed Conference Proceeding Publications (Full citation required. Please include DOI if available):

1) none

### Books and Book Chapters:

1) none

### Presentations at Meetings, but not Published in Conference Proceedings:

1) none

### Patents, Patent Applications, and IP Disclosures:



1) none

***Doctoral Degrees Awarded During Reporting Period (First and Last Name):***

none

***Master's Degrees Awarded During Reporting Period (First and Last Name):***

none

**ISN Project Number: 2.2**

**Project Title: Mid- & LW-Infrared Detector Arrays on Flexible Substrates**

**Principal Investigator(s): Tomas Palacios, Dirk Englund, Jing Kong**

**Summary of Accomplishments:**

**1. Materials growth and characterization**

During the past year, we have focused on improving the quality of two dimensional materials such as graphene and hexagonal Boron Nitride (hBN), while developing the synthesis of other transition metal dichalcogenide (TMD) materials. For graphene, our single crystalline flake size can be  $500\ \mu\text{m}$ , while for monolayer hBN we obtain domain sizes of  $50\ \mu\text{m}$  and continuous film. In addition, we have used Raman spectroscopy to characterize the quality of the materials in further detail, for graphene, we used a quantitative analysis for strain and doping concentration in the sample, providing a new insight into the characterization of CVD grown graphene. For the other TMD materials, we have developed an in-situ vapor generation growth method which allows us to successfully grow mono- to multilayer  $\text{TiS}_2$ , and we have verified that this method is applicable to other TMD materials such as multilayer  $\text{SnS}_2$  or  $\text{VS}_2$  as well.

**2. Graphene-polymer thermomechanical bolometer**

Uncooled Mid-infrared (Mid-IR) detection and imaging technologies are highly desired for night vision, security surveillance, remote sensing, industrial inspection, medical and environmental chemical sensing, etc. Traditional mid-IR detection technologies operating at room temperature are all associated with thermal related phenomena that transfer the optical signals into electrical signals through changes of temperature on the device. Here we propose and implement a new signal transducing scheme where the energy transfer path is optical-thermal-mechanical-electrical. By combining the highly sensitive strain sensors made with percolative graphene nano-flake films synthesized by Marangoni self-assembly method, and the highly efficient polymer opto-thermo-actuators, we were able to demonstrate the proof-of-concept bolometric type mid-IR detectors (Figure 2) that could be more sensitive than the state-of-the-art technologies. Two types of photoresponse behaviors were observed in our devices: a gradual change in resistance in terms of temperature (Figure 3(a)), which may be associated with the average overlap area decrease of adjacent nano-flakes; and an abrupt “switch” like response (Figure 3(b)) that are presumably due to the decrease of the number of conduction paths of the percolative film. Microscopic characterizations and theoretical modeling were carried on to understand such behaviors. Theoretical analysis showed that our new technology could be at least one order of magnitude more sensitive than the fundamental limit of existing uncooled mid-IR technologies (Figure 2(c)).

**3. Antenna-coupled multispectral graphene mid-IR imager**

On the electromagnetic device design side, we have begun working on a multispectral imager device concept most similar, but not quite identical to “Device Concept 3” from the proposal. Our approach takes advantage of the small size of dipole antennas and their electromagnetic near-fields relative to their absorption cross-sections. This allows us to engineer metasurfaces of tiled, differently-tuned antennas which absorb almost all of the light incident upon them over a wide wavelength range, sorting the light into different sets of antennas by wavelength. We have shown via simulation that if the antennas are sufficiently detuned and sufficiently far away from each other, they do not interact and can absorb as much light as if they are isolated; this simulation represents a proof of concept for this design idea. While we initially used electrical dipole antennas in our simulations for this project, we have decided to prioritize investigating slot antennas, or “magnetic dipole antennas”, the complement of normal dipole antennas. Such antennas benefit from a better mode match to 2D materials and more design flexibility (the antenna susceptance can be tuned freely by changing the slot depth), and the lithography resolution and alignment

requirements are not as stringent. We have fabricated such antennas by etching slots into silicon (a few microns long, 1.5–2 microns deep, and a few 100's of nm wide) and depositing ALD platinum as the conductor. We are currently in the process of characterizing the optical properties of these antennas.

### Research Plans for Next Year:

1. In the coming year we plan to continue improving the quality of graphene and hBN materials through synthesis optimization, while improving on the transfer process. We are planning to develop a vacuum-based dry transfer technique to minimize issues of trapped air and water and wrinkles. In addition, we plan to synthesize high quality graphene-hBN heterostructures and heterostructures of other 2D materials for our photodetector applications.
2. Optimization and scaling of the graphene-polymer thermo-mechanical bolometer: We will perform an optimization in the full design space of the device and further improve the sensitivity, response time and yield of the technology. The key factors to consider include the heat dissipation, the electrical/mechanical hysteresis, the uniformity of the assembled graphene film, and the self-calibration during measurements. Furthermore, we will start working on a large-scale CMOS compatible process for the technology and attempt to incorporate our sensing structure with the spectrum selection structure that we have also been working on.
3. In the coming year, we would like to get to the point of being able to iterate between fabrication and device measurement in order to optimize the antenna properties. This will require either finding a setup on campus which is suitable for performing free-space mid-IR cross-polarized reflectometry measurements, or buying a mid-IR tunable laser and building one. At the same time, we will begin fabricating graphene photodetectors on the antennas in order to perform an initial demonstration of multispectral functionality utilizing 2D materials grown by Jing Kong's lab.

### Representative Image and Caption:

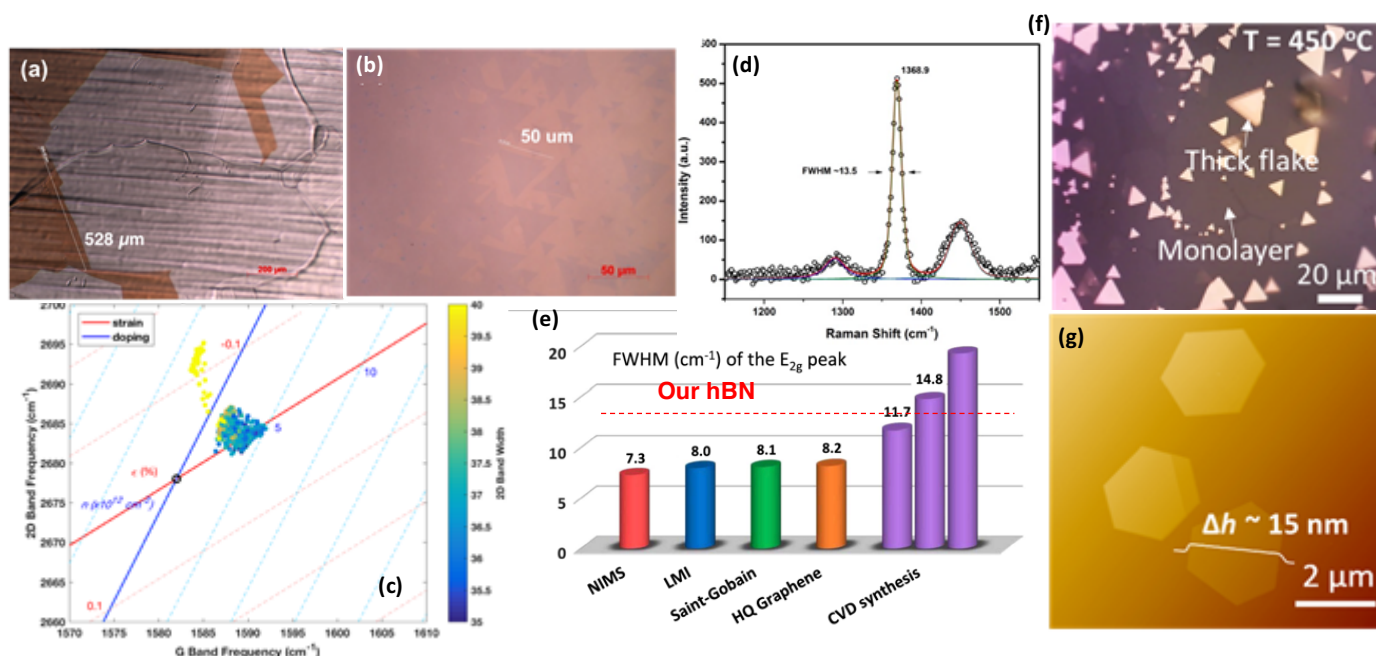


**Figure 1.** (a) Optical Microscope image of as-grown CVD graphene on copper foil showing the single crystalline grain size of  $>500\mu\text{m}$ . (b) Optical Microscope image of our CVD monolayer hBN flakes transferred onto Si/SiO<sub>2</sub> substrate. (c) Graphene G band Raman vs 2D band Raman frequency analysis, the doping and strain information for the graphene can be analyzed. In this case, the graphene is p-doped (carrier concentration  $\sim 10^{12}\text{cm}^{-2}$ ) with a very low strain ( $<0.05\%$ ). (d) Raman spectrum of a single crystalline hBN flake, the peak position of hBN E<sub>2g</sub> band at  $1368.9\text{ cm}^{-1}$  is the peak position for monolayer hBN, and the FWHM of  $13.5\text{ cm}^{-1}$  indicate high quality hBN. (e) Raman FWHM of hBN E<sub>2g</sub> band comparison, indicating our hBN quality is getting closer to the exfoliated high quality hBN. (f) Optical microscope image of our CVD grown TiS<sub>2</sub> flakes on Mica (triangular, synthesized under  $450^\circ\text{C}$ ) and (g) AFM image of the TiS<sub>2</sub> flakes (hexagonal, synthesized under  $600^\circ\text{C}$ ).

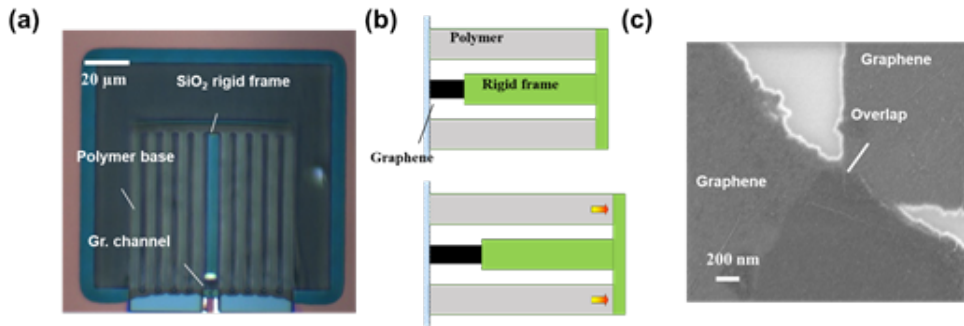


**Figure 2:** (a) Microscopic image, and (b) schematic of the new graphene-polymer thermo-mechanical bolometer developed in this project. (c) Scanning electron microscopic (SEM) image of the percolative graphene film, indicating an overlap region of around 50 nm.

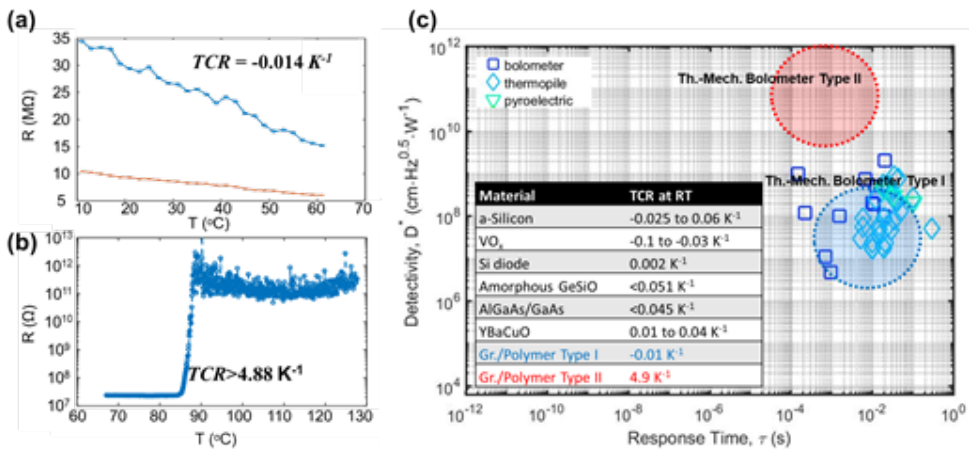


**Figure 3:** Temperature responses of the graphene-polymer thermo-mechanical bolometer. (a) Gradual change temperature dependent resistance. (Type I). (b) Abrupt change temperature dependent resistance (Type II). (c) Estimated detectivities vs. response time of our devices in comparison with mainstream thermal mid-IR detectors. The inset table summarizes the typical values of temperature coefficient of resistance (TCR) of various bolometric materials.

**Papers Published in Peer-reviewed Journals** (Full citation required. Please include DOI if available):

None

**Peer-Reviewed Conference Proceeding Publications** (Full citation required. Please include DOI if available):

- 1) Lin, Y., Ma, Q., Shen, P.-C., Dresselhaus, M., Jarillo-Herrero P., Ling, X., Kong, J. & Palacios. (March 2018). T. Broadband photoresponse from asymmetric hot-carrier thermalizations in atomically thin lateral heterojunctions. American Physical Society (APS) March Meeting, Los Angeles.

- 2) Shen P.-C., Lin, Y., Wang, X., Ling, X. Palacios, T. & Kong J. (March 2018). Unraveling the effect of multiple defect states in synthetic monolayer MoS<sub>2</sub>. American Physical Society (APS) March Meeting, Los Angeles.

***Books and Book Chapters:***

None

***Presentations at Meetings, but not Published in Conference Proceedings:***

- 1) Jing Kong (2018, 7) “Defects in 2D Materials: Characterization, Manipulation and Utilization”, NT18, the 19<sup>th</sup> International Conference on the Science and Application of Nanotubes and Low dimensional Materials, Beijing, China. (invited talk).

***Patents, Patent Applications, and IP Disclosures:***

- 1) Lin, Y., Ji, X., Kong, J. & Palacios, T. (2018) Ultrasensitive thermo-mechanical bolometer. US 62/689104 (provisional).

***Doctoral Degrees Awarded During Reporting Period (First and Last Name):***

None

***Master’s Degrees Awarded During Reporting Period (First and Last Name):***

None

**ISN Project Number: 2.3**

**Project Title: Room Temp LWIR-THz Detection via E-field Enhancement-Induced QD Upconversion**

**Principal Investigator(s): Mounqi Bawendi, Vladimir Bulovic, Keith Nelson, Adam Willard**

### **Summary of Accomplishments:**

*THz-induced electroluminescence (EL), electroabsorption (EA), and photoluminescence (PL).* Terahertz (THz) field effects were measured in the Nelson group on five types of core-shell semiconductor quantum dots (QDs) with different band gaps, sizes, and compositions. Measurements were also conducted on high quality perovskite (CsPbBr<sub>3</sub>) nanocrystals that were synthesized in the Bawendi group. All the samples were deposited onto THz metamaterial field-enhancement structures consisting of parallel gold lines that were 98 microns wide with 2-micron gaps between them, on silica glass substrates. (See Fig. 1a.) All five QD samples showed EL intensities that began to increase above THz threshold field strengths of about 120 kV/cm. It is encouraging that we see strong THz-induced EL from a variety of QD samples, indicating the generality of the effect. The EL threshold for the perovskite NCs from Bawendi group was around 105 kV/cm, somewhat lower than the thresholds for all the other samples, indicating a lower threshold for field-induced dot-to-dot charge transfer between NCs for the perovskite sample than for the conventional core-shell QD samples.

We conducted THz-induced electroabsorption measurements on perovskite NCs, i.e. the change in absorption due to the THz field. As expected, the THz field induces a red-shift (a Stark shift) of the spectrum. The spectral shift follows the THz field strength profile dynamically, indicating rapid shifting of the perovskite electronic levels as the field grows and diminishes. Based on the difference spectrum at one selected time point in the THz field profile (one of the field maxima), it is clear that in addition to the red-shift that causes absorption to increase on the red side of the spectrum and decrease on the blue side, there is also a net decrease in the total absorption so that the decrease on the blue side is far stronger than the increase on the red side. This effect was not seen in the other samples and remains under study.

Preliminary measurements of THz-induced photoluminescence from the QD samples were conducted using optical photon energies  $E_p$  that were tuned to be lower than the QD bandgap values  $E_g$  by roughly the same amount, 0.2-0.3 eV, for each sample. This was done to test whether, with the same difference energy  $\Delta E = E_g - E_p$ , approximately the same THz field threshold would be needed to induce photoluminescence when the THz field and the sub-bandgap optical pulse were time-coincident at the sample. We found that the PL threshold values were not similar but that they increased with the bandgap values despite the similar  $\Delta E$  settings. A more complete set of measurements will be undertaken with variable optical photon energies for each sample to provide a more detailed understanding of the THz-induced PL behavior. It is clear already that very THz-induced red-shifts in the photon energy needed to induce PL are observed, as in our previous report in which shifts exceeding 0.5 eV were measured [Pein 2017].

*Electrically driven photophysics.* In the Bulovic group, SiO<sub>2</sub>/QD/SiO<sub>2</sub> planar capacitor structures were fabricated using the same type of CdSe-CdS core-shell quantum dots that exhibited THz-driven EL. Using differential absorption measurements, we confirmed that no external charges are injected under electric field up to 1MV/cm, while a strong Stark shift is seen. This platform will enable an alternative way to study the photophysics of field-driven ionization and exciton generation in quantum dot arrays to support the physical understanding of THz-driven luminescence.

*Theoretical Modelling.* The Willard group solved for the electronic structures of CdSe/CdS nano-crystal using a full-atomistic, semi-empirical tight binding model with OMEN package [Luisier 2006]. The materials parameters are obtained from Ref. [Lippens 1990, Lippens 1989]. The crystals were modeled as defect-free and unstrained, and a lattice constant of 5.82Å was used. The electric field was introduced into the tight-binding Hamiltonian by shifting



the on-site energies by the potential  $V(\vec{R}_i)$  extracted at each atomic position  $\vec{R}_i$ , and  $V(\vec{r}) = e \vec{E} \cdot \vec{r}$  where  $e$  is the electron charge and  $\vec{E}$  is the applied electric field. The oscillator strength of transitions between electron and hole states are proportional to the optical matrix elements  $P$ , which are calculated by  $P = |\langle \psi_e | \vec{p} | \psi_h \rangle|^2$ , where  $|\psi_e\rangle$  ( $|\psi_h\rangle$ ) is the electron (hole) wavefunction and  $\vec{p}$  is the momentum operator. Thus the field effects on optical absorption could be calculated.

We found that the bending of the conduction and valence bands under externally applied electric fields gives rise to reduced bandgaps (see Fig. 1d). This contributes to the observed redshift of the absorption spectrum. Since electron and hole are oppositely charged, their wavefunctions shift in opposite directions under the external electric field. Consequently, wavefunction overlap between electron and hole is reduced, leading to decreased oscillator strength. The electron (blue) and hole (red) wavefunctions with (right) and without (left) electric field are plotted in Fig. 1d. The hole wavefunction remains confined within the core for field  $< 1V$  due to the large valence band offset between the core and the shell. These results can reasonably model the observations reported to date.

### ***Research Plans for Next Year:***

A high priority is measurement of THz-induced QD EL and PL in oxide-coated metamaterial structures that are being fabricated presently in the Bulovic group and by outside sources. Oxide coatings prevent field emission from the gold structures, which we believe may be responsible for the similar EL thresholds observed in the QD samples. The structures will be fabricated with gap spacings of 2.0, 1.0, and 0.5  $\mu m$  to permit considerably greater THz field enhancement than we now realize with 2.0  $\mu m$  gaps only. Additionally, some of the gold lines will be connected electrically and wired in an interdigitated pattern to permit DC voltage to be applied across the gap regions in part of each structure. This will allow us to assist the THz field with a DC field, which we have already seen to reduce the THz field threshold for EL. The new structures will allow us to complete many of the measurements planned for this year. We will send the new structures with samples to our ARL collaborator, Dr. Blair Connelly, for measurements at IR wavelengths to complement our THz measurements, in order to discover the frequency limits up to which the very large field-induced effects we have seen so far occur. This will likely define the frequency range in which efficient detectors based on the effects can be designed.

Further studies on the size, band gap and composition of the aforementioned materials are warranted. This is especially true for lead halide perovskites, where facile exchange of halide ions post synthesis can be employed to tune optical properties over a wide range while leaving their size virtually unchanged. For the CdSe system, different shell architectures have been demonstrated, enabling detailed study of the potential barrier established by shells made of CdS, ZnS or alloys thereof. Additionally, shape effects are likely to play a significant role in exciton generation. Therefore, nanoplatelets will be generated to explore morphology effects.

We also plan to study properties of AC-electroluminescence in planar capacitors using the same nanostructured materials that exhibit THz-driven EL. By measuring the differential absorption spectrum and time-resolved photoluminescence spectrum, we will be able to characterize the rates of field-ionization and recombination as a function of electric field, which can then be compared to those in THz-based systems to confirm the physical mechanism of light generation.

Theoretically, we plan to carry out Kinetic Monte Carlo simulations of synthesized CdSe/CdS/SiO<sub>2</sub> QDs to investigate the hypothesized THz-driven EL mechanisms (i.e., charge injection, field-driven ionization, or inter-dot tunneling). The details of each KMC simulation will be parameterized based on the results of electronic structure calculations (such as those described above) and benchmarked against experiment. This kinetic modeling will provide dynamic signatures that can be used to validate or rule out different possible mechanistic hypotheses.



## Representative Image and Caption:

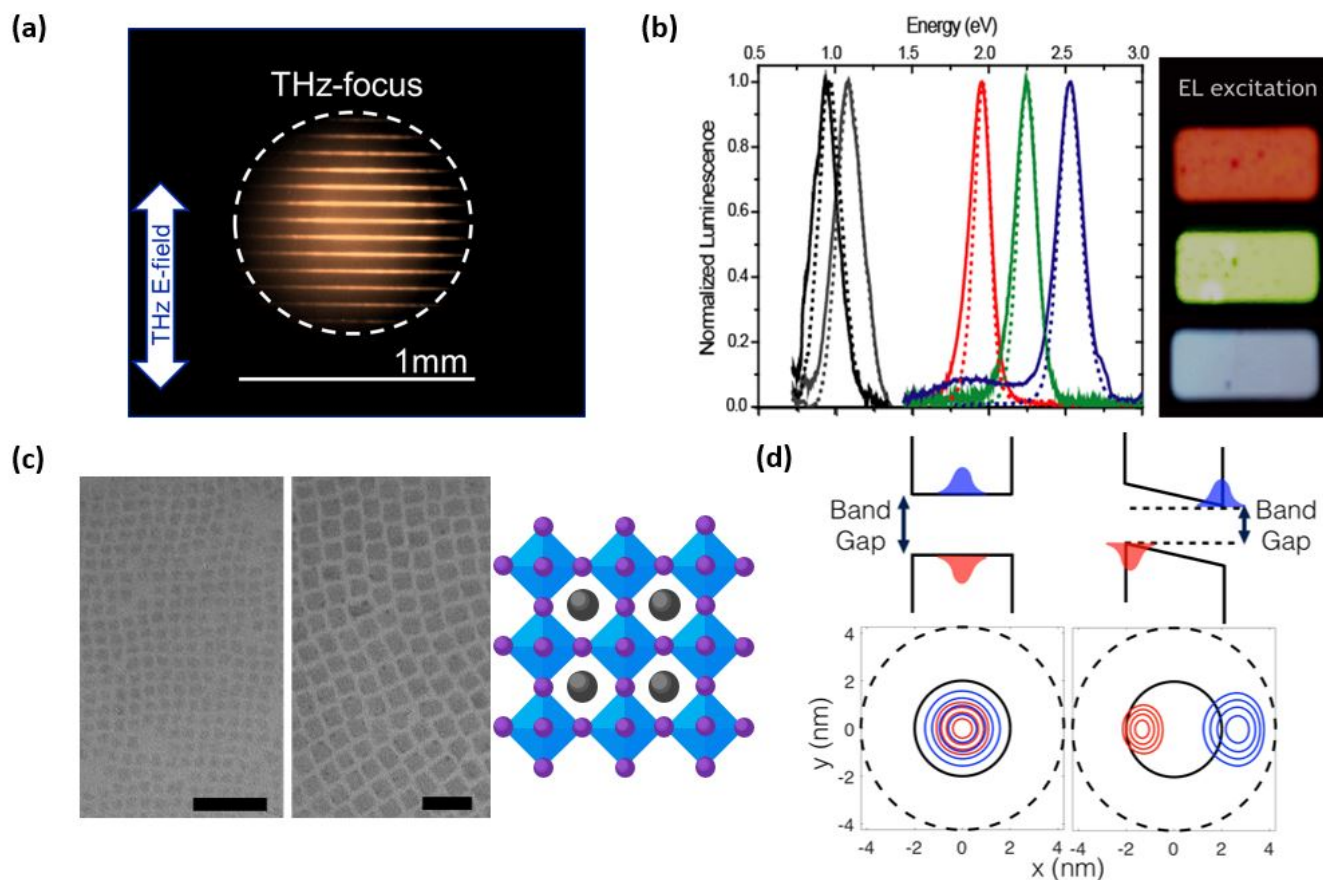


**Figure 1** (a) THz field-enhancing microslits and THz-driven QD electroluminescence from the 2- $\mu\text{m}$  gaps between 98- $\mu\text{m}$  gold lines. (b) Photographs showing electroluminescence of pixels containing red, green, and blue QD luminescent layers (right). The narrow electroluminescence (solid lines) and photoluminescence (dashed lines) spectra of QDs in completed device structures (left). (c) High-resolution TEM images of perovskite nanocrystal arrays, exhibiting high uniformity and size tunability, and the perovskite crystal structure. (d) The bending of the conduction and valence bands under externally applied electric field (upper). Electron (blue) and hole (red) wavefunctions with (lower right) and without (lower left) electric field, showing the separation of the wavefunctions and the reduced bandgap induced by the field.

## References

- [Pein 2017] B. Pein, W. Chang, H.Y. Hwang, J.M. Scherer, I. Coropceanu, X. Zhao, X. Zhang, V. Bulovic, M.G. Bawendi, K.A. Nelson, Terahertz-driven Luminescence and Colossal Stark Effect in CdSe:CdS Colloidal Quantum Dots, *Nano Letters* 2017, 10, 1021.
- [Luisier 2006] M. Luisier, A. Schenk, W. Fichtner, G. Klimeck. Atomistic simulation of nanowires in the  $s p^3 d^5 s^*$  tight-binding formalism: From boundary conditions to strain calculations. *Phys. Rev. B* 2006, 74, 205323.
- [Lippens 1990] P. Lippens, M. Lannoo. Comparison between calculated and experimental values of the lowest excited electronic state of small CdSe crystallites. *Phys. Rev. B* 1990, 41, 6079.
- [Lippens 1989] P. Lippens, M. Lannoo. Calculation of the band gap for small CdS and ZnS crystallites. *Phys. Rev. B* 1989, 39, 10935.

***Papers Published in Peer-reviewed Journals*** (Full citation required. Please include DOI if available):

- (1) We are publishing a detailed analysis of THz-induced spectral shifts in the MIT QD sample that includes theoretical work by MIT colleague Prof. Adam Willard and his group.

***Peer-Reviewed Conference Proceeding Publications*** (Full citation required. Please include DOI if available):

None

***Books and Book Chapters:***

None

***Presentations at Meetings, but not Published in Conference Proceedings:***

None

***Patents, Patent Applications, and IP Disclosures:***

None

***Doctoral Degrees Awarded During Reporting Period (First and Last Name):***

None

***Master's Degrees Awarded During Reporting Period (First and Last Name):***

None

**ISN Project Number: 2.4**

**Project Title: *Particulate Fluid Fiber Processing for Novel Fabric Architectures***

**Principal Investigator(s): *Yoel Fink, John Joannopoulos, (A. Stolyarov as Collaborator)***

***Summary of Accomplishments:***

Optical fibers are being used extensively for distributed sensing of temperature, pressure and strain - but not magnetic fields. To achieve distributed magnetometry, we introduce a new type of fiber detection architecture that integrates photodiodes (PD), a silica hollow-core waveguide and microfluidic channel that hosts nitrogen vacancy (NV) centers as the magnetic sensing element. The NV's red-shifted light is collected by the monolithically embedded Si photodiodes in the fiber to facilitated distributed magnetic field measurements along the fiber. We demonstrate a 300 meters-long-water-immiscible fibre with a diode spacing of 17 cm and a DC sensitivity of 81.45 nT Hz<sup>-1/2</sup>. Such distributed optical fibre magnetometer offers a diverse range of applications, including remote detection of ferrous metals, geophysics, and biosensing. The figure below demonstrates an initial proof-of-concept for fiber optical magnetic detection.

***Research Plans for Next Year:***

Next year we will expand on this concept and introduce a scalable approach to harmonize the performances of semiconductor devices with the form factor of fibers. Our approach will involve the incorporation of functional semiconductor devices and electrical conductors into a macroscopic preform, which will be subsequently drawn into extended lengths of functional fiber with discrete high-performance devices axially dispersed and electrically connected throughout its length. Specifically, during our thermal draw, we will insert a hollow-core silica fiber together with two copper wires into a polycarbonate preform containing the photodiodes for magnetometry. The magnetic field measurement relies on nitrogen vacancies in microdiamond crystals located inside the hollow silica channel. Due to the intrinsic scalability of the thermal draw technique, hundreds of meters of functional fibers can be produced. Moreover, we will evaluate the durability of these fibers when submerged under water while performing magnetic measurements of an external magnet.

In the proof-of-concept demonstration, we have already achieved a sensitivity of  $\sim 81 \text{ nT}/\sqrt{\text{Hz}}$  at each detection site at the DC limit. In separate experiments, sensitivities below 1 pT/hz have been demonstrated (albeit at higher frequency, where this is easier). Our architecture is extendible to such sensing approaches with better diamond sensors or the use of dynamic decoupling approaches. In principle, nitrogen-vacancies-based magnetometry can reach sensitivity values in the range of 1 fT/ $\sqrt{\text{Hz}}$ , comparable to those of the state-of-the-art SQUID magnetometers, where instead of operating in cryogenic conditions, our fiber can operate under ambient conditions. Such a sensing ability can pave the way for biosensing of the human nervous system and even wearable technology. We plan to further explore limits of detection of this technology next year.

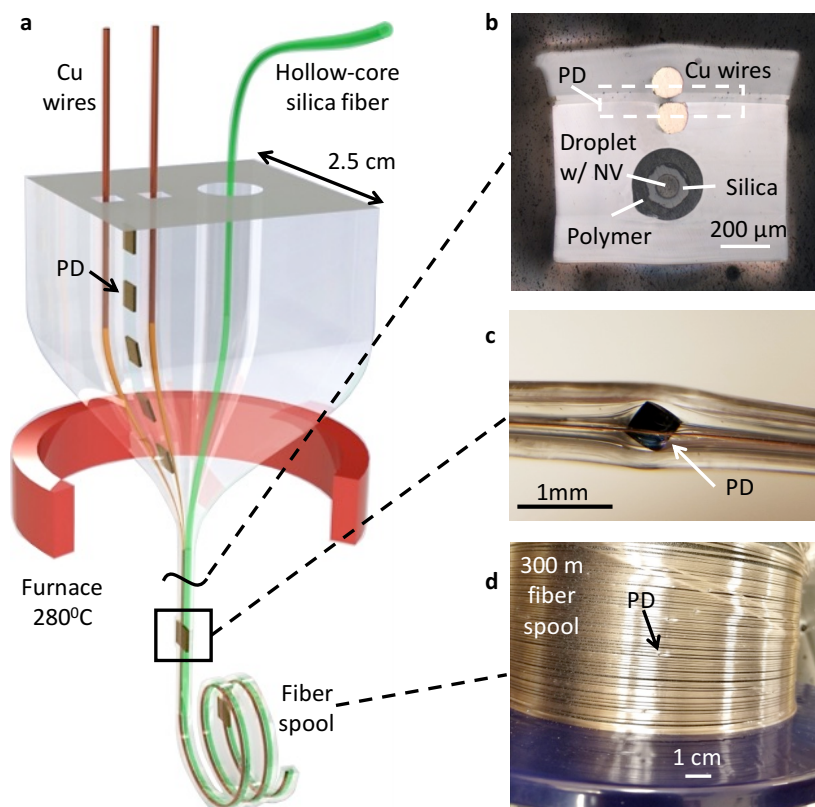
This initiative marks an important advancement in distributed fiber sensor technology. Today, distributed fiber sensors are widely used to measure strain, temperature, or pressure but not magnetic fields. Our fiber, which can be deployed underground or underwater, marks the first example of the integration of spin-based quantum sensors into a distributed fiber sensor. Such spin-based distributed optical fiber magnetometers offer a diverse range of applications, including remote detection of ferrous metals and other uses in geophysics and biosensing.

In summary, next year's research will focus on:

- The demonstration of electrically connected, discrete high-performance photodiodes in thermally drawn fibers containing high-purity silica waveguide in their core.

- The integration of arrays of nitrogen-vacancies (NV) detection sites enabling the first-time measurement of the magnitude, distance, and orientation of a magnetic objects in fiber using optically detected magnetic resonance (ODMR).
- The detection of magnetic fields by ODMR in aqueous environments.
- Characterization of limits of detection under different environmental conditions.
- The integration of a microfluidic channel within an optical fiber to enable scanning of NV micro-diamond.

**Representative Image and Caption:**



**Fibre fabrication.** *a*, Illustration of the fibre preform structure and fibre fabrication process. We embed a series of closely packed PD chips in a polycarbonate (PC) cladding. During our thermal draw, we insert two copper wires, and a hollow-core silica fibre, prepared in advance, through holes in the PC. To achieve the required dimensions of the final device, the feed and draw speed of the PC are controlled. *b*, Micrograph of the cross-section of the fibre. The bright circles are the inserted copper wires. The dashed box represents the location of embedded diodes. *c*, Close-up on a small section of the fibre with an embedded diode. *d*, A 300 m spool of the fibre.

**Papers Published in Peer-reviewed Journals** (Full citation required. Please include DOI if available):

- 1) none

**Peer-Reviewed Conference Proceeding Publications** (Full citation required. Please include DOI if available):

- 1) none



***Books and Book Chapters:***

- 1) none

***Presentations at Meetings, but not Published in Conference Proceedings:***

- 1) none

***Patents, Patent Applications, and IP Disclosures:***

- 1) none

***Doctoral Degrees Awarded During Reporting Period (First and Last Name):***

none

***Master's Degrees Awarded During Reporting Period (First and Last Name):***

none

ISN Project Number: 2.5

Project Title: **Nano-plasmonics for Soldier Applications**

Principal Investigator(s): **Marin Soljačić, Jing Kong, Steven Johnson**

### Summary of Accomplishments:

With the ultimate goal of pushing the frontiers of plasmonics science, to discover novel phenomena that will enable applications of importance to Soldier survivability, the groups focused on three important Soldier applications enabled by plasmonics. **Soljačić's** group developed a proof-of-concept based on an electron microscope and investigate the Smith-Purcell effect. The conventional Smith-Purcell effect describes light emission due to collective excitation induced by free electrons coupling to the electromagnetic modes of a periodic structure. The group obtained results on a range of samples from sub-100 nm pitch gratings to periodic high aspect ratio silicon nanowire structures to engineered metasurfaces using low-energy electrons (2.5 -40 keV) and experimentally and theoretically showed that samples not commonly thought to be appropriate for Smith-Purcell emission (because of theoretical and experimental misbeliefs), namely non-electrically conductive structures, can be strong emitters. In addition, the group theoretically derived and experimentally probed universal upper bounds for the electron emission and energy loss of free electrons. In Figure 1, the group showed that the bounds, built upon passivity constraints, depend solely on the material composition and on the electron velocity and trajectory.

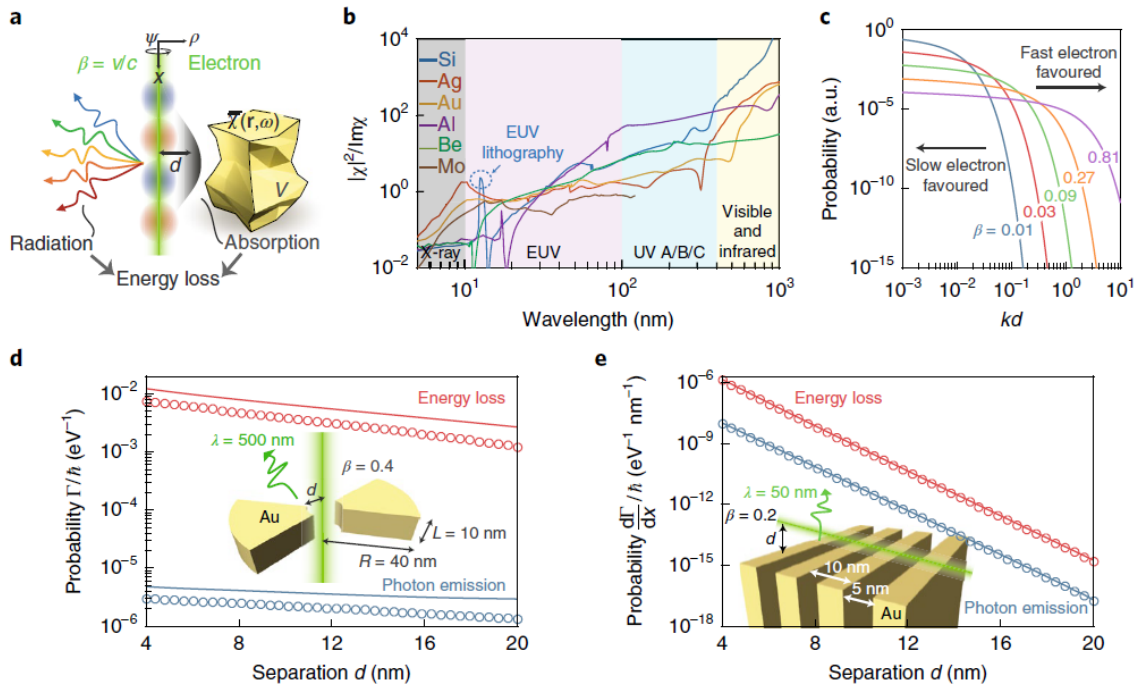


**Figure 1 (Representative Image) Theoretical framework and predictions.** (a) The interaction between a free electron and an obstacle defined by a susceptibility tensor ( $\chi(r, \omega)$ ) within a volume  $V$ , located at a distance  $d$ , generates electron energy loss into radiation and absorption. (b)  $|\chi|^2/\text{Im}\chi$  constrains the maximum material response to the optical excitations of free electrons over different spectral ranges for representative materials. At the X-ray and extreme ultraviolet (EUV) regime, Si is optimal near the technologically relevant 13.5 nm (dashed circle). Contrary to the image charge intuition for the optical excitations of electrons, low-loss dielectrics (such as Si in the visible and infrared regimes) can be superior to metals. (c) Shape-independent upper limit showing superiority of slow or fast electrons at small or large separations; the material affects only the overall scaling. (d,e) Numerical simulations (circles) compared to analytical upper limits for (d) and for (e), respectively) for the radiation (blue) and energy loss (red) of electrons penetrating the center of an annular bowtie antenna (d) and passing above a grating (e).

In order to facilitate the plasmonic applications toward the study of how 2D-plasmonic materials could lead to numerous novel secure communications, as well as chemical sensing capabilities for Soldiers, the quality of the



CVD grown 2D materials needs to be as high as possible. For this, **Kong's** group has focused on the synthesis of single crystalline graphene and hexagonal Boron Nitride (hBN) flakes to sizes as large as possible. Currently, they successfully grew large area and single-crystal graphene on Cu with a grain size of  $500\ \mu\text{m}$ , which can obtain high quality and large single domain hBN on Cu with a domain size of  $50\ \mu\text{m}$  and continuous film. In addition, they have used Raman spectroscopy to characterize the quality of the materials in further detail. For graphene, they used a quantitative analysis for strain and doping concentration in the sample, providing a new insight into the characterization of CVD grown graphene.

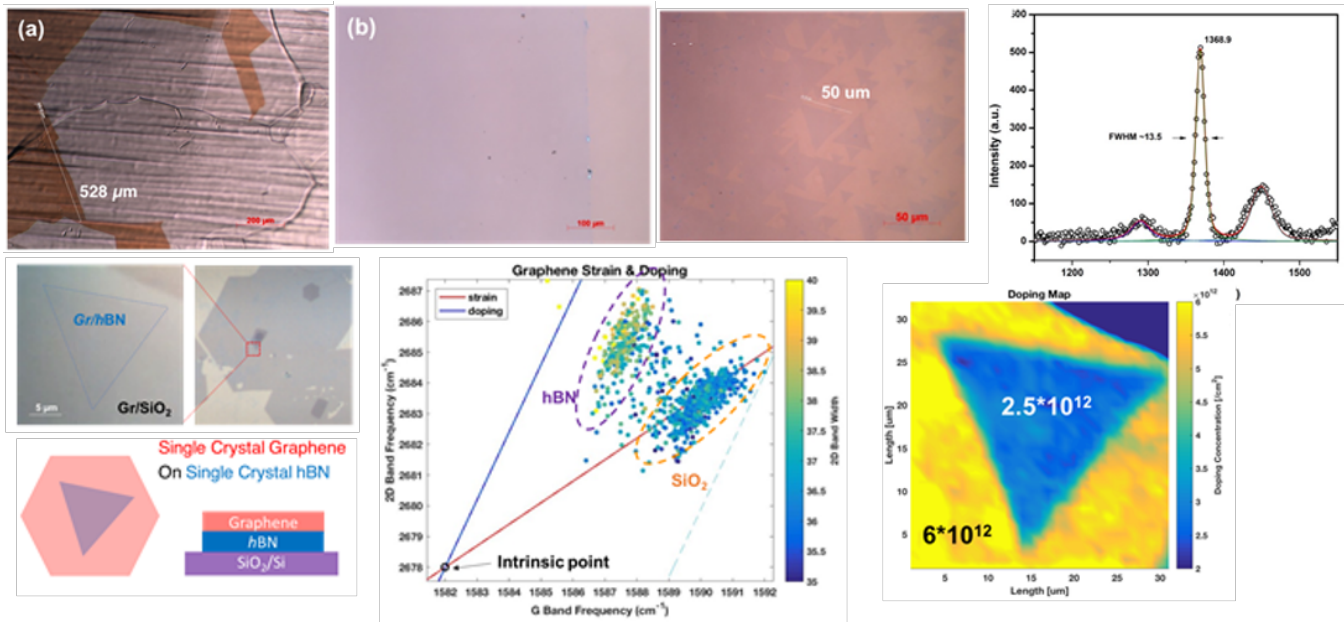


**Figure 2** (a) Optical Microscope image of as-grown CVD graphene on copper foil showing the single-crystalline grain size of  $>500\mu\text{m}$ . (b,c) Optical Microscope image of our CVD hBN continuous monolayer (b) and triangular flakes (c) transferred onto Si/SiO<sub>2</sub> substrate. (d) Raman spectrum of a single-crystalline hBN flake; the peak position of hBN E<sub>2g</sub> band at  $1368.9\ \text{cm}^{-1}$  is the peak position for monolayer hBN, and the FWHM of  $13.5\text{cm}^{-1}$  indicates high quality hBN. (e-g): Raman characterization of graphene on hBN: (e) optical microscope image and schematic illustration of the stacked graphene/hBN on SiO<sub>2</sub>/Si; (f) Graphene G band Raman vs 2D band Raman frequency analysis, indicating different doping and lattice strains for graphene on hBN vs. graphene on SiO<sub>2</sub>/Si; (g) the Raman mapping for different doping concentrations of graphene on hBN or on SiO<sub>2</sub>/Si.

Optimizing patterns for coupling plasmons in/out of the surface is of utmost importance. **Johnson's** group carried out a theoretical investigation into the limit of the absorption by metaparticle arrays. One of the most influential theoretical results for solar-cell design has been the Yablonovitch limit, which provides a bound to how much surface texturing can enhance the performance of an absorbing film averaged over a broad band-width and angular range. They obtain approximate broad-band/angle absorption limits for a case in which the traditional Yablonovitch result is not useful: dilute arrays of “metaparticles” (synthetic discrete scatterers). In optics contexts, dielectric and plasmonic

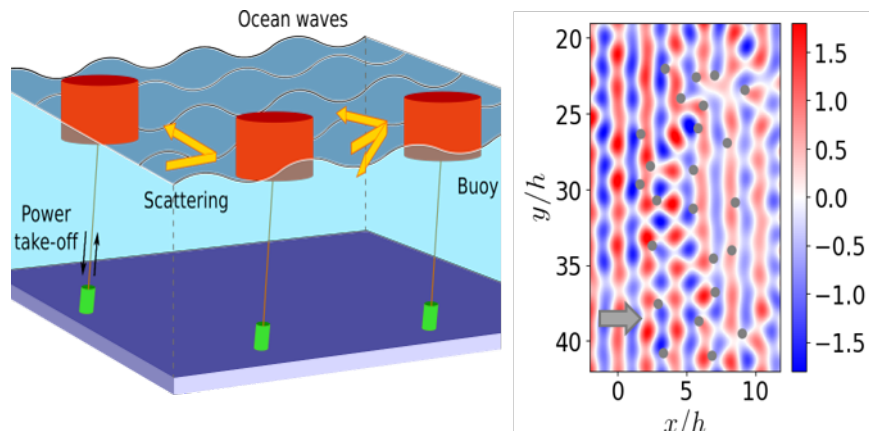


**Figure 3** (a) Bounded absorption for very general arrays of “particles”, including arrays of buoys that extract energy from ocean waves. (b) Ocean surface displacement for a cylindrical buoy array with incident waves. (c) Effect of the index contrast and scattering cross on the maximum bandwidth-averaged enhancement at normal incidence for  $3 \times 30$  arrays of buoys in heave motion (radius=0.3, draft=0.3, water depth=1 and with scattering cross section  $\sigma_s$ ). We tune the index  $n$ , along a strip surrounding the array, with  $n_0$  being the index of the array's ambient medium. We suppose that the buoy has new scattering cross section ( $\tilde{\sigma}_s$ ).

particles can for example be used to enhance absorption in thin-film or dye-sensitized solar cells. In their work, motivated by arrays of buoys designed to extract energy from ocean waves depicted in *Figure 3*, they found limits on the absorption for arrays of particles that can be described by the radiative-transfer equation (RTE), a natural extension of the ray-optics approximation to scattering media. They show that within RTE, an isotropic diffusive regime is optimal for maximizing absorption. This will allow to both obtain analytical upper bounds and identify the ideal operating regime of absorbing metaparticle arrays.

### **Research Plans for Next Year:**

**Experimental Setup:** Soljačić's group plans to investigate the Smith-Purcell effect with even lower energy electrons, and in a variety of materials (including dielectrics) as well as to investigate quantum corrections to dielectric response of materials at nano-scales.

**Device Preparation:** In addition to the high quality synthesis, effective transfer which can maintain the quality of the as-grown materials is critically needed. Up to now, the direct transfer technique developed by the group was the method of use. The technique avoids the polymer residues in between the 2D layers. Nevertheless, there are still trapped water and air in between them. Kong's group is planning to setup a vacuum dry transfer technique in the coming year which will minimize this issue. In addition, for hBNs to be used as a substrate or dielectric, high quality few-layer hBNs are needed. They are planning to develop new strategies toward higher quality uniform few-layer hBN synthesis. Apart from these, they are also planning to extend the synthesis to other 2D materials which are also important for the plasmonic applications in the near future.

**Theoretical Approach:** While most previous work focused on numerical optimization and showed promising results through the design of buoy/particle positions, the question Johnson's group is trying to answer is more general: given the absorbing/scattering properties of an individual metaparticle, is there a limit on the total enhancement and how can it be reached? Such limits can now be applied to many broadband wave effects. This includes solar-cell enhancement with plasmonic/dielectric scatterers as well as emission enhancement (fluorescence, sensing ...). Important theoretical guidance for this project is provided by the recent technique for upper bounds on light-matter interactions developed in part by the groups. Although most of the bounds thus far have been single-frequency results (with the exception of the metaparticle-array bounds above), they have exciting preliminary results on a new technique allowing extension of these results to any arbitrary frequency bandwidth, which they hope to publish in the coming year. Furthermore, they are looking into new plasmonic cavity geometries and extension to various nonlinear effects such as surface-enhanced Raman scattering (SERS) for sensing applications.

### **Papers Published in Peer-reviewed Journals** (Full citation required. Please include DOI if available):

- 1) "Maximal Spontaneous Photon Emission and Energy Loss from Free Electrons" Yi Yang, Aviram Massuda, Charles Roques-Carmes, Steven E. Kooi, Thomas Christensen, Steven G. Johnson, John D. Joannopoulos, Owen D. Miller, Ido Kaminer & Marin Soljacic. *Nature Physics*, DOI: 10.1038/s41567-018-0180-2 (2018).
- 2) "Superlight inverse Doppler effect" Xihang Shi, Xiao Lin, Ido Kaminer, Fei Gao, Zhaoju Yang, John D. Joannopoulos, Marin Soljacic, Baile Zhang. *Nature Physics*, DOI: 10.1038/s41567-018-0209-6 (2018).
- 3) "Control of semiconductor emitter frequency by increasing polariton momenta" Yaniv Kurman, Nicholas Rivera, Thomas Christensen, Shai Tsesses, Meir Orenstein, Marin Soljacic, John D. Joannopoulos & Ido Kaminer. *Nature Photonics* Vol.12, p.423 (2018).
- 4) "Large Photothermal Effect in Sub-40 nm h-BN Nanostructures Patterned Via High-Resolution Ion Beam" Josue J. Lopez, Antonio Ambrosio, Siyuan Dai, Chuong Huynh, David C. Bell, Xiao Lin, Nicholas Rivera, Shengxi Huang, Qiong Ma, Soeren Eyhusen, Ido E. Kaminer, Kenji Watanabe, Takashi Taniguchi, Jing Kong, Dimitri N. Basov, Pablo Jarillo-Herrero and Marin Soljacic. *Small*, DOI: 10.1002/sml.201800072 (2018).



- 5) "Controlling Cherenkov angles with resonance transition radiation" Xiao Lin, Sajan Easo, Yichen Shen, Hongsheng Chen, Baile Zhang, John D. Joannopoulos, Marin Soljagic, Ido Kaminer. *Nature Physics*, DOI: 10.1038/s41567-018-0138-4 (2018).
- 6) "Quantum plasmons with optical-range frequencies in doped few-layer graphene" Sharmila N. Shirodkar, Marios Mattheakis, Paul Cazeaux, Prineha Narang, Marin Soljagic, Efthimios Kaxiras. *Phys. Rev. B* Vol.97, p.195435 (2018).

***Peer-Reviewed Conference Proceeding Publications*** (Full citation required. Please include DOI if available):

- 1) Jing Kong (2018, 7) "Defects in 2D Materials: Characterization, Manipulation and Utilization", NT18, the 19th International Conference on the Science and Application of Nanotubes and Low dimensional Materials, Beijing, China. (invited talk).
- 2) **Plenary Talk:** "A few novel nanophotonic phenomena". M. Soljagic. From Solid State to Biophysics IX in Cavtat, Croatia, 2018.

***Books and Book Chapters:***

- 1) N/A

***Presentations at Meetings, but not Published in Conference Proceedings:***

- 1) N/A

***Patents, Patent Applications, and IP Disclosures:***

- 1) Hsu; Chia Wei, Qiu; Wenjun, Zhen; Bo, Shapira; Ofer, Soljagic; Marin, (issued March 2018) "Methods and apparatus for transparent display using scattering nanoparticles" US Patent 9,927,616
- 2) Ilic; Ognjen, Kaminer; Ido, Soljagic; Marin, Lahini; Yoav (issued June 2018) "Systems and methods for particle guiding" US Patent 10,004,135

***Doctoral Degrees Awarded During Reporting Period (First and Last Name):***

N/A

***Master's Degrees Awarded During Reporting Period (First and Last Name):***

N/A

## Strategic Research Area 3

### Transformational Nano-optoelectronic Soldier Capabilities

**SRA-3** primarily focuses on understanding fundamental optical, electronic and transport/reaction phenomena in nano-structured materials and learning how to apply these phenomena to enable major advances in portable power, communications, signal processing and detection. One project will harness non-Planck thermal radiation spectra from photonic crystal surfaces and near field surface emission phenomena to provide compact TPV and TPV/TE solid state electric power generators in the 1-100 W<sub>e</sub> range. Another project will study fundamental mechanisms of photon transport in 3-D and 2-D materials to enable 2-D optical integrated circuits for LIDARs, displays, communications and ultra-fast architectures for neuromorphic computing. A third team will capitalize on unusual optical resonances in condensed matter arising from Weyl points, other exceptional points, and *stable* topological bound states within the continuum to advance the state-of-the-art in high power IR and THz lasers for applications to amplifiers, spatial modulators, optical sensing and optical image processing. Another project will combine first-principles and analytical studies with novel device design and materials synthesis to explore use of topological phenomena (both photonic and electronic) in novel communications, signal detection and signal processing. The fifth project will seek to establish the basic principles to eventuate multi-scale 3D printing of high functionality fiber devices through synergistic integration of thermal fiber device drawing with 3D printing of the draw tower feed material. Benefits would include: recursive-manufacturing processes able to introduce nanoscale features into macroscale products in a highly controlled manner; by understanding fluid instability growth rate, new paradigms for creating solid state multimaterial “inks” for conversion into or functionalization of fibers; and capabilities to create non-equilibrium micro- and nano-structured multi-material solids of unusual shapes (e.g. Janus and beach ball like spherical particles) within fibers through capillary breakup of multimaterial cores.

.

**ISN Project Number: 3.1**

**Project Title: Solid State Power Generation at Millimeter Scales**

**Principal Investigator(s): Ivan Celanovic, Marin Soljačić, Peter Fisher**

***Summary of Accomplishments:***

During this period we have made significant progress in design, optimization, and fabrication of the first of a kind, standalone, fully functional, portable 20 W, solid state TPV generator as shown in *Figure 1. (c)*. The unit features new parallel-channel reactor, custom built control electronics, air delivery system, vacuum packaging, and custom built recuperator. In addition, we have scaled 2D-PhC fabrication to 4 inch tantalum wafers and made significant fabrication progress towards hafnia filled-cavity PhC selective emitter.

***TPV System Development:***

We focused our effort into three main areas: a larger 4x4 cm microcombustor capable of driving a 15-20 W system, a recuperator to recover heat from the exhaust, and balance of plant components.

We designed, fabricated, and tested a 4x4 cm microcombustor. We adopted a parallel channel design (we previously used a single meandering channel) in order to reduce pressure drop while maintaining the sufficient residence time within the microcombustor and sufficient catalyst area for the reaction to occur. To accomplish this, we used a combination of analytical modeling, numerical CFD simulations, and experimental testing. The final design has 24 parallel channels, each with a width of 1.1 mm and length of 28 mm. An inlet plenum distributes gas from the inlet tube to the channels; and exhaust plenum collects gas from the channels into the exhaust tube. For fabrication, we used the same diffusion brazing process developed for the 2x2 cm microcombustor. We designed and built all necessary jigs and fixtures. The parallel channel design relies on uniform channel width to distribute the flow of gases evenly among the 24 parallel channels, necessitating an involves set of jigs to maintain the spacing during fabrication. We fabricated 5-10 microcombustors as part of the fabrication process development. We performed testing of the microcombustor both in air and in vacuum with fuel flows ranging up to 900 W, twice the target operating point. We measured temperature and are currently in the process of analyzing exhaust gas composition. We will complete the characterization of the microcombustor next year, focusing on determining the range of conditions that result in complete combustion.

Additionally, we performed initial work on a recuperator to transfer heat from the exhaust gas stream to the inlet air stream. Our design methodology was to use a combination of analytical modeling, numerical simulations, and simple experiments. The final design is a multichannel primary surface heat exchanger built around a piece of corrugated foil. We designed and built the jigs and fixtures necessary to form the recuperator components from sheet metal. The components were assembled by spot welding then potted in refractory cement to minimize heat loss. We fabricated an initial experimental prototype and conducted some preliminary tests with the microcombustor. Currently, we are actively characterizing performance of the recuperator and this activity will continue into next year. A second iteration of the design may be necessary to optimize performance.

Finally, we performed initial work on balance of plant components. Propane is delivered by a commercial miniature mass flow controller (MFC) similar to our benchtop experiment. Air is supplied by a miniature centrifugal blower (eg for electronic cooling) and monitored by a miniature air flow sensor (eg for HVAC applications). We built a digital control system to servo the power delivered to the blower to maintain the reading from the air flow sensor at a set point. The control system also controls propane flow through the MFC in order to deliver both the required fuel and air to the microcombustor. We tested the control system experimentally with the microcombustor. These preliminary tests indicate that this a viable approach. The control system was able to operate the microcombustor over a wide range of power levels and was robust against changes in pressure drop. This activity will also continue next year, with emphasis improved robustness (replacing breadboards with soldered connections, refactoring code, etc.) and operating from a single power source with wide voltage range to mimic the output of the TPV cells.

### *Photonic Crystal Fabrication*

We have pursued 1) numerical simulations to design easier-to-fabricate filled photonic crystals (PhCs) based on in-band power as an evaluation metric and 2) the development of a fabrication process with for larger 4-inch wafer substrates with new resist.

#### 1) Numerical simulations for designing an easier-to-fabricate PhC with high in-band power

We have performed numerical simulations of realistic filled PhC designs and have evaluated these designs using a new metric, in-band power. In-band power is a measure of the absolute power emitted by the PhC. We have hypothesized that the radius must be increased in order to increase the in-band power. In our designs we have varied the radius as well as the period, but we have kept the period as small as possible with sidewall thicknesses of 100nm. We also have taken into account the previously-identified fabrication imperfections of the filled PhC, which are a hollow core due to incomplete cavity filling and a thick layer of hafnia on top of the PhC. It is unclear how the size of the hollow core and hafnia layer thickness change with the increased radius, so we have performed two kinds of simulations: (a) either the hollow core radius and hafnia layer thickness change proportionally with the radius or (b) they do not change. Our simulations were performed at 45° incidence angle (which is a good approximation of the hemispherical emittance) and room temperature, and we calculated in-band power at 1200K for a 2um photovoltaic cell bandgap.

According to our simulations, increasing the radius generally increases the in-band emitted power and it is theoretically possible to achieve ~25 to 36% increase in-band emitted power compared to a conformal PhC for a 2um PV cell bandgap at 1200K. In these designs the radii range from 0.23 to 0.25um and the periods from 0.58 to 0.60um. The design that achieves the highest improvement at 36% is a filled PhC with period 0.58um, radius 0.24um, and a hollow core and hafnia layer proportionally wider and thicker respectively. The impact of the hafnia layer thickness and hollow core size on the in-band emitted power will be the subject of future investigation.

#### 2) Development of a fabrication process for larger 4-inch wafer substrates with new resist

We have pursued two fabrication processes: a) Conformal PhC for TPV system demonstration and b) Filled PhC.

a) Conformal PhC for TPV system demonstration: We have tested the fabrication of the conformal PhC on dummy silicon substrates. During this we encountered two problems with the new resist. One, that the resist cross-linked during ashing and once cross-linked the PhC cavities could not enlarge to their target size and the resist could not be removed by dry etching or plasma ashing processes. To overcome this issue, we added an additional plasma ashing step in another layer, that of the anti-reflective coating (ARC), so that we could enlarge the PhC cavities to their target size. The second issue was that the resist adhered poorly despite the use the adhesion promoter HMDS. We have heard anecdotally that the adhesion promoter can be unreliable and have identified an alternative adhesion promoter to be used in future processing.

For the large area fabrication on the 4-inch Ta wafer, we have monitored the cavity sizes at different points on the wafer (using a polar coordinate system) to check the uniformity across the wafer. At the current stage, where we have finished the first ashing step, we have measured 60-100nm of variation in cavity diameters from edge to center. This issue may be mitigated by changing the interference lithography setup.

b) Filled PhC: We are currently working on fabricating the filled PhC with 0.58um period and 0.24um radius on Si. First we have designed a tri-layer resist stack with resist, SiO<sub>2</sub> interlayer, and ARC to minimize reflectivity and aspect ratio while ensuring that resist is thick enough for pattern transfer. We have identified the proper exposure dose, and have completed the pattern transfer into the ARC. Once the fabrication process in silicon is finished we will perform the fabrication on the tantalum substrate.

### ***Research Plans for Next Year:***

Our research plan regarding the system development for the next year is to integrate the system components (microcombustor, recuperator, and balance of plant) as well as the photonic crystal and low bandgap PV cells. The first step is to complete the component-level work indicated in the previous section: analysis of the microcombustor exhaust gases, and characterization of the recuperator's performance over

a range of flows and temperatures. When we are confident that the microcombustor-recuperator assembly is working, we will simultaneously begin to integrating the balance of plant and to package the microcombustor with IR-transparent windows such that it can be used with PV cells. Initial work will be done without the photonic crystal, and the photonic crystal will be added once sufficient confidence has been gained in the system. The final result will be a self-contained TPV system.

Our research plan regarding the photonic crystal development is to fabricate and measure the emittance of both conformal and filled PhCs. If the measured emittance deviates from the simulated emittance, we will use a combination of focused ion beam imaging and simulations to identify the fabrication imperfections and their impact on the PhC performance. We will consider dry etching or Ar ion sputtering to better control the thickness of the top hafnia layer. We will also investigate the thermal stability of the filled PhC, in particular to see if thermal expansion stresses affect the interface between tantalum and hafnia.

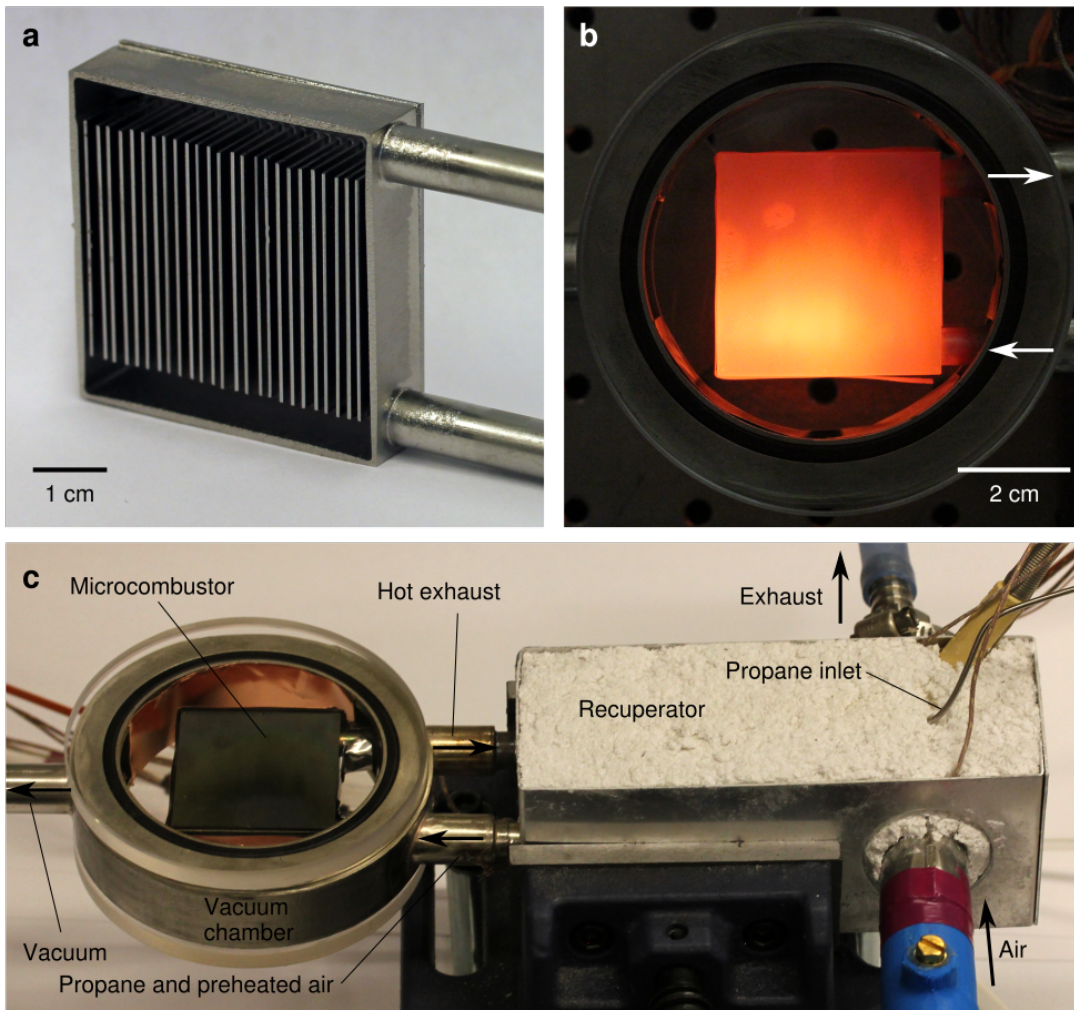


**Figure 1.** (a) Parallel channel microcombustor without its lid. (b) Microcombustor in operation. (c) Experimental setup with the microcombustor connected to the recuperator, which is potted in refractory insulation.



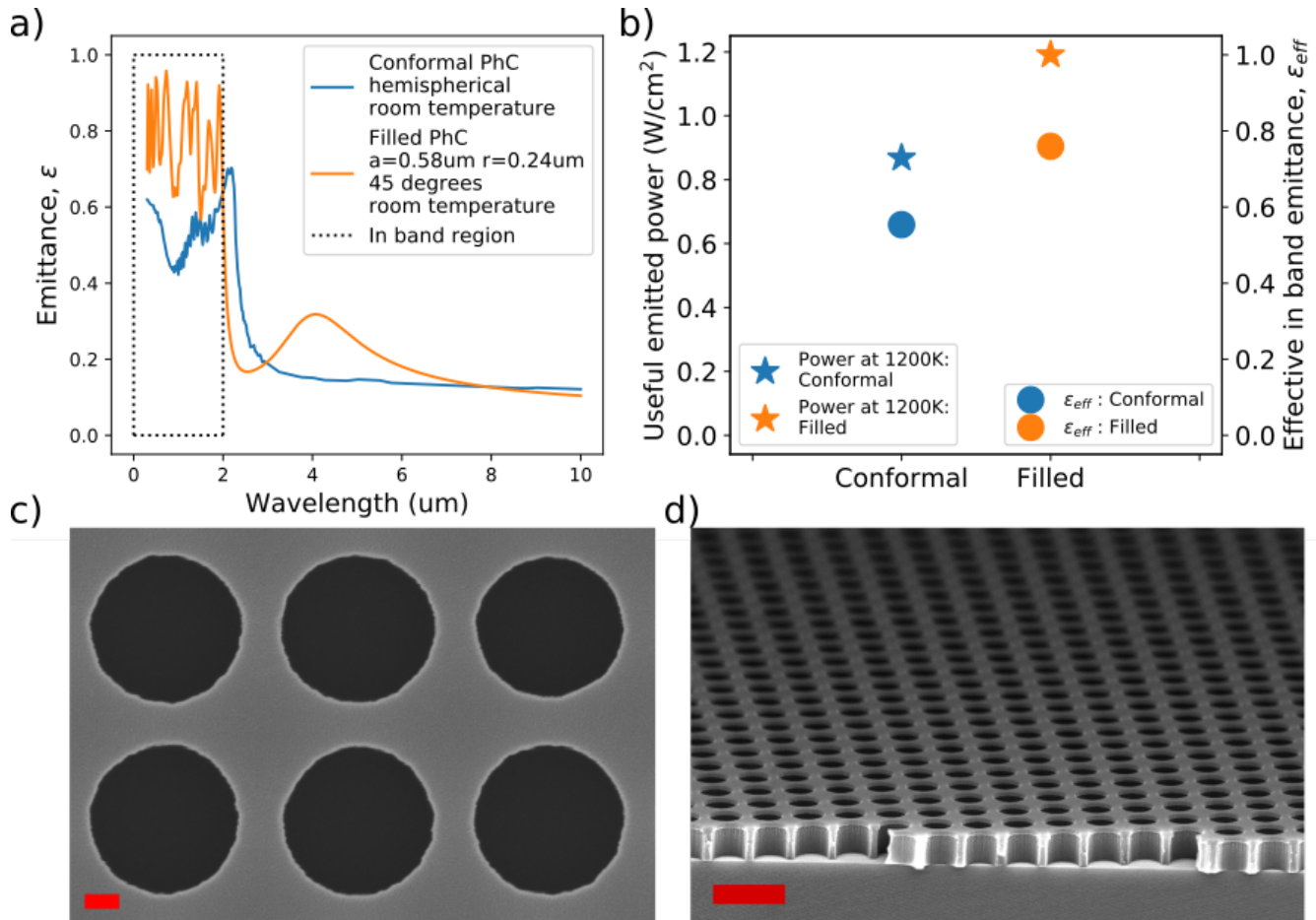


**Figure 2.** Simulation and fabrication of the filled PhC. Its simulated in-band emittance is higher than that of the conformal PhC (a), so that the filled PhC has 15.2% higher in-band emitted power (b). The filled PhC on silicon is currently being fabricated, with the top view in (c) and the cross section in (d).

**Papers Published in Peer-reviewed Journals** (Full citation required. Please include DOI if available):

- 1) "Active Radiative Thermal Switching with Graphene Plasmon Resonators" Ognjen Ilic, Nathan H. Thomas, Thomas Christensen, Michelle C. Sherrott, Marin Soljacic, Austin J. Minnich, Owen D. Miller, and Harry A. Atwater. *ACS Nano*, Vol.12, p.2474, (2018).

**Peer-Reviewed Conference Proceeding Publications** (Full citation required. Please include DOI if available):

- 1) **Plenary Talk:** "A few novel nanophotonic phenomena". M. Soljacic. From Solid State to Biophysics IX in Cavtat, Croatia, 2018. [Also reported in other ISN projects, since I talked about a few different topics.]
- 2) W. R. Chan, V. Stelmakh, S. Karnani, C. M. Waits, M. Soljacic, J. D. Joannopoulos, I. Celanovic, "Towards a portable mesoscale thermophotovoltaic generator." *J. Phys.: Conf. Ser.* 1052 012041, doi :10.1088/1742-6596/1052/1/012041, <http://iopscience.iop.org/article/10.1088/1742-6596/1052/1/012041>
- 3) R. Sakakibara, V. Stelmakh, W. R. Chan, S. Karnani, C. M. Waits, M. Soljacic, J. D. Joannopoulos, and I. Celanovic (Dec. 2018). "Improved Omnidirectional 2D Photonic Crystal Selective Emitter for Thermophotovoltaics." *J. Phys.: Conf. Ser.* 1052 012056, doi :10.1088/1742-6596/1052/1/012056, <http://iopscience.iop.org/article/10.1088/1742-6596/1052/1/012056>



---

***Books and Book Chapters:***

none

***Presentations at Meetings, but not Published in Conference Proceedings:***

- 1) Presenter, F.M. (year, month). Title of paper or poster. Paper or poster session presented at the meeting of Organization Name, Location.

***Patents, Patent Applications, and IP Disclosures:***

- 1) David Bierman, Ivan Celanovic, Walker Chan, Gang Chen, Daniel Kraemer, Andrej Lenert, Kenneth McEnaney, Young Suk Nam, Marin Soljatic and Evelyn Wang, (2018). “Spectrally-engineered solar thermal photovoltaic devices,” US patent No. 9,929,690

***Doctoral Degrees Awarded During Reporting Period (First and Last Name):***

none

***Master’s Degrees Awarded During Reporting Period (First and Last Name):***

none

ISN Project Number: 3.2

Project Title: **Photonic Integrated Circuits for LIDARs, Displays & Low-power Computing**

Principal Investigator(s): **Dirk Englund, Marin Soljačić**

### Summary of Accomplishments:

#### Task 1: LIDAR

##### General principle and implementation

A schematic of this lens-based beam-steering device is seen in Fig. 1. First, a tunable IR source centered at  $\lambda_0 = 1.55 \mu\text{m}$  is fiber-coupled to an on-chip, silicon nitride ( $\text{Si}_3\text{N}_4$ ) waveguide. Next the signal is routed through a switch matrix composed of a depth tree of Mach-Zehnder interferometric switches (of size  $N$ ) which use integrated thermo-optic (TO) phase shifters. Then, light from the waveguide enters a slab waveguide, where it is diffracted and then refocused by an aplanatic lens, formed from a patterned amorphous silicon (a-Si) layer. Finally, the collimated beam propagates into a 1D grating where it is scattered out-of-plane. Beam steering for the chip is achieved through two mechanisms. (1) Port switching changes the in-plane angle of propagation into the lens and consequently the azimuthal angle,  $\phi$ , enabling wide-angle steering. (2) Wavelength ( $\lambda$ ) tuning changes the polar angle,  $\theta$ , at which the collimated beam is scattered out of the grating and into the far-field. Switching ports translates the emitted beam in the plane (side-to-side). Tuning  $\lambda$  translates the beam up and down.

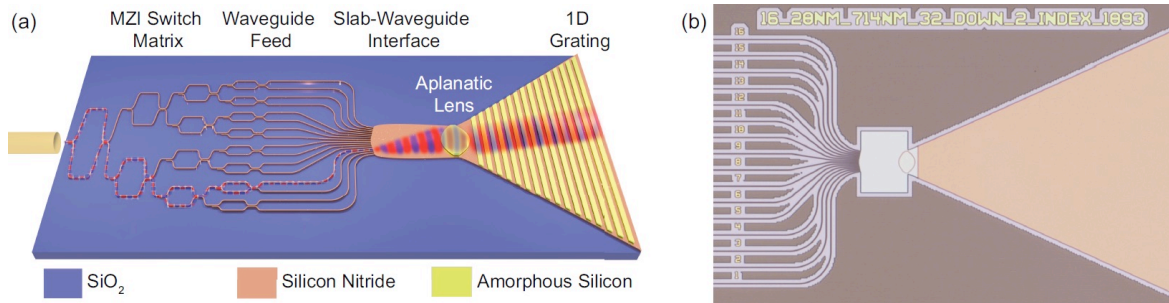


**Figure 1:** Schematic of the LIDAR lens-based beam steering device.

##### Comparison with other optical beam steering techniques

This architecture has several advantages over traditional phased-array approaches. First, because only a sub-set of the switches are used simultaneously, the phase-shifter power requirements scale as  $\log_2 N$ , where  $N$  is the number of ports, whereas phased-array architectures scale with  $N$ , where  $N$  is the number of antenna elements. This can lead to large power savings when a large number of far-field spots are desired. Second, this approach avoids the phasing architecture necessary to cohere phased-arrays, greatly reducing the complexity of both the transmit and receive side control architectures while also increasing stability to temperature and environmental variations. Finally, we can emit multiple beams from the device (e.g. exciting all ports simultaneously) without any penalties in beam quality.

##### Experimental results

As a proof of concept, we measure a 16 port device with a  $\text{Si}_3\text{N}_4$  slab=197 nm, a-Si=24.5 nm, and grating pitch  $\Lambda=714$  nm. Far-field measurements are shown. The azimuthal angle range is  $\phi_{\text{range}} = 38.8^\circ$  from  $\phi = (21.0^\circ \text{ to } -17.8^\circ)$  with a mean angle step increment of  $\overline{\Delta\phi} = 2.58$  via port switching. The polar angle range is  $\theta_{\text{range}} = 12.0^\circ$  from  $\theta = (22.6^\circ \text{ to } 34.6^\circ)$  with a mean angle step increment of  $\overline{\Delta\theta} = 0.12^\circ/\text{nm}$  via  $\lambda$  tuning from 1500 nm to 1600 nm. Collaboration with MIT Lincoln Laboratory.



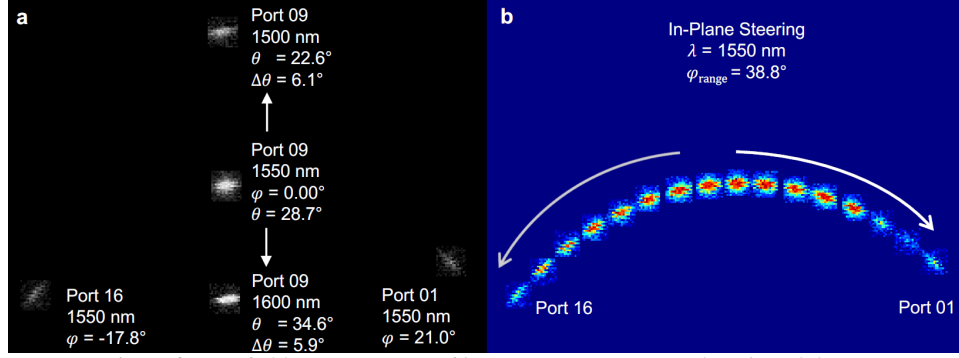


**Figure 2:** Far-field measurements of beam steering using our lens-based device.

## Task 2: Optical Computing

*General principle and implementation.* An N-spin Ising problem without an external magnetic field can be formulated as follows: *finding the minimum of the Hamiltonian*:  $H = -\sum_{1 \leq i < j \leq N} K_{i,j} \sigma_i \sigma_j$ , where  $K_{i,j}$  is the interaction term between spins  $\sigma_i$  and  $\sigma_j \in -1, 1$ . It has been shown that recurrent Neural Networks (NN) architectures could be used to find local minima and good approximate solutions of Ising problems. Both architectures rely on, at each recurrent loop, the implementation of a matrix multiplication and a non-linear threshold function. We here use a modified noisy Little NN. Its dynamics, in a long-time and high noise limit, are given by a Gibbs distribution minimizing the Ising Hamiltonian  $H$ .

The general principle of the Photonic Recurrent Ising Sampler (PRIS) is shown in Figure 3. For example, the linear optical interference unit can be achieved with MZI network, diffractive optics, ring resonator filter banks, and free space lens-SLM-lens system, the optical drop-out can be implemented with simple electro-optical absorber, modulator or a single MZI, the nonlinearity unit can be implemented with optical nonlinearity, or simple analog/digital electronics.

*Theoretical performance and estimated on-chip performance.* Our system can theoretically solve general Ising problems. We evaluated the performance for MAX-CUT and spin glasses graphs. Implemented on a GHz-platform, as can be realized with recent advances in integrated photonics, this algorithm could outperform other optical Ising machines by several orders of magnitude.

*Comparison with other sampling techniques.* Our algorithm can also be used to probe critical behaviors and their critical exponents. We benchmarked our system against the famous Metropolis-Hastings algorithm on the toy model 2D ferromagnetic Ising model.

### Experimental results.

We experimentally demonstrated the PRIS on a programmable nanophotonic processor (PNP) made of an array of Mach-Zehnder Interferometers fabricated in the silicon-on-insulator (SOI) process. We obtained ground state of a wide library of 4-spin Ising models and demonstrated our ability to use dynamic extrinsic noise to power the ground state search (here, dynamic noise is implemented by the reshuffling of the phase-shifters configuration at every step of the algorithm).

A single iteration of the experimental recurrent sampler architecture consists of four separate passes through the photonic integrated chip. Each desired unitary operation ( $U$  and  $U^\dagger$ ) requires two passes through the chip to implement a variant of homodyne detection in which output mode amplitudes and phases are measured relative to adjacent modes and using a single idler with known amplitude as a global reference. Not all of the elements of the sampler are unitary, however, and the remaining operations are performed in CPU. These include application of the diagonal matrix  $D$ , Gaussian noise, and the nonlinear thresholding function.

We observe boosted ground state probabilities for a range of 4-spin compared to a random search. In addition, the measured ground state probabilities agree very closely with simulated PNP behavior and Little Model theoretical

ground state probabilities. We also observe signature of a noise-assisted sampling regime, where one can tune the extrinsic noise level to maximize the enhancement in the ground state probability.

### Research Plans for Next Year:

We plan to improve our LIDAR system using novel components, including:

- Luneburg lenses to achieve a much wider field of view and greater resolution with greater robustness to manufacturing tolerances
- Curved and bi-directional gratings to increase power efficiency and decrease off-axis aberrations

Regarding optical computing, our plans include:

- Investigate scaling of PRIS with different optical architectures
- Efficient mapping of PRIS to other NP-hard problem solvers
- Investigate interplay between optical nonlinearities and learning of correlations
- Publish two papers on the PRIS

### Representative Image and Caption:

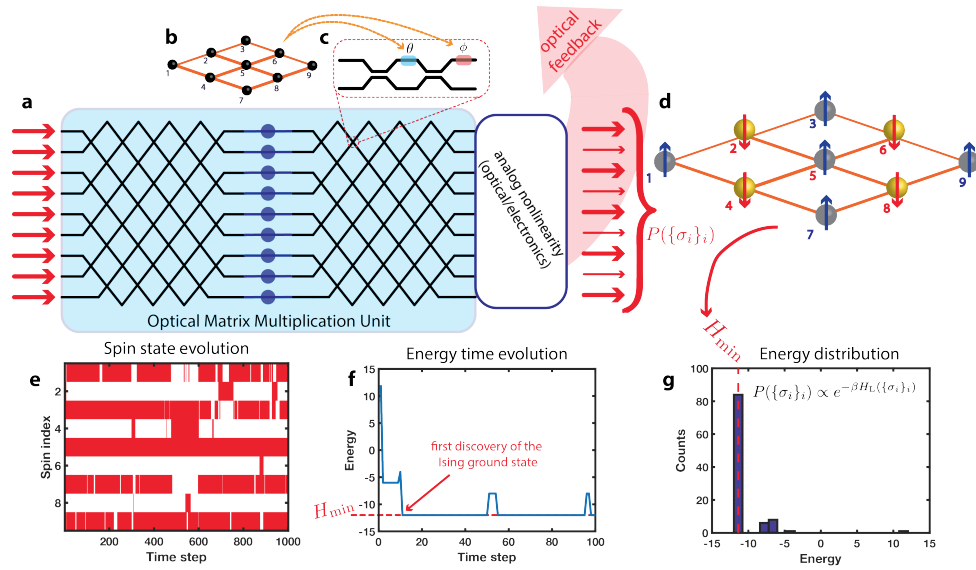


**Figure 3: General concept of a recurrent Optical Ising Machine.** (a) In-phase optical signal, encoding a spin state, is fed to an Optical Matrix Multiplication Unit. An arbitrary Ising problem (here, 9-spin 2D ferromagnetic (b)) is encoded into the phases of the MZI network (c). The signal then goes through an analog nonlinear unit and is fed back to the chip input. After a finite number of iterations, the optical output encodes the ground state (d) of the Ising problem. The spin state (resp. energy) evolution as a function of time is shown in (e) (resp. (f)). The optical signal converges in probability to the Gibbs distribution of the associated Ising problem (f), for which the ground state (d) is exponentially more likely.”

***Papers Published in Peer-reviewed Journals (Full citation required. Please include DOI if available):***

- 1) "Nanophotonic particle simulation and inverse design using artificial neural networks" John Peurifoy, Yichen Shen, Li Jing, Yi Yang, Fidel Cano-Renteria, Brendan Delacy, Max Tegmark, John D. Joannopoulos, Marin Soljacic. *Science Advances*, Vol.4, no.6, eaar4206, (2018). [Also reported in ISN 3.3. because of overlap of research.]

***Peer-Reviewed Conference Proceeding Publications (Full citation required. Please include DOI if available):***

- 1) ***Plenary Talk:*** "Artificial Neural Networks in Nanophotonics". M.Soljacic. JST Workshop in Tokyo, Japan, 2018. [Also reported in ISN 3.3, since I talked about a few different topics.]
- 2) ***Keynote Talk:*** "Some recent results in active nano-photonics". M.Soljacic. IEEE Photonics Society Summer Topical Meeting Series in Kona (HI), USA, 2018. [Also reported in ISN 3.3, since I talked about a few different topics.]
- 3) ***Plenary Talk:*** "A few novel nanophotonic phenomena". M. Soljacic. From Solid State to Biophysics IX in Cavtat, Croatia, 2018. [Also reported in other ISN projects, since I talked about a few different topics.]
- 4) ***Invited Talk:*** "Planar-lens Enabled Beam Steering for Chip-scale LIDAR", Josue Lopez, Scott Skirlo, Dave Kharas, Jamison Sloan, Jeffrey Herd, Paul Juodawlkis, Marin Soljacic, and Cheryl Sorace-Agaskar. CLEO in San Jose (CA), USA, 2018.
- 5) ***Invited Talk:*** "D Englund, "Semiconductor Quantum Technologies for Secure Communications and Scalable Quantum Networks," Brigham Young ECEN Colloquium, BYU, Provo, Utah (2018)"
- 6) ***Invited Talk:*** D Englund, "The Dawn of the Quantum Information Era," The Future of Nanoscale Electronics (2018)
- 7) ***Invited talk:*** D Englund, "Large-Scale Programmable Photonic Circuits and Applications in Quantum Information Processing," QCMC 2018, Baton Rouge, LA (2018)

***Books and Book Chapters:***

- 1) N/A

***Presentations at Meetings, but not Published in Conference Proceedings:***

- 1) N/A

***Patents, Patent Applications, and IP Disclosures:***

- 1) U.S. Patent Application Number: 16/032,737

***Doctoral Degrees Awarded During Reporting Period (First and Last Name):***

N/A

***Master's Degrees Awarded During Reporting Period (First and Last Name):***

Charles Roques-Carmes, MS in Electrical Engineering and Computer Science

Mihika Prabhu, MS in Electrical Engineering and Computer Science

**ISN Project Number: 3.3**

**Project Title: Nanophotonics-Enhanced Systems for the Soldier**

**Principal Investigator(s): Steven Johnson, Marin Soljačić, John Joannopoulos**

### Summary of Accomplishments:

**THz gas laser design and modeling:** We have developed a new theoretical model to understand the molecular gas optically pumped far-infrared (OPFIR) laser behavior. Unlike previous OPFIR-laser models involving only a few energy levels that failed even qualitatively to match experiments at high pressures, our newly developed ab-initio theory matches experiments quantitatively at all pressures with no free parameters. Our new model includes a vast number of physical processes, from nonlinear collisions to diffusion, that were previously neglected, taking advantage of a new numerical method that is capable of solving the millions of coupled nonlinear rate equations that are required. Not only does the model match experiments quantitatively; it also unexpectedly shows that our compact laser exhibits remarkable conversion efficiency, up to 39% of the Manley–Rowe limit. Our compact laser is **1000× smaller** in volume while delivering more than **10× greater efficiency** than the best commercial OPFIR lasers, as shown in Figure 1 (at end).

**Inverse design of large-area metasurfaces:** We developed a prototype framework for efficient optimization-based “inverse design” of large-area “metasurfaces” for applications such as broadband/angle-insensitive lenses and demultiplexers. To optimize surfaces that can be thousands of wavelengths in diameter, with thousands (or millions) of parameters, the key is a fast approximate solver for the scattered field. We employ a “locally periodic” approximation in which the scattering problem is approximated by a composition of periodic scattering problems from each unit cell of the surface, and validate it against brute-force Maxwell solutions (Fig. 2). Compared to previous design approaches, we have greatly increased flexibility, e.g. to automatically balance tradeoffs between multiple frequencies or to optimize a photonic device given only partial information about the desired field. Preliminary work indicates that our approach even extends beyond the metasurface regime to non-subwavelength structures where additional diffracted orders must be included (but the period is not large enough to apply scalar diffraction theory).

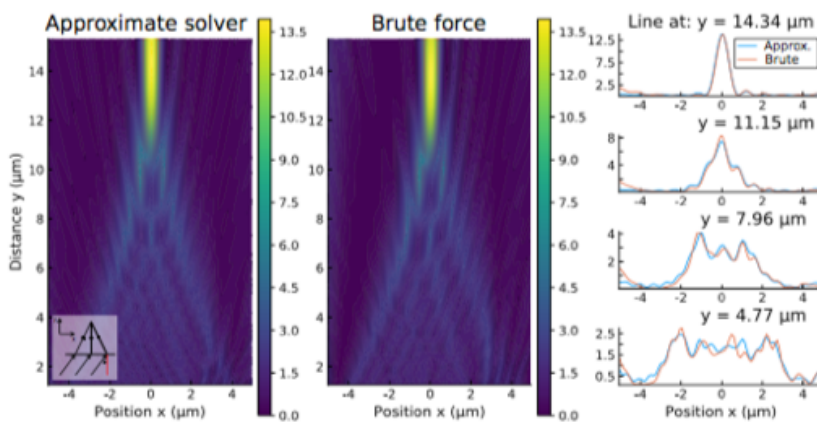


**Figure 2.** Left:  $|E|$  intensity plot of the scattered field of a metalens using our locally periodic approximate solver showing good agreement with a brute force calculation (middle). Right: the field sections computed by the two solvers show perfect agreement close to the focal lines (top). This agreement starts to deteriorate the closer the section is to the metasurface (bottom).

At a theoretical level, we also developed a precise theory of “locally uniform” metasurface approximations like those that have been used heuristically in the literature. Not only do we obtain a type of adiabatic theorem showing that the “zeroth-order” locally uniform approximation converges in the limit as the surface varies more and more slowly, including a way to quantify the rate of convergence, but we also obtain an infinite series of higher-order corrections. These corrections, which can be computed to any desired order by performing integral operations on the surface fields (shown in Fig. 3), allow rapidly varying surfaces to be modeled with arbitrary accuracy, and also allow one to validate designs based on the zeroth-order approximation (which is often surprisingly accurate) without resorting to expensive brute-force Maxwell solvers. We showed that our formulation works arbitrarily close to the

surface, and can even compute coupling to guided modes, whereas in the far-field limit our zeroth-order result simplifies to an expression similar to what has been used by other authors.

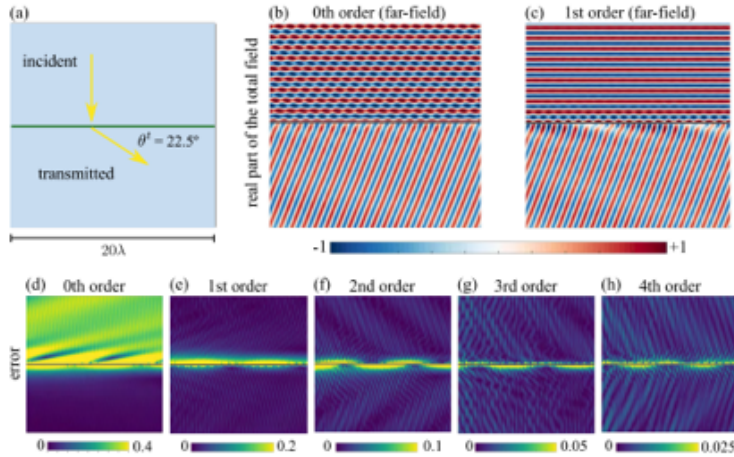


**Figure 3.** High-order corrections to the ray optics approximation. (a) Geometrical configuration of the problem under consideration which corresponds to an unit amplitude planewave impinging at normal incidence on a metasurface that renders a transmitted planewave with wavevector forming an angle of  $22.5^\circ$  with respect to the metasurface. (b) and (c): Real part of the total field 0th and 1st order approximation. (d), (e), (f), (g) and (h): Absolute errors for  $N= 0, 1, 2, 3, 4$ , respectively, in zeroth, first, second, third and fourth order corrections to the ray optics approximation. The color scales were adjusted according to the maximum error displayed in each figure.

**Neural-network photonics design:** We investigated (*Science Advances*, Vol.4, no.6, eaar4206, (2018).) a method to use artificial neural networks to approximate light scattering by multilayer nanoparticles. We find the network needs to be trained on only a small sampling of the data in order to approximate the simulation to high precision. Once the neural network is trained, it can simulate such optical processes orders of magnitude faster than conventional simulations. Furthermore, the trained neural network can be used to solve nanophotonic inverse design problems by using back-propagation – where the gradient is analytical, not numerical.

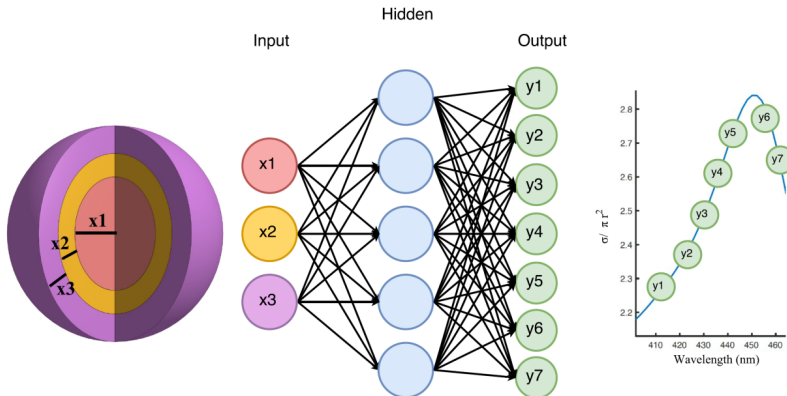


**Figure 4:** The neural network architecture has as its inputs the thickness of each shell of the nanoparticle, and as its output the scattering cross section at different wavelengths of the scattering spectrum. Our actual neural network has four hidden layers.

While we focused here on a particular problem of light scattering from nanoparticles, the approach presented here can fairly easily be generalized to many other nanophotonic problems. This approach offers both the generality present in numerical optimization schemes (where only the forward calculation must be found), and the speed of an analytical solution (owing to the use of an analytical gradient). Conceptually, there are a number of reasons why the approach used here is useful for a myriad of branches of physics. After the neural network is trained, it allows us to obtain approximate answers quickly (orders of magnitude savings), enabling inverse design and optimization.

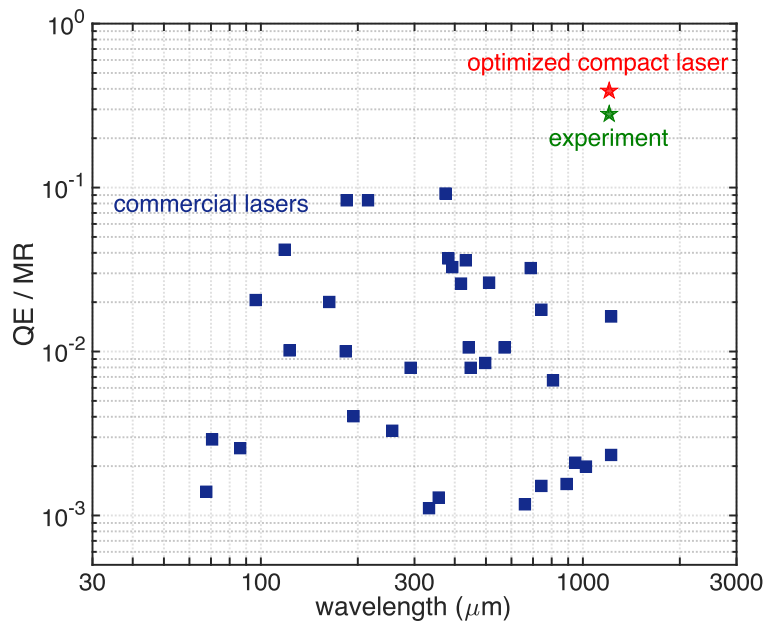
### Research Plans for Next Year:

- **THz OPFIR:** we will extend our work to **new gases** (such as CO and  $N_2O$ ) for efficient high-power sources at other THz wavelengths, as well as demonstration of a fully compact OPFIR laser system with wide frequency tunability by replacing CO<sub>2</sub> pump laser with quantum cascade laser.
- **Laser theory:** we have a prototype technique to solve the SALT equations of micro-laser theory orders of magnitude faster than published work, while exploiting off-the-shelf photonics solvers, that we intend to refine and apply to large-area surface-emitting lasers. We will also work on understand the stability of such lasing modes, which has never been explored in a fully nonlinear theory.



- *Metasurface design*: extension to fully three-dimensional designs, new applications at a variety of frequencies, curved surfaces, and coupling to large-scale “topology” optimization over 100s or 1000s of parameters per unit cell.
- *Neural networks*: We plan to work on one-sided emission from photonic crystal slabs: this is important for integration of planar devices to the free-space propagation. We also plan to investigate novel inverse design techniques with artificial neural networks, including Generative Adversarial Networks (GANs).

### Representative Image and Caption:



**Rep. Image:** Total quantum efficiency ( $QE = \text{THz power out/IR power in}$ ) of commercial “CH.F OPFIR lasers and our compact OPFIR laser, normalized by the Manley–Rowe (MR) limit on QE. Our experimentally demonstrated laser achieves a QE that is 29% of the MR limit which improves to 39% after cavity optimization. Both are 10× better than the best commercial laser at the same frequency (0.25 THz or 1.2 mm wavelength), while being 1,000× smaller. (Published in PNAS, 2018.)

### Papers Published in Peer-reviewed Journals (Full citation required. Please include DOI if available):

- 1) F. Wang, J. Lee, D. J. Phillips, S. G. Holliday, S.-L. Chua, J. Bravo-Abad, J. D. Joannopoulos, M. Soljačić, S. G. Johnson, and H. O. Everitt, (June 26, 2018). “A high-efficiency regime for gas-phase terahertz lasers”, *Proceedings of the National Academy of Sciences*, **115** (26), 6614–6619 (2018). doi: <https://doi.org/10.1073/pnas.1803261115> John Peurifoy, Yichen Shen, Li Jing, Yi Yang, Fidel Cano-Renteria, Brendan Delacy, Max Tegmark, John D. Joannopoulos, Marin Soljačić, “Nanophotonic particle simulation and inverse design using artificial neural networks”. *Science Advances*, Vol.4, no.6, eaar4206, (2018). [Also reported in ISN 3.2. because of overlap of research.]
- 2) Hengyun Zhou, Chao Peng, Yoseob Yoon, Chia Wei Hsu, Keith A. Nelson, Liang Fu, John D. Joannopoulos, Marin Soljačić, Bo Zhen. “Observation of Bulk Fermi Arc and Polarization Half Charge from Paired Exceptional Points”. *Science*, 10.1126/science.aap9859 (2018). [Also reported in ISN 3.4, because of the overlap of the topics of research.]

### Peer-Reviewed Conference Proceeding Publications (Full citation required. Please include DOI if available):

None.

***Books and Book Chapters:***

None.

***Presentations at Meetings, but not Published in Conference Proceedings:***

- 1) ***Plenary Talk:*** M. Soljačić. (2018). “Artificial Neural Networks in Nanophotonics”. JST Workshop in Tokyo, Japan, 2018. [Also reported in ISN 3.2, since the author talked about a few different topics.]
- 2) ***Keynote Talk:*** M. Soljačić. (2018). “Some recent results in active nano-photonics”. IEEE Photonics Society Summer Topical Meeting Series in Kona (HI), USA, 2018. [Also reported in ISN 3.2, since author talked about a few different topics.]
- 3) ***Plenary Talk:*** M. Soljačić. (2018). “A few novel nanophotonic phenomena”. From Solid State to Biophysics IX in Cavtat, Croatia, 2018. [Also reported in other ISN projects, since author talked about a few different topics.]
- 4) ***Plenary Talk:*** S. Johnson (June 2018), “Real physics from ‘unphysical’ simulations,” ICERM workshop: Computational Aspects of Time-dependent Electromagnetic Wave Problems in Complex Materials, Brown University USA.
- 5) ***Invited Talk:*** S. Johnson (May 2018), “Theory and optimization of slowly varying electromagnetic metasurfaces,” Inverse Problems: Modeling and Simulation, Malta.

***Patents, Patent Applications, and IP Disclosures:***

None.

***Doctoral Degrees Awarded During Reporting Period (First and Last Name):***

None.

***Master’s Degrees Awarded During Reporting Period (First and Last Name):***

None.

**ISN Project Number: 3.4**

**Project Title: *Applications of Novel Topological Phenomena***

**Principal Investigator(s): *Liang Fu, Nuh Gedik, Marin Soljačić***

***Summary of Accomplishments:***

Since this project started in January 2018, our team has published 2 papers in top journals on topological photonics, completed a major instrumentation upgrade/integration, and started thin film growth of topological materials.

**Topological Photonics:**

In a collaboration between 3 ISN affiliates Soljačić, J.D. Joannopoulos and L. Fu, we theoretically proposed and experimentally demonstrated a bulk Fermi arc formed in an open photonic crystal slab due to the presence of non-Hermitian radiative losses. Discovered and characterized the existence of half-integer topological charges in the polarization of far-field radiation around the bulk Fermi arc. Both phenomena were shown to be direct consequences of the non-Hermitian topological properties of exceptional points. The work published in Science [1] spans the fields of topological photonics, non-Hermitian physics, and singular optics.

Soljačić's group theoretically proposed a scheme for realizing charged flux tubes, by placing a charged object with an intrinsic magnetic dipole moment between two blocks of a high-permeability material. The scheme can be used as a stepping stone to the realization of Wilczek's anyons—a composite state of charged particles and magnetic flux tubes—particles obeying fractional statistics. The work published in Physical Review Letters [2] spans the fields of optical metamaterials and interacting many-body topology.

**Topological Materials:**

Recent discovery of  $\text{Pb}_{1-x}\text{Sn}_x\text{Te}$  as topological crystalline insulator predicted by Fu, with bulk and surface band structure that can be modulated with doping, thickness and structural distortions, has created new opportunities to fabricate samples suitable for quantum infrared radiation (IR) detection. Gedik's group has recently built a combined MBE (molecular beam epitaxy) - trARPES (time and angle resolved photoelectron spectroscopy) system, which provides an ideal platform to systematically investigate and tune the electronic and optical properties and enables us to study how band structure of a material changes after excitation by electromagnetic radiation such as IR. His group also has a time domain terahertz spectroscopy setup, which enables us to measure changes in photoconductivity of a material following illumination by IR. Both these setups will be extensively used to optimize  $\text{Pb}_{1-x}\text{Sn}_x\text{Te}$  films for quantum IR detection.

Presently Gedik's group has finished integrating the MBE system to his existing trARPES setup and are growing films of topological insulator  $\text{Bi}_2\text{Se}_3$  to optimize the MBE system (see Image). At the same time, his group has calibrated the deposition rate of Sn source in our MBE. Within next few months Te and Pb sources will be introduced in the MBE chamber and be calibrated. We aim to start growing and measuring films of  $\text{Pb}_{1-x}\text{Sn}_x\text{Te}$  once the calibration routine is complete (see Research Plan).

***Research Plans for Next Year:***

Topological crystalline insulators for infrared detection: Gedik's group initially intend to develop a recipe for MBE growth of high quality films of  $\text{SnTe}$  by measuring their structural and electronic properties as a function of growth parameters such as substrate preparation, growth temperature and growth rate. Once a growth recipe is established, Gedik and Fu' group will study different ways to modulate the band structure and the chemical potential of the films with the aim of increasing their sensitivity towards IR detection. Firstly, we will study effect of thickness on bandgap



of SnTe using trARPES, where a large increase in bandgap (up to 0.5 eV) is expected with decreasing thickness.<sup>3</sup> Since SnTe is p-type doped, we also intend to study  $\text{Pb}_x\text{Sn}_{1-x}\text{Te}$  as a function of Pb doping concentration,  $x$ , which affects carrier doping (increasing  $x$  leads to increased n-type tendency) as well as the bandgap of the material, both of which are important parameters for optimal performance of IR detector.<sup>3</sup> We also intend to study effect of strain induced by lattice mismatched substrates on these films, which is expected to modulate their band gap.<sup>3</sup> An important part of our study of these films using trARPES setup will be to excite them using IR pulses and measure the resulting change in band structure. trARPES allows us to *visualize* the photocarrier generation due to IR absorption and their subsequent relaxation, which will guide us to optimize growth parameters to obtain films with best detector performance. Furthermore, as a direct probe for establishing functionalities of these materials as IR detectors, we will use time domain terahertz spectroscopy setup in our lab to study changes in their optical conductivity upon illumination by IR. Measuring changes in photoconductivity as a function of illuminating IR frequency, Pb doping, thickness and strain will allow us to systematically chart the effectiveness of  $\text{Pb}_x\text{Sn}_{1-x}\text{Te}$  films for application in quantum IR detection.

Synthetic gauge fields and Floquet topology: Soljačić's group plans to investigate photonic synthetic gauge fields in Floquet systems via dynamic modulation. Modulation-based  $T$  breaking, though a well-established notion, was recently revitalized in the context of Floquet topology. We will design and realize traveling-wave polarization encoder/transceiver and isolator/circulators. From a scientific point of view, we will experimentally achieve nontrivial Floquet photonic topology. Application wise, our device will strike a balance between footprints, bandwidth and insertion loss.

Time-invariant topological photonics and non-Abelian Berry phases: Soljačić's group will extend and apply theoretical tools employing the non-Abelian Berry phase—developed in condensed matter theory for the analysis of the quantum spin Hall effect—to the analysis of symmetry-protected two- and three-dimensional photonic topological phases.

Utilizing exceptional point for sensing: Fu's group will build on his recent theory of non-Hermitian topological phenomena to study sensitivity of perturbation at exceptional points, including high order ones. In particular, we will quantify the figure of merit for improved sensitivity and find the optimum condition for sensing near exceptional points. We will continue to collaborate with Soljačić's group to demonstrate exceptional sensitivity in photonic systems, and explore the physical realization of exceptional points in quantum solids.

### ***Representative Image and Caption:***

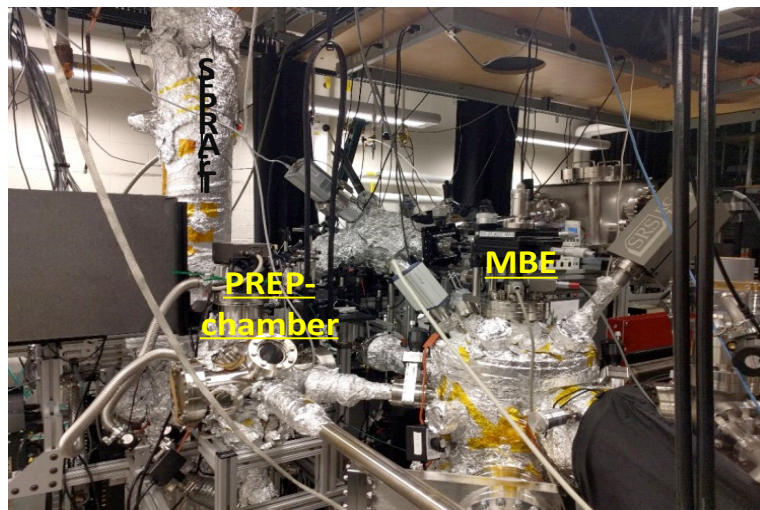


**Figure:** Layout of the combined MBE-trARPES system. Films grown in the MBE chamber will be transferred in situ to trARPES chamber via the prep chamber.

***Papers Published in Peer-reviewed Journals*** (Full citation required. Please include DOI if available):

- 1) H. Zhou, C. Peng, Y. Yoon, C.W. Hsu, K.A. Nelson, L. Fu, J.D. Joannopoulos, M. Soljačić, B. Zhen. (2018). *Observation of bulk Fermi arc and polarization half charge from paired exceptional points*, Science **359**, 1009.
- 2) M. Todorić, D. Jukić, D. Radić, M. Soljačić, H. Buljan, *Quantum Hall effect with composites of magnetic flux tubes and charged particles*, Phys. Rev. Lett. **120**, 267201 (2018).

***Peer-Reviewed Conference Proceeding Publications*** (Full citation required. Please include DOI if available):

- 1) ***Plenary Talk:*** "A few novel nanophotonic phenomena". M. Soljagic. From Solid State to Biophysics IX in Cavtat, Croatia, 2018. [Also reported in other ISN projects, since I talked about a few different topics.]

***Books and Book Chapters:***

- 1) N/A

***Presentations at Meetings, but not Published in Conference Proceedings:***

- 1) N/A

***Patents, Patent Applications, and IP Disclosures:***

- 1) N/A

***Doctoral Degrees Awarded During Reporting Period (First and Last Name):***

N/A

***Master's Degrees Awarded During Reporting Period (First and Last Name):***

N/A

**ISN Project Number: 3.5**

**Project Title: Novel Multimaterial Inks for Multiscale 3D Device Printing**

**Principal Investigator(s): Yoel Fink, John Joannopoulos, (A. Stolyarov as Collaborator)**

### ***Summary of Accomplishments:***

Additive manufacturing has been rapidly advancing with an increasing range of materials and with increasing speed. However, what is still elusive is the ability to introduce functionalities in printed products due to difficulties in printing and combining different material classes necessary to fabricate a device. The objective of this project is to demonstrate the use of a universal multimaterial filament with functional micro- or nano- structured domains as an “ink” for the fabrication of functional printed architectures. In the previous year, we introduced a new print technique termed Filament Surface Heating, engineered an apparatus for printing of multimaterial fibers, simulated the temperature profile of the fiber upon extrusion from a heated nozzle, and printed several novel photodetecting three-dimensional devices from a photodetecting fiber including the first-ever printed lens-less omnidirectional localized light-sensing device. For these few months, our main achievements have been:

- Understanding the wetting phenomenon of a viscous heated filament.
- Fabrication and characterization of a pixelated light-emitting filament using the phenomenon of in-fiber capillary breakup.
- Utilizing our modified print process (Filament Surface Heating) to print macro (centimeter-scale) optoelectronic systems of high device resolution (50  $\mu\text{m}$ ) from the light-emitting filaments.
- Creating the first-ever 360° light-emitting printed display.

### ***Wetting of viscous multimaterial filament***

In order to determine the suitable range of print speed and nozzle temperature for printing these multimaterial filaments, we make use of a filament that contains two conducting polyethylene (CPE) blocks that are spaced apart at a fixed distance to characterize the impact of wetting onto these heated filaments. As shown by the schematic in Figure 1a, at high temperature and low speed, there is a tendency for the CPE blocks to be pushed apart by the spreading and flowing encapsulating thermoplastic. Such spreading can, however, be controlled through the deposition speed of the filament through the nozzle. As the deposition speed increases, the duration for heat to diffuse into the domain containing the CPE blocks decreases. This results in a condition at which the polymer core surrounding the CPE blocks remain in its solid state with little deformation, while the surface of the filament is hot enough so that polymeric chains between individual printed lines can inter-diffuse into each other to form fusing bonds. This hypothesis is illustrated and proven in the inset of Figure 1b, for which increasing the speed reduces the spacing between the 2 CPE blocks, while still maintaining good adhesion to the underlying substrate. Measuring the CPE spacing (Plot of Figure 1b) further validates the point as the CPE spacing of the printed filaments tends towards the CPE spacing of the original pristine filament as the speed is increased. Increasing the speed, however, reduces the surface temperature of the filament for fusion, resulting in peel-off or non-adhesion of the deposited filaments. Within this plot, regions which inform good or poor adhesion can be identified through a visual check if the printed lines remain adhered to the print bed. Eventually, the optimal condition to retain the structure and functionality of the printed filament is determined by the range of speed at which one can obtain both good adhesion and CPE spacing similar to the original filament (yellow region in Figure 1b plot).

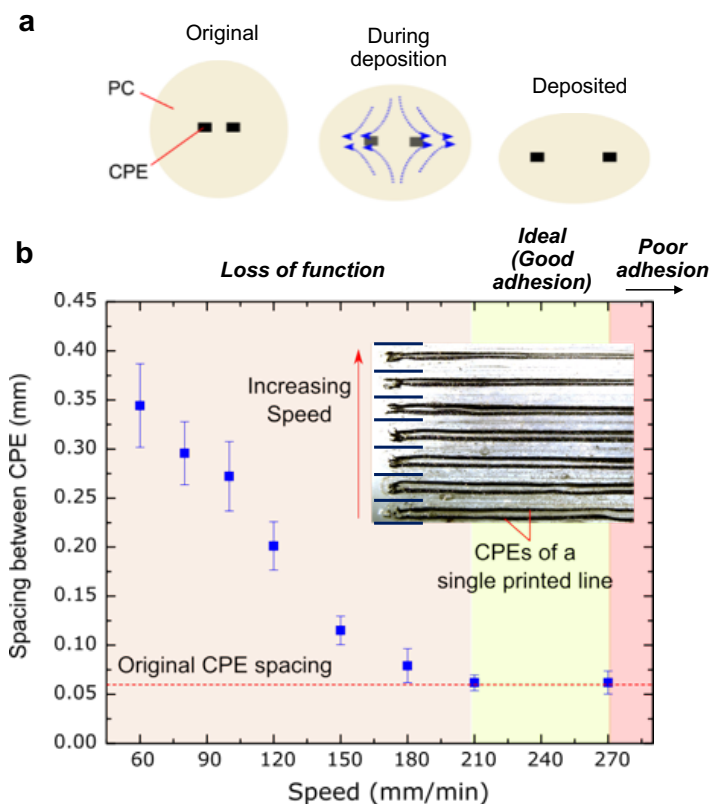


**Figure 1. Understanding and controlling wetting.** (a) Common wetting phenomenon of a heated filament that occurs as it is being deposited on a print bed. Carbon-loaded polyethylene (CPE) within the thermoplastic, Polycarbonate (PC), is initially spaced closely together but becomes spread-out during the deposition due to wetting. (b) Plot of CPE spacing vs speed of deposition which shows the decrease in spreading of the CPE spacing as one increases the speed of deposition for a fixed nozzle temperature. The inset shows a top view optical micrograph of multiple CPE blocks within each filament printed at increasing speeds. Note that for increasing speeds, the fusion between the printed lines will be weaker.

### Fabrication of pixelated light-emitting printable filament

The capability to print light-emitting inks can be useful in a multitude of applications ranging from customized displays, robotics, to communication between printed functional objects (Internet of things). We thus demonstrate a printable pixelated electroluminescent light-emitting filament (Figure 1a-1c) which consists of a metallic bismuth-tin (BiSn) core, electrically-conducting tungsten (W), an electroluminescent zinc sulfide (ZnS), insulating cladding polycarbonate (PC) and a print adhesion layer cyclic olefin copolymer (COC). To co-draw materials of very different melting points (e.g. melting point of tungsten is  $\sim 3000$  °C and the glass transition temperature of PC is 150 °C), we made use of a method called convergence draw whereby we feed high melting point tungsten and ZnS wires into pre-drilled channels within the preform. During the draw, these channels will narrow and reduce to a dimension similar to the diameter of these wires. These channels upon narrowing eventually drag, pull and incorporate these wires into their narrowed channels. Key to the formation of spatial light-emitters is the use of programmably-placed microspheres (Figure 1d). The geometry and scale of these BiSn microspheres with ZnS and W enables 0-dimensional electroluminescent pixels within a larger 3D-printed macrostructure. To form these spheres, the BiSn cylindrical core confined within the transparent viscoelastic PC matrix is subjected to laser-induced capillary breakup (Figure 2d), transforming the core into thermodynamically-stable BiSn spheres of larger diameter than the BiSn core which subsequently bridge the distance between the W and ZnS wires (Figure 2e). By connecting W and Cu to an alternating voltage source, these electrically conductive spheres link the electric potential from W towards the outer surface of ZnS, creating high electric field localized to these spheres positions and enabling sufficient electric field strength (Fig. 2f) to induce light emission from the ZnS layer via electroluminescence.

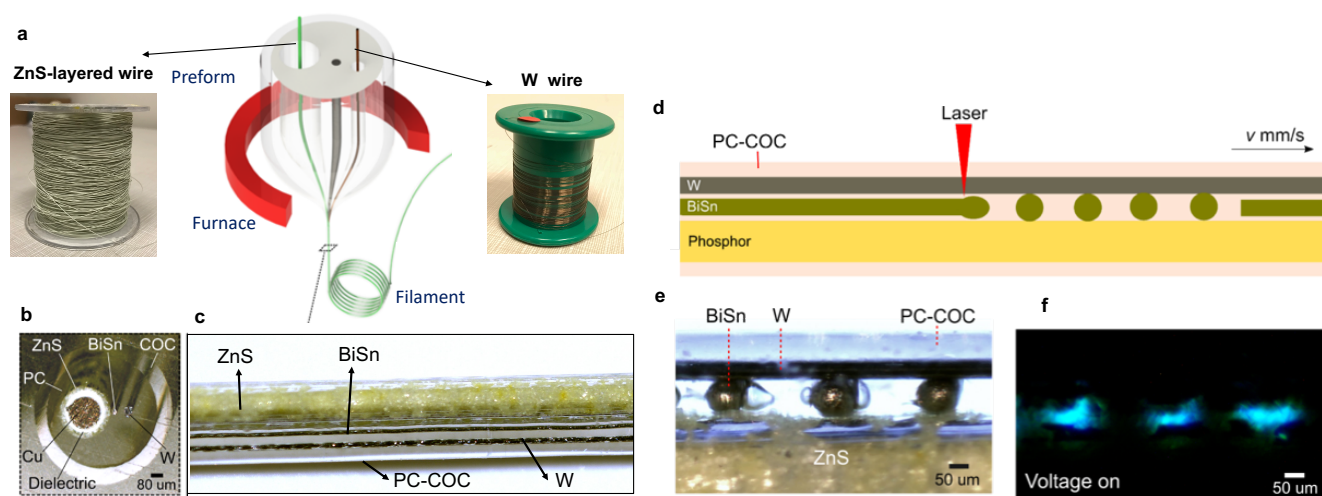


**Figure 2. Fabrication of a pixelated light-emitting filament.** (a) Thermal-drawing of the preform with high melting point wires fed into its hollow channels during the draw to form a multimaterial filament containing light-emitting metal-insulator-semiconductor 3D microstructures. (b) Cross-sectional and (c) Planar optical micrographs of the drawn filament. (d) In-filament capillary breakup of the instable cylindrical BiSn to create metallic conductive spheres by using a laser of 808 nm wavelength transparent to the cladding materials. (e) Optical micrograph of the in-filament low melting-point BiSn conductive spheres interfacing high melting-point W and ZnS. (f) Electroluminescent light-emission from ZnS at distinct sphere locations in (e) as an AC voltage is applied across the W and Cu wires.

### Printing light-emitting filament into 3D displays

The opportunity to combine microscale materials within the filament offers the potential to incorporate abundant micro-devices in a printed macro structure. Such advantage is ideal and highly applicable towards the printing of displays since modern display systems require large density of high resolution pixels. To advance towards the printing of the light emitting filaments, we make use of a lower glass transition thermoplastic COC ( $T_g \sim 80^\circ\text{C}$ ) cladding around a high  $T_g$  thermoplastic PC core so that filament surface heating can be done at a lower temperature or faster speed. Such an encapsulating layer further averts the detrimental wetting effect on the functional structures internal to the filament while still ensuring that the polymeric surface is at a temperature above its critical temperature for polymer fusion between printed lines (Figure 3a-3b). Using our technique, macro printed objects (Figure 3c) can then contain prescribed microfeatures and materials that are previously unprintable and not combinable (Figure 3d). Exploiting our technique to spatially write lighted pixels and later print them, we showcase a printed cylindrical ring (Figure 4a) capable of displaying designed stripe patterns of light created by a collection of 90 microscale pixel-spheres (Figure 4b and 4c), in which each lighted spot corresponds to 2 pixel-spheres. Comparing to previous work on printed light-emitting diodes having resolution in the order of mm due to wetting of low-viscosity inks, the pixel resolution of our printed display is limited only by the sphere size and is shown to be in the microscale (55  $\mu\text{m}$ ). Furthermore, we demonstrate that the curved cylinder is capable of light emission around its geometry, offering a 360° continuous viewpoint which is largely applicable for 3D displays and interactive robotics. In addition, in contrast to previous work that requires a bulk platform for embedding devices and printing interconnects, our micro-devices are already connected during deposition. This reduces large amount of external connectorization, enabling the formation of as-formed 3D objects of structurally-thin walls (order of mm) integrated with devices.



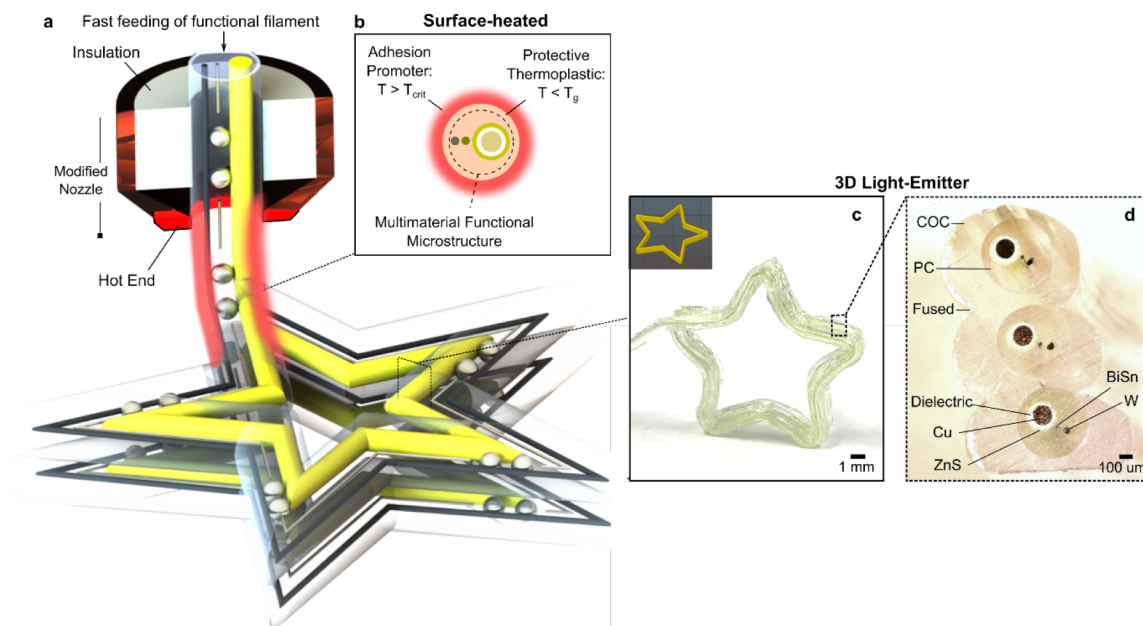


**Figure 3. Filament Surface Heating (FSH) of pixelated light-emitting filament.** (a) The light-emitting filament is fed quickly through a short hot end and becomes heated on the surface to be deposited into tailored shapes. (b) FSH generates a surface-heated effect with the filament surface temperature rising beyond its critical fusing temperature ( $T_{crit}$ ) while maintaining the temperature of the inner surrounding polymer at a temperature below its glass transition ( $T_g$ ). (c and d) A macro star printed from the light-emitting filament, via FSH, with its cross-sectional optical micrographs showcasing a hierarchical assembly of fused lines with preserved interfacial microstructures of different material classes.

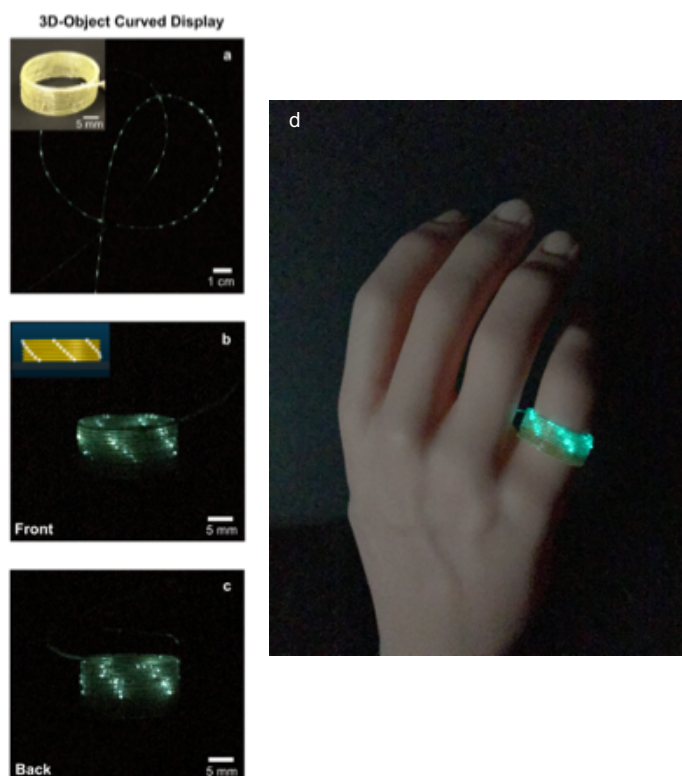


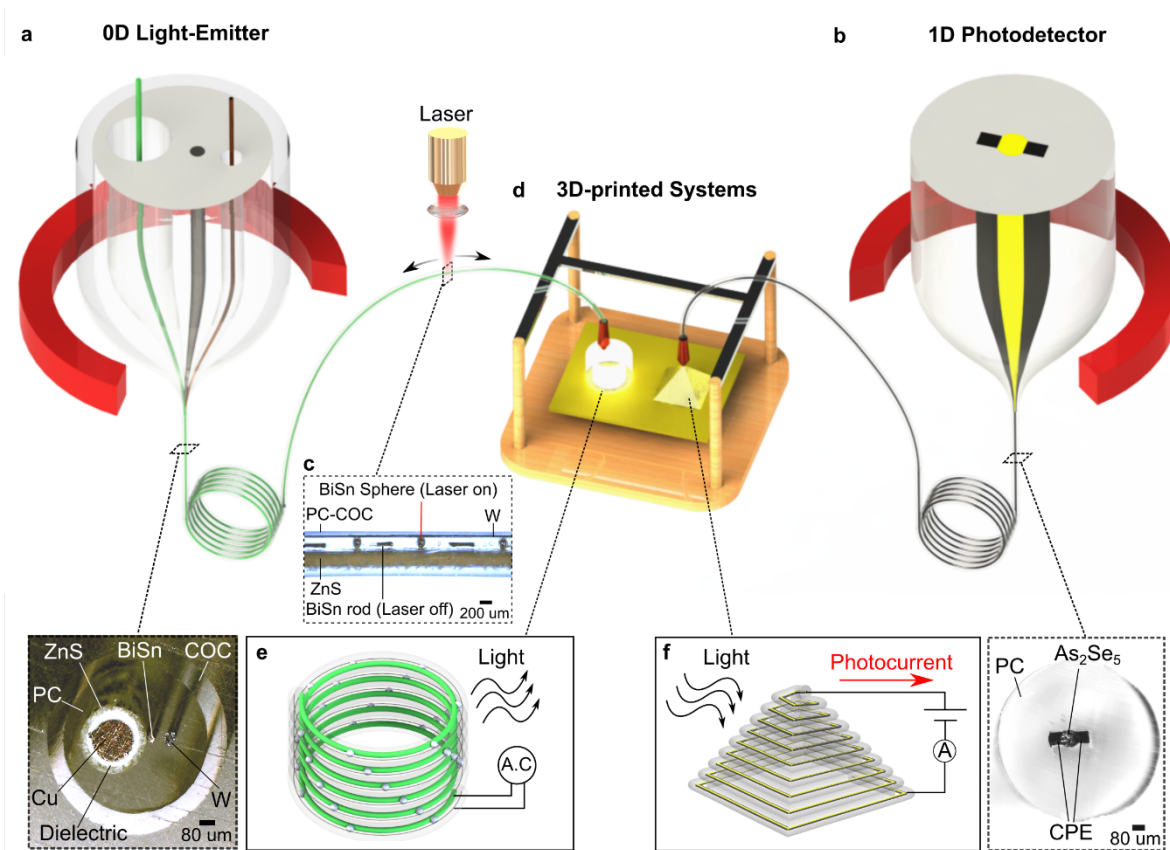
**Figure 4. Three-dimensional printed display** (a) Photograph of a filament dotted with pixelated light emitters. The inset shows the cylindrical ring printed from this filament, which is capable of (b and c) displaying electrically-activated stripe patterns all around its body. The inset of (b) shows the desired light design. (d) A photograph of the printed ring worn by a fake mannequin hand illustrating how a printed wearable can be used as a light-emitting display.

---

**Research Plans for Next Year:**

- **Theoretical model of wetting:** Measuring the spacing of CPE versus different deposition speeds and nozzle temperatures as in Figure 1 allows us to gather data and develop a theoretical wetting model for our heated filaments.
- **Multifunctional Objects:** We will fabricate apparatus as well as develop design strategies to print and combine two or more device functionalities, such as photodetecting and light-emitting, within a single object.
- **Porous Scaffolds:** Using the porous fibers produced from the thermal drawing process, we will print them to create tailored porous implants with engineered channels to aid nerve growth specifically for spinal cord applications.
- **Omni-directional retroreflective fiber from printed preforms:** In collaboration with Dr. Michael Ghebrebrhan at Natick Laboratory, we have obtained preliminary results and will further develop the strategy of thermal drawing *3D-printed preforms* of complex cross-sections and of disparate materials specifically for optical applications such as an omnidirectional retroreflective fiber.
- **Recursive printing (Cyclic print and re-draw):** In collaboration with Dr. Eric Wetzel from US. Army Research Laboratory, we will focus on two thrusts: (1) Recursive printing for hierarchical in-fiber lattice architectures of complex functionalities. We aim to print periodic lattice made up of multimaterial units of the individual fibers and redraw the printed lattice to obtain metamaterial fibers with nanoscale lattices, and (2) Deterministic mixing of immiscible polymers via recursive printing. Polymers such as PC, COC, ABS and more are not miscible in each other. In this thrust, we aim to look at the controlled nanoscale mixing of these polymers via recursive printing to create composites of novel mechanical properties.

### Representative Image and Caption:



**Representative Image: Additive Manufacturing of Three-dimensional Functional Systems from Structured Multimaterial Filaments.** Thermal-drawing of multimaterial preforms into (a) 0-dimensional light-emitting and (b) 1-dimensional light-detecting filaments, with their corresponding cross-sectional optical micrographs of metal-insulator-semiconductor 3D microstructures. (c) Spatially-resolved laser-induced capillary formation of discrete BiSn spheres to form programmably-placed pixels within the light-emitting filament. (d) These 3D-microstructured filaments are fed into a regular Fused Filament Fabrication printer with a modified nozzle, enabling the formation of customized electrically-activated three-dimensional systems capable of spatial (e) light-emission and (f) light-detection from its entire structure.

### Papers Published in Peer-reviewed Journals (Full citation required. Please include DOI if available):

- 1) Loke, G., Yuan, R., Rein, M., Jain, Y., Joannopoulos, J. & Fink, Y. Structured multimaterial filaments for high-resolution printing of three-dimensional optoelectronic systems. Submitted to Nature Communications.

### Peer-Reviewed Conference Proceeding Publications (Full citation required. Please include DOI if available):

- 1) none





***Books and Book Chapters:***

- 1) none

***Presentations at Meetings, but not Published in Conference Proceedings:***

- 1) none

***Patents, Patent Applications, and IP Disclosures:***

- 1) Fink, Y., Loke, G. Yuan, R. Multimaterial 3D-Printing With Functional Fiber, 62/423,825. Patent Pending.

***Doctoral Degrees Awarded During Reporting Period (First and Last Name):***

- 1) Michael Rein

***Master's Degrees Awarded During Reporting Period (First and Last Name):***

none